ISOMERIZATION AND FRAGMENTATION OF $[b_5]^+$ IONS AND $[b_5 - H]^{\bullet +}$ RADICAL CATIONS IN THE GAS PHASE

Bai-Han Backen Wu

A THESIS SUBMITTED TO THE FACULTY OF GRADUATE STUDIES

IN PARTIAL FULFILMENT OF THE REQUIREMENTS

FOR THE DEGREE OF

MASTER OF SCIENCE

GRADUATE PROGRAM IN CHEMISTRY

YORK UNIVERSITY

TORONTO, ONTARIO

APRIL 2017

ABSTRACT

In this thesis, we examined the CID spectra of the closed-shell $[A_4W_{\alpha\text{-Me oxa}} + H]^+$ ions, which are completely identical, and indicates sequence scrambling. There are some unique fragmentation patterns from this set of ions that have been analyzed in details.

The second part of this thesis is the study of the open-shell $[A_4W_{\alpha\text{-Me oxa}}]^{\bullet+}$ radical cations. In this study, we noticed no sequence scrambling, which is a distinctive characteristic. This is attributed to the formation of a stable structure with a captodative radical at the N-terminus.

We also studied the open-shell $[A_4Y_{oxa}]^{\bullet+}$ and $[A_4M_{oxa}]^{\bullet+}$ ions and summarized some similarities that are shared between the $[A_4G_{oxa}]^{\bullet+}$, $[A_4Y_{oxa}]^{\bullet+}$, and $[A_4M_{oxa}]^{\bullet+}$ ions. All three systems exhibit some isomerization before dissociation; but CID spectra of different sequences are non-identical, with different relative abundances. Loss of CO_2 is frequently the most dominant peak in all three systems.

ACKNOWLEDGEMENTS

I would like to express my deepest gratitude to my supervisor, Professor Alan C. Hopkinson, for all his supports, patience, and motivation. During his guidance, he shared knowledge, passion in scientific research, as well as humor. Without his wisdom, guidance, and dedication in editing, it would be tremendously more difficult for my research, publications, and thesis writeup.

In the same way, I would also like to express my most sincere thanks to my supervisor, Professor K. W. Michael Siu, for his guidance and constant motivation. He always shares great insights and wisdoms, and has always been there to help and support. He has been a huge influence for my research passion during the time. Without hit guidance, I would not have achieved what I have done.

I would also like to show my sincere gratitude to my colleagues. First and foremost, I would like to give special thanks to Dr. Justin Kai-Chi Lau for the enormously amount of supports and advises. All DFT calculation works shown in this thesis are the results of his dedication and patience, which provide great support for my works. He has been my mentor in both research and personal development, and also my friend. I want to thank Dr. Udo H. Verkerk for his useful advices and detail tutorials in both organic synthesis and instrumentation with his expertise. I also want to thank my former colleague, Dr. Cheng-Han (Ethan) Hung from Taiwan, for being my great mentor in mass spectrometry instrumentation when I first started my research. I want to thank Dr. Cheuk-Kuen (Isaac) Lai for sharing his vast knowledge in mass spectrometry principles and instrumentation, as well as all the supports he provided. I want to thank the colleague sharing office

with me, Brian Lam, for all the supports, as well as being cheerful and encouraging all the time. I also want thank my other colleagues, Dr. Yating Wang, John Van Nostrand, and Dr. Olena Matsui, and former colleague Dr. Declan Williams and Dr. Xiao Yan Mu, for all the supports when needed.

Lastly, I feel grateful to my parents and my girlfriend, who have always been with me and supported me during my tough times, especially during the completion of this thesis. Without their accompany and encouragements, it would have been much more difficult for me.

I also want to thank Centre for Research in mass Spectrometry (CRMS) at York University and Natural Science and Engineering Council (NSERC) for allowing me to have the opportunity and all the supports to make this research happen.

TABLE OF CONTENTS

LIST OF FIGURES

LIST OF SCHEMES

CHAPTER 1: Introduction

1.1 Application of mass spectrometry (MS) in proteomics

Mass spectrometry-based proteomics has become a very powerful technique and a fast-developing field in molecular biology, following the development of soft ionization methods such as electrospray ionization (ESI) and matrix-assisted laser desorption ionization (MALDI) during the 1990s.[1-8] Modern bottom-up proteomics is able to receive protein samples and generate a list of identified proteins within the same day, without the need of additional purification steps. This is achieved by a combination of enzymatic digestion, followed by liquid chromatography (LC) separation and mass spectrometry analysis.

Even though mass spectrometry can detect masses of analytes, detection of a mixture of intact proteins can be difficult. Proteins usually undergo post-translational modifications (PTM), which makes identification difficult using only the measured *m/z* values.[6] Tandem MS (MS/MS) on intact proteins is also difficult, since collision-induced dissociation (CID) is nearly impossible due to the large size of proteins. In bottom-up proteomics, proteins are first denatured by adding surfactants to increase accessibility of the protein (**Figure 1.1**). Surfactants being used for proteomic need to be compatible with MS analysis. The surfactant either needs to be removable by organic solvents, or is acid-labile and becomes decomposed at the end of the digestion

protocol.[9-12] The denatured protein is then incubated with the added enzyme. Proteases such as Lys-C, Arg-C, Asp-N, and Glu-C are commercially available for this purpose, which cleaves peptide chains at specific sites.[2] Trypsin is one of the most commonly used proteases; it cleaves proteins at the carboxyl terminal of a lysine or arginine residue.[2,13] The peptide mixture after a protein has been digested by trypsin is referred to as tryptic digest peptides, and is ready for further separation processing.

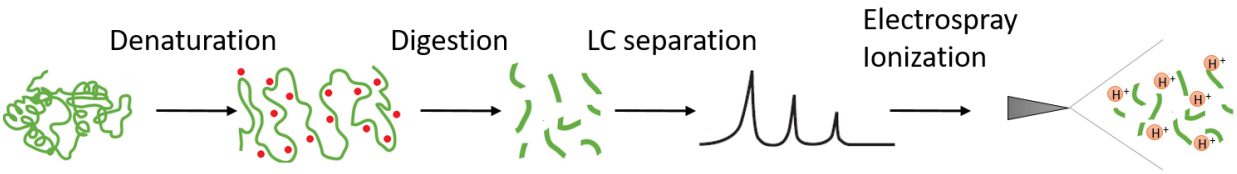

Figure 1.1 Typical workflow for generating protonated peptide ions in bottom-up proteomics.

Mass spectrometers can detect multiple peptides in one single spectrum, but there would be overlapping isobaric peptides which make it too complicated for interpretation if the peptide digest mixture is infused into the mass spectrometer all at once, especially when multiple proteins are present. The peptide digests are usually first separated using a high-performance liquid chromatography (HPLC) before introducing to the mass spectrometer.[2] The dissolved peptide digest is injected onto a capillary column packed with adsorbent material, the stationary phase, which retains hydrophobic analytes. Next, a gradient of two solvents is used to flow through the column by applying pressure, which separates the peptides based on their hydrophobicity. The end of the HPLC column is connected to an electrospray ion source that ionizes each peptide into the

gas phase for them to enter the mass spectrometer. Measuring peptide signals based on the elute only will result in a total ion chromatogram (TIC) that represents the elution profiles of the peptide digest. There will still be multiple peptides having the same or similar elution profile, but the mass analyzer is now able to detect and distinguish the different peptides based on their different *m/z* values. For more accurate identifications, MS/MS analysis is often used to further sequence each individual peptide before matching for proteins. For each MS scan, a defined number of peptides, usually the three most abundant peptide peaks, will be automatically selected for CID.

Upon CID of a protonated peptide, the peptide tends to fragment by breaking the amide bond. [14-17] This is caused by protonation on an amide nitrogen followed by nucleophilic attack by an adjacent carbonyl oxygen on the protonated amide carbon, thereby resulting in the cleavage of the amide bond. This results in $[b_n]^+$ ions from the N-terminus and/or $[y_m + 2H]^+$ ions from the C-terminus (**Figure 1.2**).[18] The *y*-type ions are believed to be truncated peptides or protonated amino

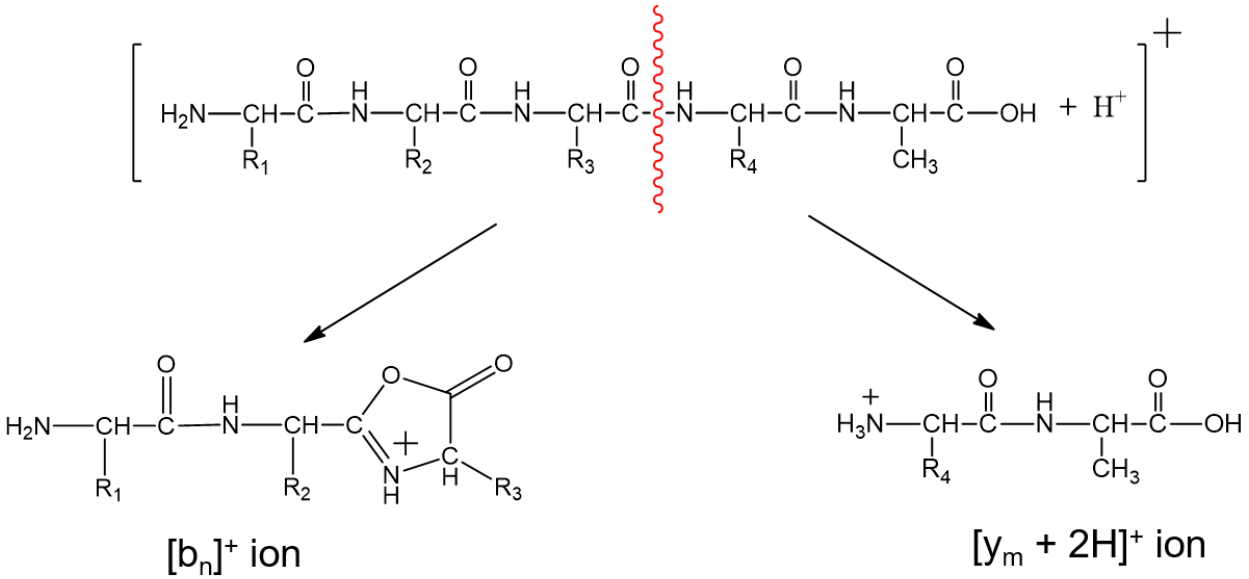

Figure 1.2 Fragmentation of gas-phase protonated peptides in MS.

acids, whereas the structures of $[b_n]^+$ ions are believed to have oxazolone structures at the C-terminus.[15,19-23] These b- and y-type ions are matched with a database to deduce the original peptide sequence.[2] After the entire HPLC-MS/MS run is completed, and a list of identified peptide is obtained, the detected peptides can be matched in the database to identify the proteins that were present in the original sample before digestion, along with any modifications.

1.2 Collision-induced dissociation (CID)

Since ESI is a soft ionization technique, the selected ions need to be further activated to observe for fragmentation and acquire structural information. In modern day instruments, collision-induced dissociation is the most commonly used ion activation method, especially for quadrupoles and ion traps.[24] Ions are activated by provision of a certain amount of kinetic energy through electric potentials, followed by inelastic collision with neutral gas molecules (nitrogen, helium, or argon), such that kinetic energy of the target ion is converted into internal energy Q in the form of molecular vibration. The maximum Q, in which the collision is inelastic, is defined by the center-of-mass internal energy of the ion (E_{CM}), and is expressed by the relationship:

$$E_{CM} = E_{lab} \frac{m_N}{m_N + m_{AB}} \quad \textbf{(1)}$$

where E_{lab} is the kinetic energy applied to the ion, m_N is the mass of the neutral gas molecule, m_{AB} is the mass of the precursor ion.[25-28] This internal energy is then rapidly redistributed throughout the molecule in the form vibrations. The final internal energy of the precursor ion after collision can be expressed as:

$$E_{AB}^{\neq} = E_{AB} + Q \quad \textbf{(2)}$$

When $E_{AB}^{\neq}$ is sufficient to cause dissociation of the precursor ion, the most fragile bonds will break. The overall CID process can be described as:

$$AB^+ + N \xrightarrow{energy} AB^{+\neq} + N \rightarrow A^+ + B + N \quad \textbf{(3)}$$

where A^+ and B represent the product ion and the neutral loss, respectively, and N represents the neutral collision gas molecule. The first step represents the ion activation created by accelerating the ion in an electric field, which spans a larger time frame than the second step, which represents the dissociation of the ion.

The extent of fragmentation in a CID spectrum depends on several factors: the amount of collisional energy provided; the duration of time over which the ions are being activated; the instrumental time scale for ions to travel before they reach the detector; how rapidly the target ion redistributes the internal energy; and the efficiency of the CID.[24]

The factor that influences fragmentation in CID that is the easiest to understand is the collisional energy that the ion acquires in the system. From equation **(1)** described above, the collisional energy, which is the total internal energy of the precursor ion after collision, depends on the kinetic energy applied on the ion, the mass of the neutral gas molecule, and the mass of the

precursor ion. First, of course, the maximum collisional energy increases with higher E_{lab}, which is the kinetic energy that the precursor ion receives as it accelerates before entering the collision cell. For example, an ion initially at rest passing through a potential of 10 V would have an E_{lab} of 10 eV. For ion trap instruments like the QTRAP 2000 and the LIT in the Orbitrap Elite, the ion is accelerated with the resonance excitation voltage at a specific frequency for the precursor's *m/z* value. A greater potential applied on the ion will result in greater collision energy. Equation **(1)** also suggests that the maximum collisional energy increases when the mass of neutral gas molecule increases or the mass of precursor ion decreases. The neutral inert gas being used in most instruments include N_2, He, Ar.[26] Experimental results have shown that heavier gases like argon or xenon will give better fragmentation compared to helium.[29] CID of large ions with small gas molecules should be difficult. However, numerous studies found that CID of large peptides can also be very efficient.[30] The inert gas that was used in the QTRAP 2000 for radical cation experiments is nitrogen (N_2) gas, and the inert gas that was used in the Orbitrap Elite for the closed-shell studies is helium.

1.3 Electron-based dissociation (ExD)

Another ion activation method that can be used orthogonally to CID is electron-captured dissociation (ECD). In CID, internal energy of the precursor molecule redistributes throughout the molecule and converts to vibrational energy before dissociation. As a result, the ion often has a sufficient timeframe for cyclization and rearrangement, and the weakest bonds in the precursor

molecule will break first.[27] For proteins and peptides, the amide bond along the backbone is the weakest bond, which results in abundant of b- and y- type ions.[31] This characteristic may be useful sometimes, but can be problematic for some studies. For instance, post-translational modifications (PTM) such as phosphorylation and glycosylation, and non-covalent protein interactions, will be cleaved first in CID, leaving no useful information in the mass spectra.

ECD emerged as a relatively new ion activation method during the past decade. The detail mechanisms for ECD-type methods are still under debate, but it is mostly believed to be a non-ergodic process, meaning that the dissociation process is fast and occurs before redistribution of internal energy.[32, 33] In ECD, an electron source is produced by a heated dispenser cathode, and comes in contact with the trapped precursor ion (**Figure 1.3**).[34] The precursor ion then captures

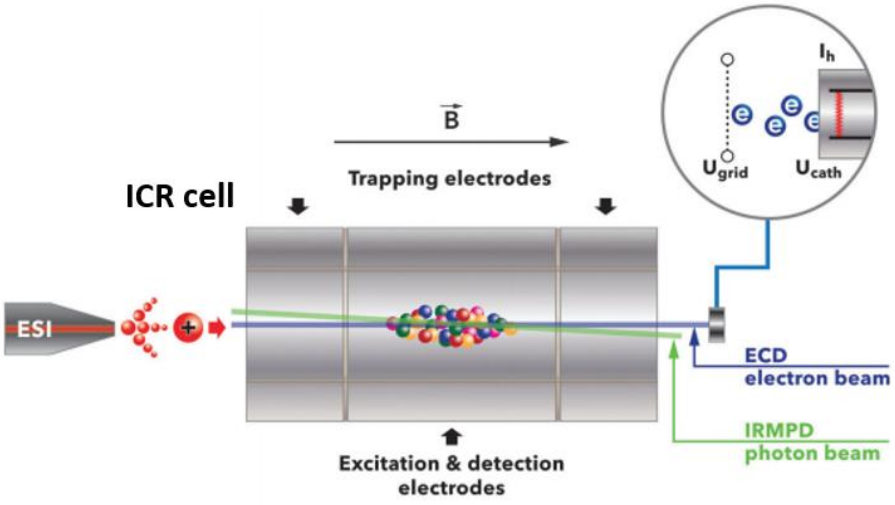

Figure 1.3 ECD in FT-ICR instruments. A heated dispenser cathode produces electron beam at the rear end of the instrument. IRMPD can also be done at the same time by applying a photon beam. Figure adapted from Zhurov et. al.[34]

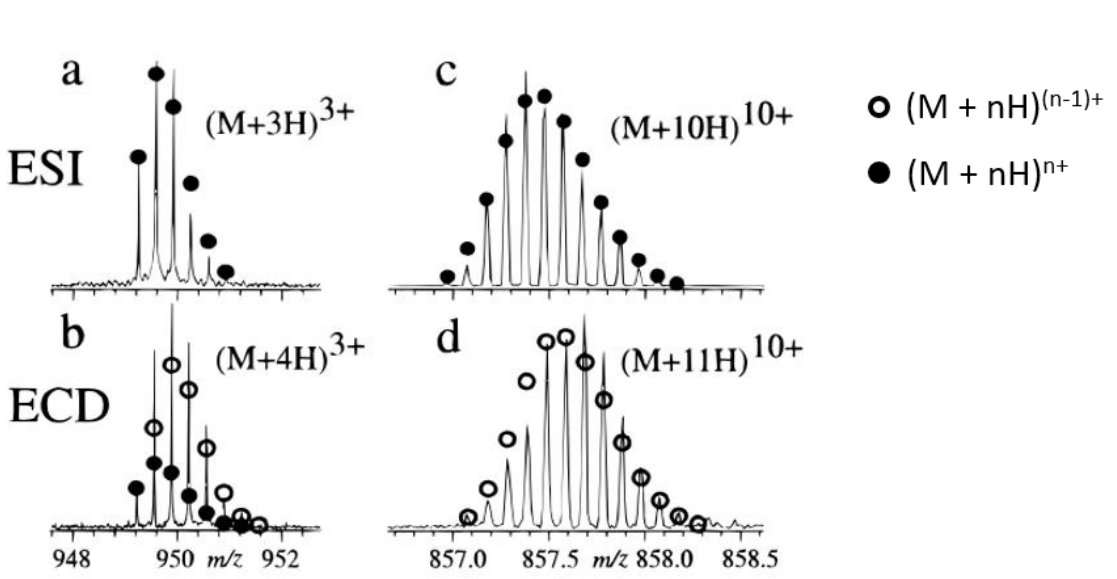

Figure 1.4 Isotopic distributions of (a, b) melittin^{3+} and (c, d) ubiquitin^{10+} ions obtained by (a, c) ESI and (b, d) ECD. Closed and open circles, theoretically predicted isotopic abundance distributions for $(M + nH)^{n+}$ and $(M + nH)^{(n-1)+}$, respectively. Figure adapted from Zubarev et. al.[35]

one electron and becomes a radical species with an odd number of electrons. In the cases of protein and peptides, the species will be shown as $(M + nH)^{(n-1)+\bullet}$, instead of $(M + nH)^{n+}$ shown in a CID spectrum with ESI (**Figure 1.4**).[35] These radical species fragment very differently from those demonstrated by CID. Instead of producing b and y ions by cleavage of the amide bond, ECD typically breaks the N-C_α bond and results in c and z ions. However, ECD is not a popular method since it can only be implemented on FT-ICR instruments.[33, 36] This is due to the fact that the electromagnetic field of the ICR cell is much better suited for trapping electrons, compared to the RF field with low mass cut-off in a quadrupole type ion trap.

To overcome the limitation of ECD and use the technique more broadly, Syka et al. introduced electron transfer dissociation (ETD) in 2004.[36] In ETD, electrons are not dispensed

directly and captured by the precursor ion. Instead, a secondary molecule is ionized into an anion through chemical ionization and acts as an electron donor, and then transfers the electron to the precursor ion. One very crucial step in this technique is to choose an efficient reagent anion that easily transfers an electron to the cation precursor, since this step often competes with proton transfer from the cation.[37] Several polyaromatic compounds have been experimented for this purpose, many of them shown electron transfer without dissociation.[38, 39] To date, fluoranthene is the most preferred reagent, although its efficiency in electron transfer is only 40%.[37] One of the most popular commercial instrument that employs ETD is the Orbitrap. In the Orbitrap Elite.[40] Fluoranthene anion is produced through negative chemical ionization in the ETD module at the back end of the instrument. The ETD process can be described in the following steps:

$$N_2 + e^-_{fast} \rightarrow N_2^{\bullet +} + e^-_{slow} + e^-_{fast}$$

$$\text{fluoranthene} + e^-_{slow} \rightarrow \text{fluoranthene}^{\bullet -}$$

$$[M + nH]^{n+} + \text{fluoranthene}^{\bullet -} \rightarrow [M + nH]^{\bullet (n-1)+} + \text{fluoranthene}$$

Nitrogen gas is used as a carrier gas that sweeps fluoranthene into the gas phase. As negative chemical ionization, hot electrons (70 eV) are emitted from a filament, and knock electrons off from the nitrogen gas molecules. These electrons are captured by the fluoranthene molecules to create anions, which are then ready to transfer to the ion trap through quadrupole ion guides.

There are also variations in ECD, one of them is electron-induced dissociation (EID), for singly charged ions. Typical ECD techniques use low energy electrons (< 0.2 eV). When a singly charged ion $[M + H]^+$ is exposed to high energy electrons (> 10 eV), which exceeds its first

ionization energy, it can be further ionized to become $[M + H]^{\bullet 2+}$, and this is called tandem ionization.[41-43] The $[M + H]^{\bullet 2+}$ will then re-capture a low energy electron. The end result will be a singly charged ion that has the same *m/z* and same number of electron with the original species, but is electronically excited. The process can be described as below:

$$[M + H]^{+} + e^{-}_{fast} \rightarrow [M + H]^{\bullet 2+} + e^{-}_{slow} + e^{-}_{fast}$$

$$[M + H]^{\bullet 2+} + e^{-}_{slow} \rightarrow [M + H]^{+\neq}$$

Since the electron-capture process is exothermic and the ion is electronically excited, it will undergo fragmentation. The fragmentation pattern from EID has similarities with PD, since the ions are both electronically excited.[43] EID is usually used on small singly charged molecules that are difficult to acquire multiple charge, such as small peptides, polyketides, and small pharmaceutical molecules.[42,44,45]

For studies on anions, such as acidic peptides, several variations of ECD for negative mode have been published.[33] These include electron detachment dissociation (EDD), negative electron transfer dissociation (NETD), and negative ion ECD (niECD). EDD has similarities with EID, which involves tandem ionization of a multi-deprotonated anion by collision with a high energy electron (> 10 eV).[33, 46]

$$[M - nH]^{n-} + e^{-}_{fast} \rightarrow [M - nH]^{\bullet (n-1)-} + e^{-}_{slow} + e^{-}_{fast}$$

The electron detachment process is exothermic, and the resulting multi-deprotonated radical anion will fragment primary by the cleavage of C_{α}–C bond, which produces a- and x-type ions.[46, 47]

NETD is another negative mode technique that is analogous to ETD. Instead of producing a radical anion with fluoranthene that donates an electron, NETD employs EI to produce radical cation fluoranthene, by removing the carrier gas supply and maintain sufficient vapor pressure of fluoranthene by increasing the temperature.[47]

$$\text{fluoranthene} + e^-_{fast} \rightarrow \text{fluoranthene}^{\bullet +}$$

$$[M - nH]^{n-} + \text{fluoranthene}^{\bullet +} \rightarrow [M - nH]^{\bullet (n+1)-} + \text{fluoranthene}$$

For singly charged anions, Yoo et al. introduced negative ion ECD (niECD) in 2011.[48] They have discovered that, although it is difficult for gaseous anions to capture electrons due to repulsion, it is possible for small anions ($[M - nH]^{n-}$, $n \geq 1$) to capture an electron within a narrow energy range (~3.5 eV – 6.5 eV). Fragmentation through niECD follows a similar mechanism with that through ECD and produces primary c- and z-type ions. This technique is useful for studies of PTMs in small acidic peptides, which is difficult to acquire multiple charge required by EDD and NETD.

Electron-based dissociation techniques have rapidly evolved during the past decade, from ECD that is limited to only FT-ICR instruments, to the more widely-adapted ETD. Numbers of variations for negative mode and singly charged ions have also been developed, which make this type of ion activation method more feasible for different types of analytes. Electron-based dissociation has shown prominent application in top-down proteomics, where CID is inefficient for fragmentation of intact proteins, and at the same time it is easy for proteins to acquire multiple

charge. ECD or ETD is also used orthogonally with CID in proteomics since they produce different fragmentation patterns, which helps to increase sequence coverage significantly, and retains PTM information at the same time.

1.4 Hydrogen-deficient radical cation formation

Radical peptide ions that are generated using ExD techniques have high energy, which gives them the non-ergodic property and results in quick dissociation.[33] However, to study the gas phase chemistry of peptide radical cation, we need to record the onset of each fragmentation pathway starting from low energies. The hydrogen-deficient radical cations, generated from oxidative dissociation inside the mass spectrometer, are more desirable for the purpose of fundamental study. One of the most widely used methods for generating such species is by the use of copper (II) ion (Cu(II)).[50] This technique was first discovered by Chu et. al. by using diethylenetriamine (dien) as an auxiliary ligand to form a dipositive complex with Cu(II) and oligopeptides that contain both tyrosine and a basic residue (arginine, lysine, or histidine). The proposed structure for the complex consists of a dien molecule coordinating the five-coordinate Cu(II) atom with the three amines, and the peptide coordinating the other two with the N-terminal amine and the phenolic oxygen. CID of this complex yielded the reduced $[Cu(I)(dien)]^+$ and the desired $[M]^{\bullet+}$ radical peptide (**Figure 1.5**).

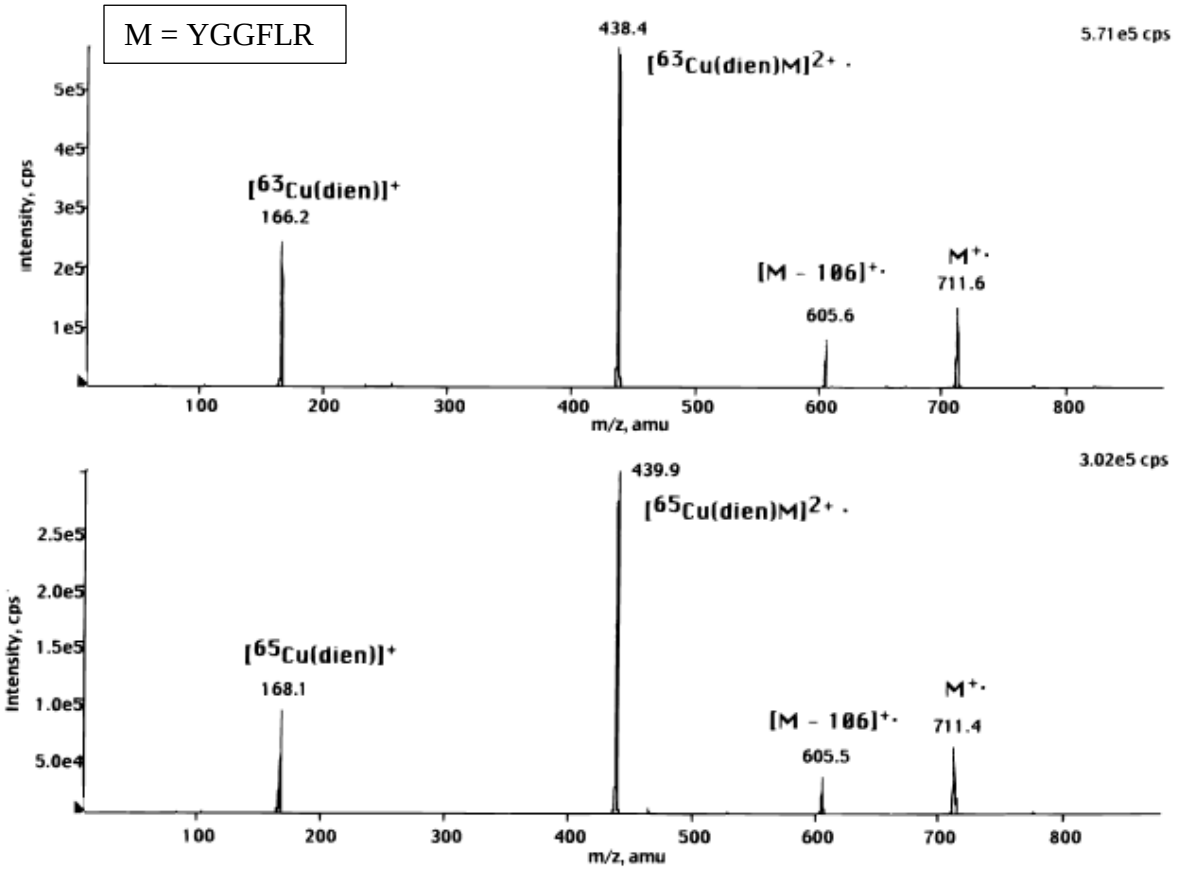

Figure 1.5 CID spectra of the [Cu(II)(dien)YGGFLR]$^{\bullet 2+}$ complex with ^{63}Cu (upper) and ^{65}Cu (lower). Figure adapted from Chu et. al.[50]

In addition to dien, there are numerous auxiliary ligands that have been employed for this application, such as 2,2,':6',2"-terpyridine (terpy) and 12-crown-4.[50-52] Dien, which was initially used, have mobile protons at the amine groups, which may facilitates proton transfer to the radical cation being produced and generates a protonated peptide. Since we want to avoid this competitive pathway when generating peptide radical cations, ligands with tertiary amines, such as terpy, had

became a better choice. Crown ether is also a popular group of ligands for binding metal ions. It acts as a planar ligand, as opposed to terpy. The size and the type of ligand needed for generating peptide radical cations depend on the size and side chains of the peptide, and also the metal being used. Throughout the study in this thesis, we selected 18-crown-6 as the auxiliary ligand. To generate the desired hydrogen-deficient radical cation from our synthesized peptides, the peptide sample was mixed with copper perchlorate hexahydrate ($Cu(ClO_4)_2 \bullet 6H_2O$) and 18-crown-6 in approximately 1:1:1 ratio in 50:50 (v/v) water : methanol. The prepared solution was continuously infused into the mass spectrometer as the ESI source, and the dipositive complex $[Cu(II)+L+M]^{\bullet 2+}$ (L = 12-crown-6, M = target peptide) was selected as the precursor ion for CID. The complex dissociates into $[Cu(I)+L]^{+}$ (*m/z* 327) and $[M]^{\bullet +}$, and the latter was selected for further analysis. The process is illustrated as follows:

$$[Cu(II)+(18\text{-crown-}6)+M]^{\bullet 2+} \xrightarrow{CID} [M]^{\bullet +} + [Cu(I)+(18\text{-crown-}6)]^{+}$$

1.5 Sequence scrambling in $[b_5]^+$ and $[b_5 - H]^{\bullet +}$ ions

The commonly used CID is a relatively slow ion activation process and is ergodic. This means that the selected and activated precursor ion has sufficient time to redistribute the internal energy throughout the molecule, and may undergo rearrangements, before dissociation.[53,54] Recent studies have shown that for the closed-shell $[b_n]^+$ ions of longer peptides, the N-terminal amine

can attack the carbonyl carbon in the oxazolone ring to form a cyclic polypeptide (**Figure 1.6**).[15,55,56] The cyclic structure of $[b_5]^+$ ions have been verified by Erlekam et al., with a protonated amide oxygen.[57] This common cyclic polypeptide will reopen and fragment at preferred sites. Consequently, the original sequence information of the peptide ion can be lost, and we call this sequence scrambling. It has also been known that sequence scrambling is significant for $[b_n]^+$ ions only when $n > 3$.[58] $[b_5]^+$ ions that contain a tyrosine or tryptophan residue along with four alanine residues have been studied previously, and both exhibited sequence scrambling.[51,59] There was a marked preference for loss of the hetero-residue, with both sets of $[b_5]^+$ ions losing approximately

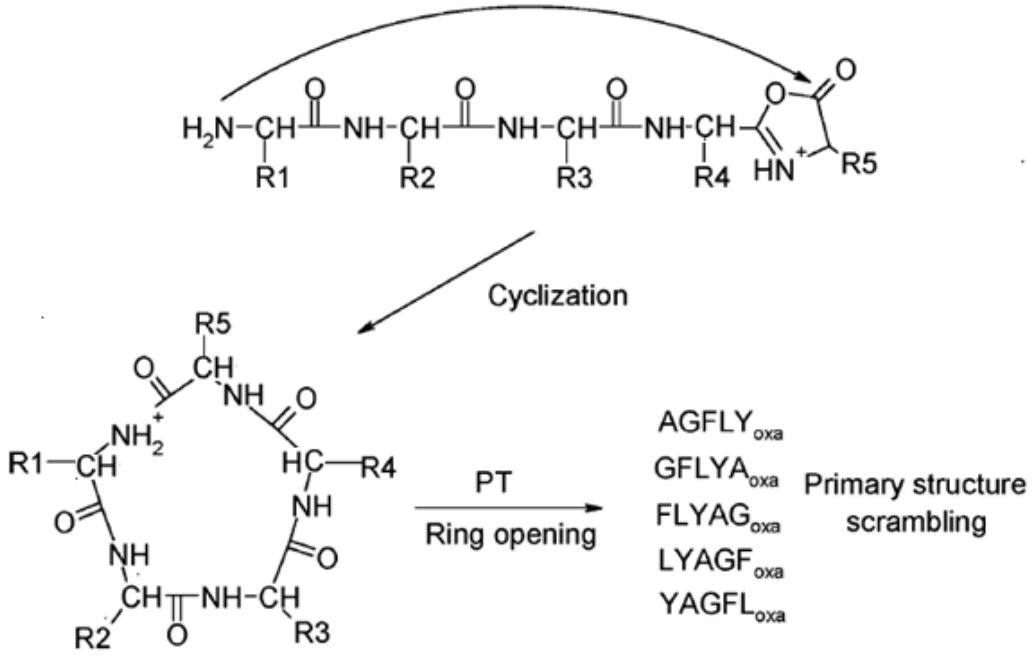

Figure 1.6 Sequence scrambling of $[b_5]^+$ ion of $[YAGFL_{oxa} + H]^+$ through macrocyclization. The subscript "oxa" denotes the oxazolone structure at the C-terminus (R1=CH_3, R2=H, R3=C_7H_7, R4=C_4H_9, R5=C_7H_7O). Figure adapted from Harrison et. al.[56]

equal amounts of the imines derived from alanine and tyrosine or tryptophan residues. Since open-shell radical cations often show richer fragmentation chemistries compared to the closed-shell ions, we are interested in studying the $[b_5 - H]^{\bullet+}$ radical cation, which is analogous to the $[b_5]^+$ ion from a protonated peptide.

Our previous studies on the $[b_5 - H]^{\bullet+}$ ions that contain four alanine residues and one tryptophan residue at different positions showed complete sequence scrambling of the ion.[59] These $[b_5 - H]^{\bullet+}$ ions form a common macrocyclic structure, followed by ring-opening into the sequence $[AAAAW_{oxa}]^{\bullet+}$, with the radical located at the α-carbon of the tryptophan (**Figure 1.7**). This α-radical is adjacent to the nitrogen atom in the oxazolone ring, where the proton is often located and this facilitates proton migration onto the backbone, thereby triggering the cleavage of peptide bonds.

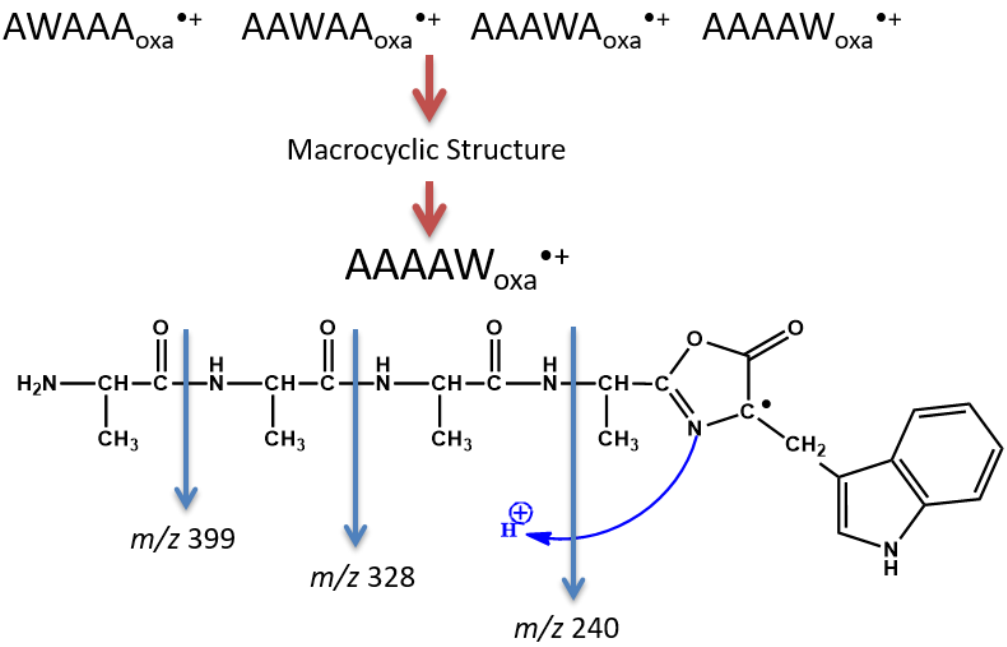

Figure 1.7 Sequence scrambling and dissociation of $[b_5 - H]^{\bullet+}$ derived from $[A_4W_{oxa}]^{\bullet+}$.[59]

In order to continue our investigation of sequence scrambling in b-type ions, we decided to examine $[b_5 - H]^{\bullet+}$ ions again with four alanine residues, but with one α-methyltryptophan residue. The formation of the α-radical is no longer possible and having a methyl group on the α-carbon of the tryptophan makes the α-carbon more sterically hindered; consequently the other three bonds connected to this α-carbon are lengthened and therefore potentially more fragile. The key structural feature in the isomer of the $[A_4W_{oxa}]^{\bullet+}$ ions that dissociated was the location of the radical on the α-carbon of the tryptophan residue in the oxazolone ring. Here we ask the questions does macrocyclization still occur and what dissociation mechanism is followed if formation of the α-radical is prevented by the presence of a methyl group on the α-carbon of the tryptophan? Based on our calculations on the isomers of $[A_4W_{oxa}]^{\bullet+}$, plausible structures for the $[A_4W_{\alpha\text{-Me oxa}}]^{\bullet+}$ ions may have (i) a captodative structure with the radical on the α-carbon of the N-terminal residue and the proton on the oxygen of the first peptide bond (**Figure 1.8** ion **I**), (ii) a β- radical on the side chain of the α-methyltryptophan residue and the proton on the peptide backbone (**Figure 1.8** ion **II**), and (iii) a structure in which both the charge and the radical are located on the aromatic system of the indole ring (**Figure 1.8** ion **III**). Macrocyclization is facilitated by having the charge on the oxazolone ring, making it susceptible to nucleophilic attack; similarly, the terminal amino should be freely available. These structural requirements suggest that both the captodative structure and the π-radical are unlikely to macrocyclize and sequence scrambling would probably not be observed from these structures.

We are also interested in the difference in fragmentation of the protonated peptides, peptide radical cations, and the $[b_5]^+$ ions when an α-methyl group is introduced on the tryptophan residue. Hexapeptides were synthesized to produce a series of $[b_5]^+$ ions that contain four alanine residues

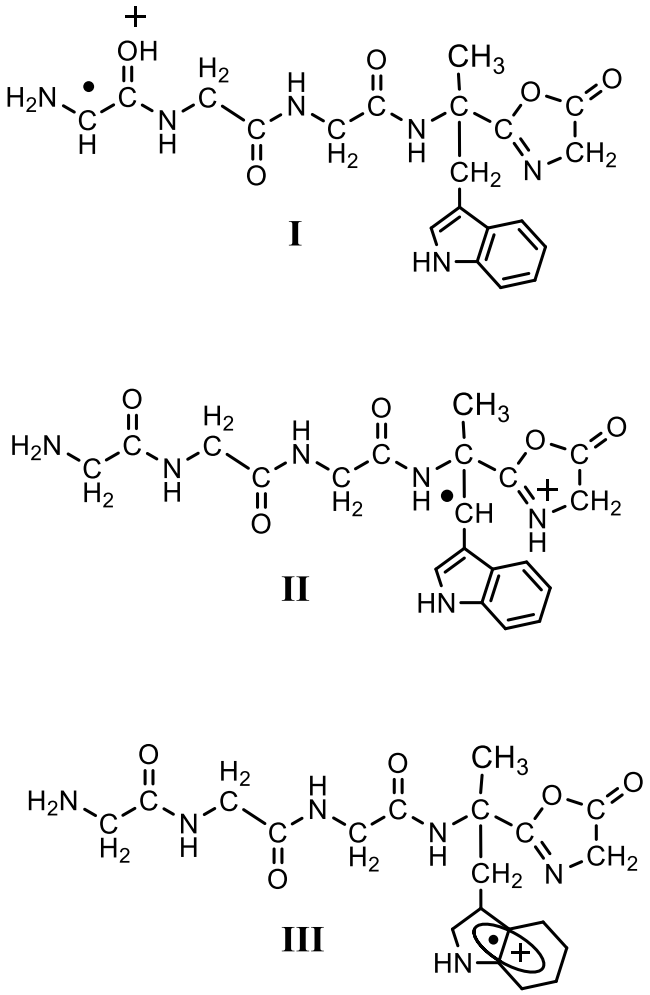

Figure 1.8 Plausible structures for the $[A_4W_{\alpha\text{-Me oxa}}]^{\bullet+}$ ions.

and one α-methyltryptophan residue, with the latter at all different positions except for the first. Results and detailed comparisons will be discussed in this thesis.

Another research direction is to study the $[b_5 - H]^{\bullet+}$ in hexapeptides that contain a methionine residue, as well as hexapeptides that contain a tyrosine residue. To date, many studies have been done on peptide radical cations with aromatic side chains, such as tryptophan, tyrosine,

histidine, and phenylalanine.[50,59-61] These ions are particularly stable because of the ability of the aromatic systems to stabilize the charge and the radical, making it easy to produce $M^{\bullet+}$. There are also studies on radical peptide radicals with cysteine, by homolytic cleavage of the S-NO bond in the nitrosylated peptide.[62-65] Also, there are studies on making radical cations with methionine amino acid and dipeptides using Cu^{2+}/acetonitrile (ACN) complexes.[66,67] Our goal is to continue to explore the open-shell $[b_5 - H]^{\bullet+}$ ion from systems containing methionine and tyrosine, and compare with those derived from the systems that have been known.

The research goal of this thesis is to understand the sequence scrambling properties and dissociation patterns of both the closed-shell $[b_5]^+$ ions and the open-shell $[b_5 - H]^{\bullet+}$ ions. We aimed to understand the behavior of these b-type ions by comparison between simple systems that contain four alanine residues and one hetero-residue at different positions. We were interested in finding out whether having different hetero-residues in the ion would change the scrambling behavior, especially for the open-shell $[b_5 - H]^{\bullet+}$ ions, as well as the effect of simple modifications such as having an α-methyl group on the hetero-residue. This information in gas phase chemistry will be needed, in order to build a stronger foundation for proteomics by improving efficiency and accuracy of the database search algorithm.

CHAPTER 2: Experimental Techniques

2.1 Electrospray ionization

In the past century, mass spectrometry has rapidly developed. The early mass spectrometers relied on an electron impact (EI) ion source, which causes fragmentation of molecules at the front end of the instrument.[68,69] To retain the structure of the analyte in the gas phase inside the mass spectrometer, soft ionization techniques, such as electrospray ionization (ESI), were developed and gained popularity.[2] ESI-MS has rapidly emerged into the proteomics field, as it can be used for structural analysis of a wide range of thermally labile biomolecules, including proteins, peptides, and drugs. However, while the intact structure is often retained using soft ionization techniques, further ion activation methods, such as collision-induced dissociation, are needed to fragment the ion for more detailed structure elucidations.

An ESI source can be very simple. The principle behind ESI is to deliver a flow of solution through a capillary with elevated voltage, relative to the orifice on the opposite side where ions enter the mass spectrometer.[2,70] This will form charged droplets from the tip of the ESI capillary, or the ESI emitter. These charged droplets undergo solvent evaporation and electrostatic repulsion and reduce in size, which will increase in charge density, and ultimately result in formation of the charged gas-phase ions (**Figure 2.1**).[71] This process happens in an atmospheric region before the

ions enter the orifice. An annular flow of inert gas, also called the sheath gas, is often used to flow in the same direction outside of the inner capillary, to assist in forming the small droplets.

For study on the closed-shell $[b_5]^+$ ions from peptides containing an α-methyltryptophan residue, all experiments were conducted on an Orbitrap Elite™ Hybrid Ion Trap-Orbitrap Mass Spectrometer (Thermo Fisher Scientific) in positive mode, with a heated electrospray ionization (H-ESI) source. In H-ESI, sample solution passes through a heated metal needle.[71] At the ESI

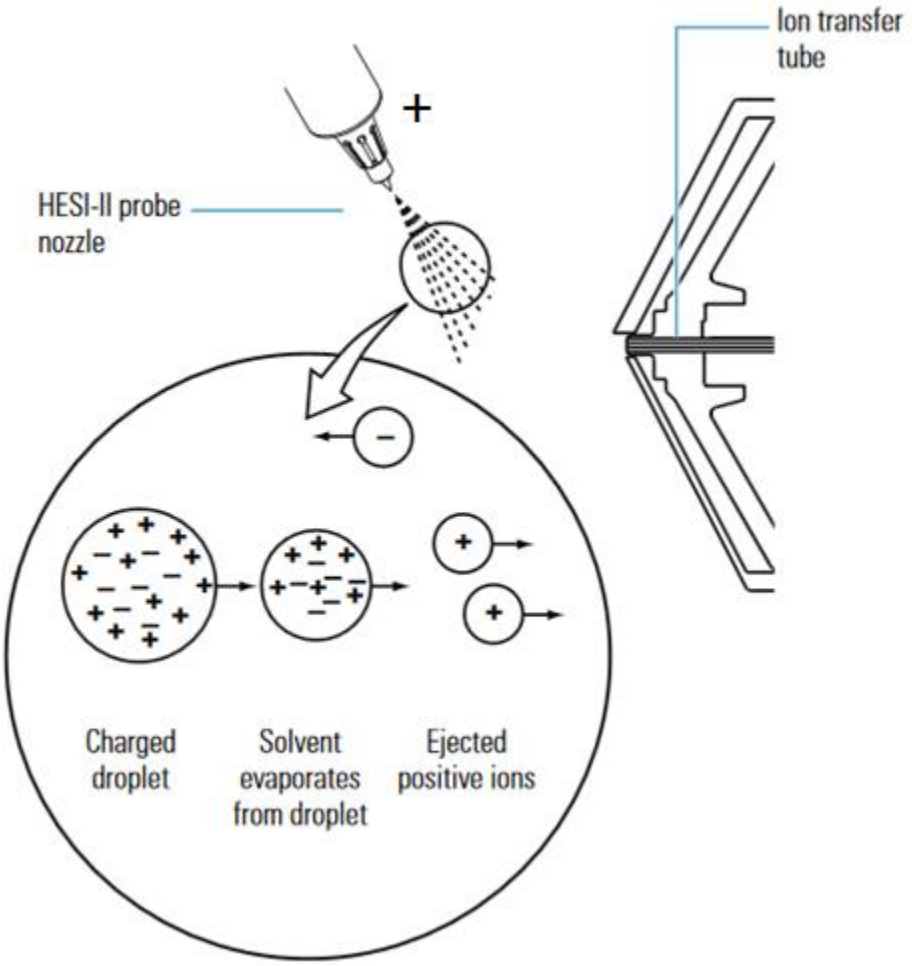

Figure 2.1 Process of ion formation from an ESI source. Figure adapted from HESI-II probe user guide.[71]

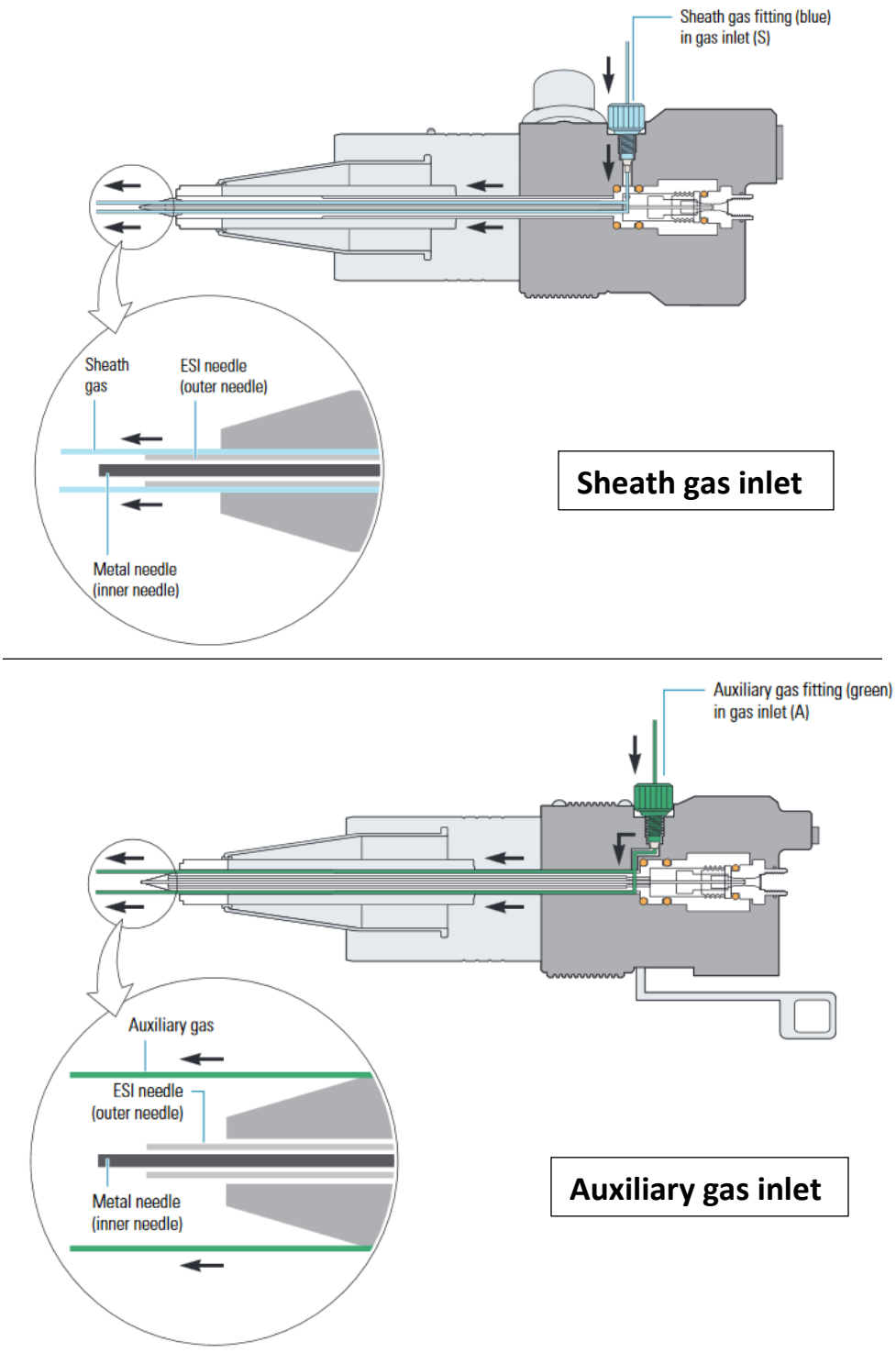

Figure 2.2 Introduction of sheath gas and auxiliary gas into H-ESI used on the Orbitrap. Figure adapted from HESI-II probe user guide.[71]

nozzle, the inner sample needle protrudes approximately 1.5 mm from the tip of an outer ESI needle (**Figure 2.2**). As the sample passes through the ESI nozzle, it receives an elevated voltage, which is typically set at 3.5 kV, and is sprayed into small droplets with the aid of a flow of nitrogen sheath gas from the outer ESI needle. There is an optional flow of nitrogen auxiliary gas (aux gas), which is also coaxial and is passed through a vaporizer on the outer ring of the ESI needle. The aux gas is heated in the vaporizer and is able to assist in solvent evaporation of the droplets. Throughout our study, the sheath gas was set at 3.5 psi and aux gas was turned off. The sample flow rate was 5 μL/min.

For study of the $[b_5 - H]^{\bullet +}$ radical cations from peptides that contain α-methyltryptophan or methionine, all experiments were conducted on a Sciex QTRAP 2000 prototype, with an ESI probe that consists of a simple capillary connected to an emitter tip. An ESI voltage of 3-4 kV is typically used and is applied near the tip of the emitter. Sample flow rate was at 3-5 μL/min.

2.2 Mass analyzers

2.2.1 Quadrupole mass filters and linear ion trap

Quadrupole mass analyzers are very common in modern commercial MS. A single quadrupole consists of four parallel electrodes. Each pair of opposite electrodes is separately applied with the DC voltage U and a radiofrequency (RF) voltage V with frequency ω (**Figure 2.3**).[26,72] When a positive ion enters the quadrupole in the z-direction, it will oscillate in both x-

and y- directions because of the alternating attraction and repulsion exerted by the electrodes with RF voltages. At a given U, V, and ω, only the ions with a specific mass to charge ratio (*m/z*) forms a stable trajectory within the quadrupole and pass through the exit lens to be detected. A quadrupole acts as a mass filter, which filters ions with one specific range of *m/z* value at a time. Keeping a specific U/V ratio and increasing the magnitude allows ions with increasing *m/z* value to pass through the quadrupole; while adjusting the U/V ratio will change the window size of the *m/z* range,

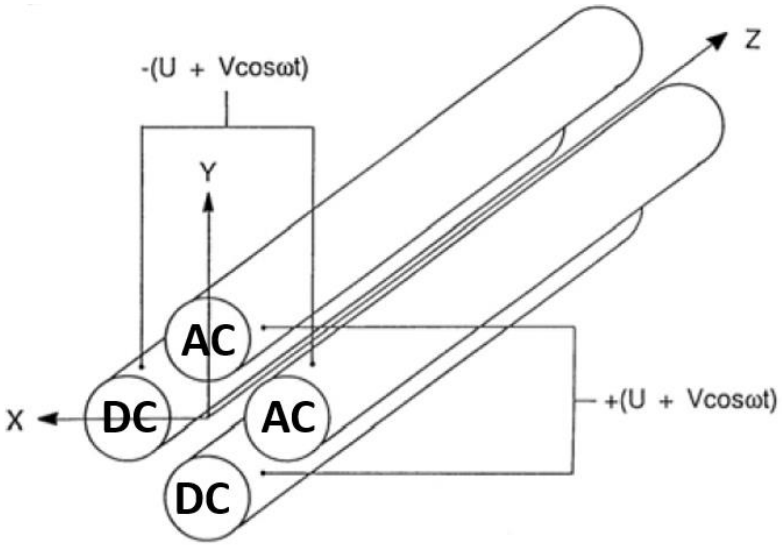

Figure 2.3 Schematic diagram of a quadrupole. Each pair of opposite electrodes consists of a DC voltage U and an alternating RF voltage V. Figure adapted from Gross.[26]

which changes the resolution and sensitivity in the mass spectrum. A final mass spectrum is produced by specifying an U/V ratio and detecting ions while increasing voltage magnitudes.

For applications of transmitting ions, applying only the RF voltage will create a wide band pass for essentially all ions.[26,73] Applying an opposite potential at both end of and RF-only quadrupole allows ion storage, which becomes a linear quadrupole ion trap. For the QTRAP 2000

(Sciex) used for all of the radical cation studies in this thesis, it consists of three main quadrupoles. The first quadrupole (Q1) selects the first precursor ion, which is always the $[Cu(II)+L+peptide]^{\bullet+}$ complex in all of the radical cation studies in this thesis. For this quadrupole, the resolution is set at a low resolution to allow bigger windows, in order to allow higher signals for later MS^n experiments. The complex selected in Q1 passes through the quadrupole and enters Q2 for CID. Q3 is a linear ion trap. Fragment ions from Q2 enter Q3, which initially traps the ion by first applying a DC voltage at the exit lens to prevent ions from exiting, then applies another DC voltage at the entrance lens after a specified fill time of 2 seconds. The second precursor is selected in Q3 by applying auxiliary RF for all other *m/z*, which gives other ions enough energies to overcome the exit potential and leave the quadrupole. Then, another auxiliary RF is applied in Q3 to activate the second precursor ion and perform CID within Q3. In addition, we modified the method table for Q3, to perform MS^n experiments by instructing the instrument to repeat the selection and activation stage before scanning.

2.2.2 Dual-pressure linear ion trap

Inside the Orbitrap Elite (Thermo Fisher Scientific) used for the closed-shell $[b_5]^+$ study is a dual-pressure linear ion trap system. It consists of two separate linear ion traps: the first trap is the high-pressure cell for CID, followed by a low-pressure cell for ion scanning (**Figure 2.4**).[40] Each of the linear ion trap consists of four hyperbolic rods, with each rod divided into three sections (**Figure 2.5**).[74] Each section of each trap has a separate DC trapping voltage during axial trapping. The high-pressure cell is supplied with helium gas for CID. Upon axial trapping of ions in the high-pressure cell, an ion isolation waveform voltage is applied to a pair of exit rods with a slot on

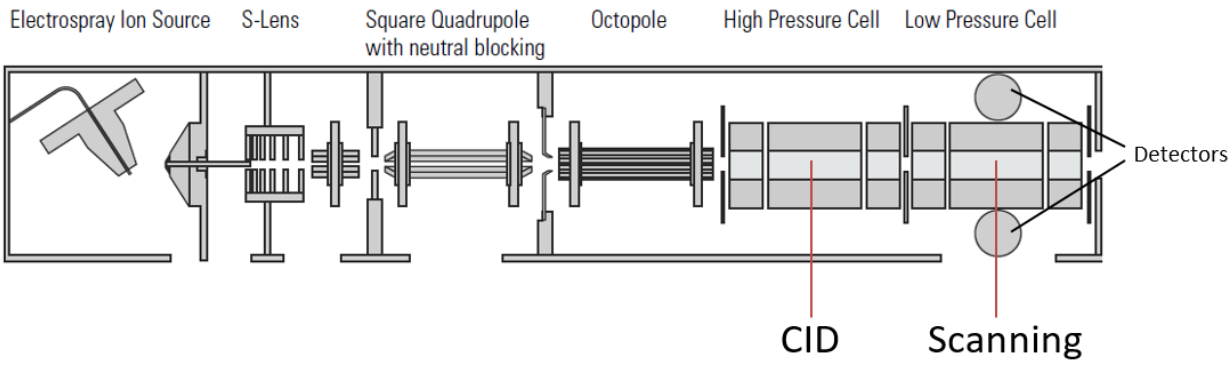

Figure 2.4 Schematic diagram of the Orbitrap Elite. Figure adapted from Orbitrap Elite hardware manual.[40]

each of them. This AC voltage works with the main RF voltage and eject all ions except the selected precursor ion. Next, a resonance excitation AC voltage is applied on the exit rods to resonate with the precursor ion. The precursor ions gain kinetic energy and collide with the helium gas molecules to cause fragmentations. After CID, all the fragment ions are transmitted to the low-pressure cell for scan-out. During scan-out, the main RF voltage ramps from low to high, and a resonance ejection AC voltage is applied on the exit rods simultaneously. This causes ions from low to high *m/z* ratio to become unstable and eject through the slots on the two exit rods (**Figure 2.6**). Outside of each of the two exit rods is an ion detector system, which consists of an electron multiplier and a conversion dynode.

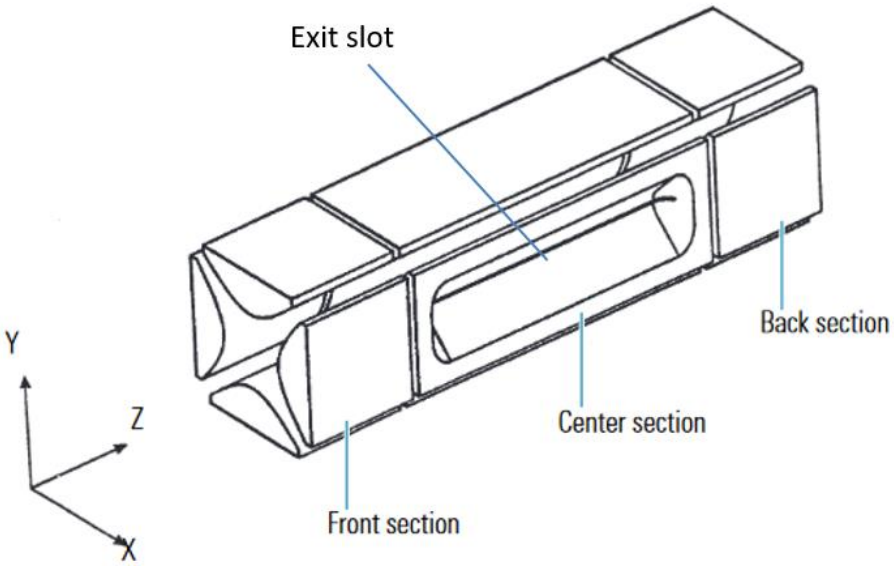

Figure 2.5 Components of a linear ion trap in the Velos Pro portion of the Orbitrap Elite. Figure adapted from LTQ series hardware manual.[74]

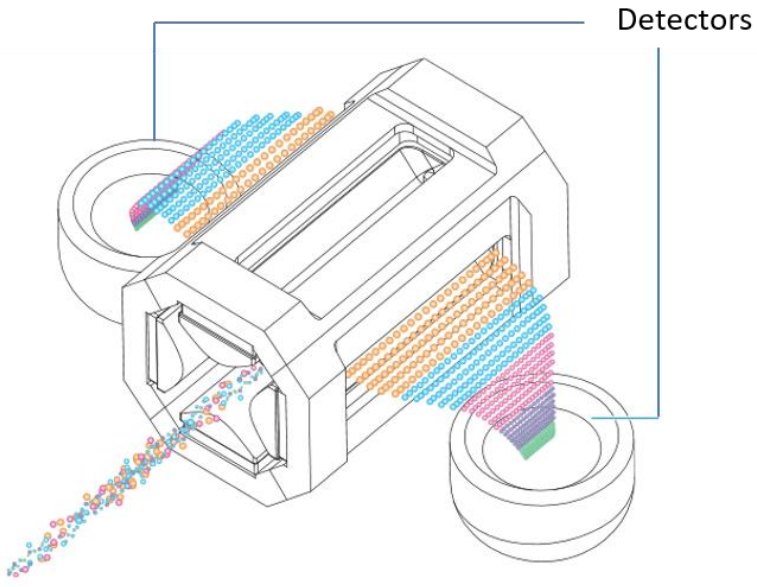

Figure 2.6 Diagram for the scan-out process in the low-pressure cell. Figure adapted from LTQ series hardware manual.[74]

2.3 Chemicals

2.3.1 Reagents

Fmoc-α-Me-Trp(boc)-OH was purchased from ChemPep (Wellington, FL). For labeled peptides, L-Ala-3,3,3-d_3-N-Fmoc and L-Ala-^{15}N-N-Fmoc were purchased from CDN Isotopes (Québec, QC). Other Fmoc-protected amino acids and synthesis reagents were purchased from Advance ChemTech (Louisville, KY).

2.3.2 ^{18}O-labeling of amino acids

In order to study the site specificity of fragments and losses that contain oxygen atoms, such as CO or CO_2, ^{18}O-labeled peptides were synthesized by exchanging the oxygen atom of the fmoc-protected amino acid with H_2O^{18} prior to solid-phase peptide synthesis (SPPS). This was achieved by acid-catalyzed ^{18}O-exchange according to the literature.[75] Detailed procedures were carried out as follows:

1. An oven-dried Schlenk flask was mounted and connected with a nitrogen gas supply on the side-arm. A magnetic stirrer was placed inside the flask.
2. The stopcock was opened and the flask was supplied with nitrogen gas. An inert gas flow was created from the side arm to the neck of the flask, to prevent air and moisture from entering.
3. Approximately 2 mL of anhydrous 1,4-dioxane was transfer using a needle syringe, from a septum-sealed bottle to the flask.

4. 1- 2 mmol of the fmoc-protected amino acid was added into the flask.
5. 1 mL of $H_2{}^{18}O$ (50 mmol) was transferred into the flask using a needle syringe.
6. 18 µL of acetylchloride (0.25 mmol) was transferred into the flask using a microsyringe.
7. The Schlenk flask was connected to a condenser, with a polytetrafluoroethylene (PTFE, or Teflon) sleeve for sealing the neck. The top of the condenser was connected to a nitrogen supply, which is also connected to an opened oil bubbler to release excess pressure. The stopcock and nitrogen gas supply on the side-arm of the Schlenk flask was then closed.
8. The round bottom of the Schlenk flask was immersed in an oil bath at 100 °C with magnetic stirring and the condenser on.
9. The exchange reaction was left to react overnight.
10. The oil bath was removed and the reaction mixture was allowed to cool to room temperature.
11. Open the stopcock and the nitrogen supply on the side-arm. Then, the condenser was removed from the Schlenk flask. The flask was then connected to a glass bridge, which is connected with a 50 mL round bottom flask. The stopcock and nitrogen supply on the side-arm were closed immediately.
12. The ^{18}O-exchanged fmoc-protected amino acid was freeze-dried. The reaction mixture in the Schlenk flask was froze by immersing in liquid nitrogen. Then, a vacuum line was connected to the side-arm of the Schlenk flask and created a low pressure system. The vacuum line was closed by the stopcock after around 1 minute.

13. Liquid nitrogen was then removed from the Schlenk flask and applied on the round bottom flask. As the frozen mixture evaporates in the Schlenk flask under reduced pressure, it traveled through the bridge and condensed in the round bottom flask.
14. The dried labeled fmoc-protected amino acid in the Schlenk flask was stored in -18 °C before use for SPPS.

2.3.3 Solid-phase peptide synthesis

Peptides used in all experiments in this thesis were synthesized by solid-phase peptide synthesis (SPPS) according to the commonly accepted procedures from the literature.[76] Detailed procedures for this technique are outlined as below:

1. Wang resin with a bound fmoc-protected amino acid was first soaked in dichloromethane (DCM) and bubbled with nitrogen gas inside a reaction vessel for around 15 minutes. This amino acid will be the C-terminal residue of the final peptide. Then the DCM was removed by filtering out the resin.
2. 20% (v/v) piperidine in dimethylformamide (DMF) was added into the reaction vessel, with about three bed volumes. The resin was left to react with the piperidine under nitrogen gas for 20 minutes. The fmoc protecting group at the N-terminus of the amino acid is now removed as illustrated in **Scheme 2.1**.

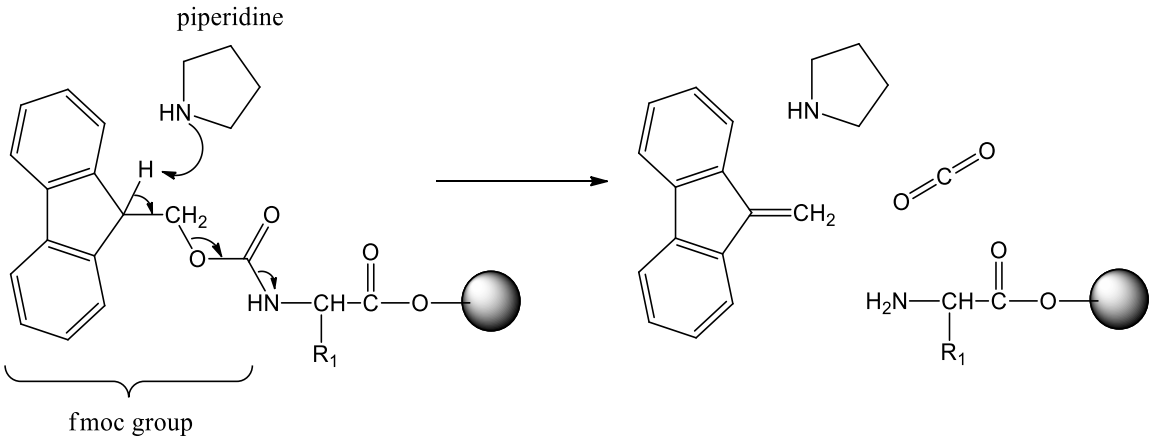

Scheme 2.1 Mechanism for cleavage of fmoc protecting group by piperidine during SPPS.

3. The resin was filtered and washed with DMF three times, and then washed with DCM three times.
4. The next fmoc-protected amino acid was added into the reaction vessel, with 3 mole-equivalence of the Wang resin added. For fmoc-α-methyltryptophan-OH, 1.5 mole-equivalence was added to save cost. 500 µL of diisopropylcarbodiimide (DIC) and 500 µL of 1-hydroxybenzotriazole (HOBt) was added to activate the carboxylic group of the added fmoc amino acid, by turning it into an activated ester which reacts readily with amines at room temperature (**Scheme 2.2**). Approximately three bed volumes of DMF was added to ensure an even mixture of the reagents. The mixture was left to react with the resin in the reaction vessel for 2 hours.

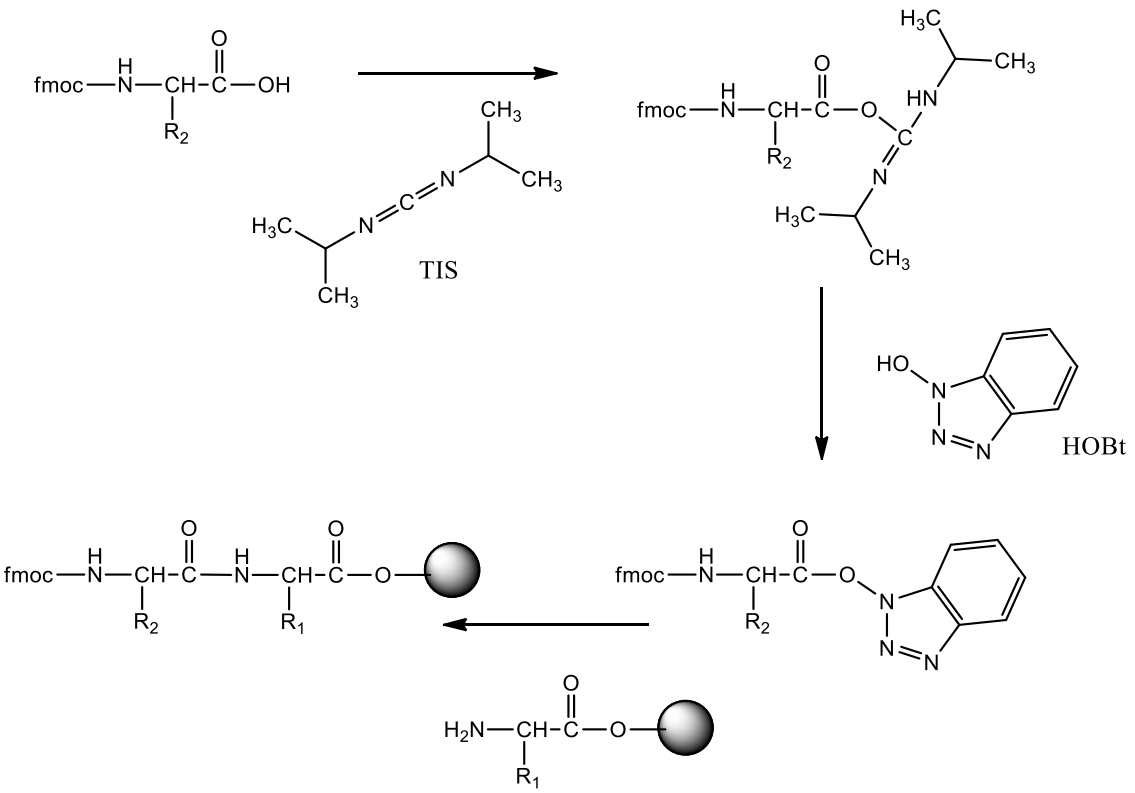

Scheme 2.2 Activation of carboxylic group into an active ester, and formation of the amide bond.

5. The resin was filtered and washed with DMF three times, then washed with DCM three times.
6. Step 2-5 was repeated multiple times to incorporate amino acid residues from the C-terminus to the N-terminus.
7. After the N-terminal residue of the desired peptide had been incorporated, repeat step 2 to remove the fmoc protecting group from the N-terminus.
8. A cleaving solution was prepared with trifluoroacetic acid (TFA), DCM, triisopropylsilane (TIS), and H_2O, in a ratio of 14:4:1:1 (v/v). Around two bed volumes of the cleaving

solution was added into the vessel for cleavage of the peptide from the Wang resin, as well as any protecting group for the side chain, such as the boc protecting group on the α-methyltryptophan side chain. The mixture was left to react for 2 hours under nitrogen.

9. The resin was filtered and the filtrate was collected. The resin was washed 3-4 times with small volumes of DCM, and the filtrates were pooled together in a 50 mL round bottom flask.
10. The pooled solution containing the synthesized peptide was left to evaporate under reduced pressure and resulted into a small volume of oil or solid. Approximately 10 mL of cold anhydrous diethyl ether was added into the flask. The flask was sonicated briefly and the solution became cloudy.
11. The solution was left in a freezer (-16 ^{o}C) for 15 minutes for the white solids to precipitate. The solution was carefully removed from the precipitate. The white precipitate, which is the synthesized peptide in solid form, was left to dry and then stored in the freezer (-16 ^{o}C) until needed for experiments.

2.3.4 Sample preparation

After the peptides were synthesized and dried into solid form, they were stored at -18 °C without further purifications. Prior to experiment, the synthesized peptides were taken out from the freezer and dissolved in 50/50 water/methanol, followed by proper dilution.

CHAPTER 3: Fragmentation of α-methyltryptophan-containing Hexapeptides and Their $[b_5]^+$ Ions

3.1 Results and discussions

3.1.1 Fragmentation of the protonated hexapeptides

CID spectra of the protonated peptides $[M + H]^+$ of α-methyltryptophan-containing hexapeptides are summarized and compared with those of their native tryptophan-containing analogs (**Figure 3.1**). In all spectra, the $[b_5]^+$ ion is the most dominant product ion, regardless of whether or not there is a methyl group at the α-carbon of the tryptophan, and is independent of where the tryptophan or α-methyltryptophan residue is located in the sequence. Other fragmentations include (i) a further loss of CO from the $[b_5]^+$ ion to produce the $[a_5]^+$ ion and (ii) loss of a dipeptide from the C-terminus giving the $[b_4]^+$ ion, the second most abundant ion in all the spectra (with the exception of $[AAAAW_{\alpha\text{-Me}}G + H]^+$, where there is essentially only one product, the $[b_5]^+$ ion). There are some small simplifications in the spectra that appear to be a function of replacing the α-hydrogen of tryptophan by a methyl group. Loss of water is a minor

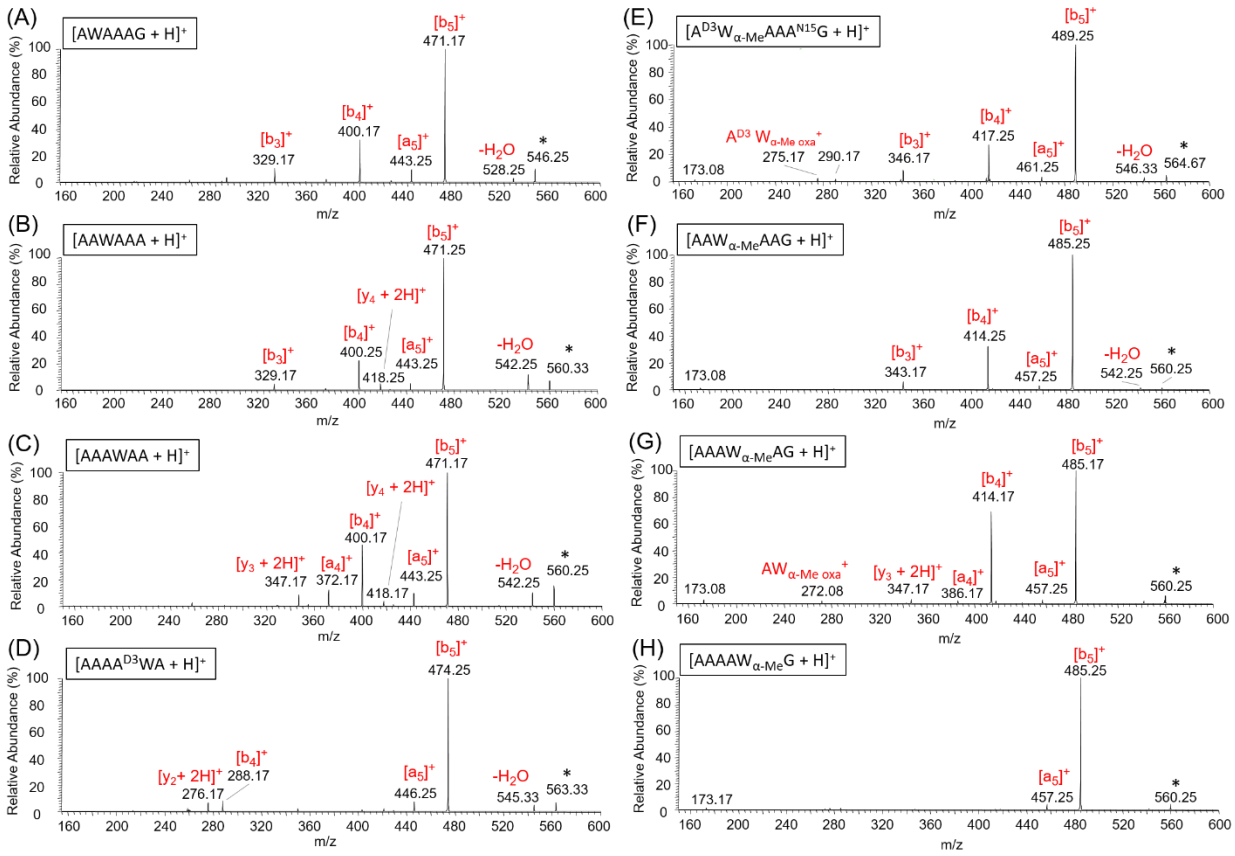

Figure 3.1 CID spectra of the protonated hexapeptides, with the hetero-residue at different positions. **(A)** – **(D)**: CID of tryptophan-containing hexapeptides. **(E)** – **(F)**: CID spectra of α-methyltryptophan-containing hexapeptides.

channel that is less prevalent for peptides containing α-methyltryptophan. Also $[y_n + 2H]^+$ ions in which the tryptophan residue is at the N-terminus are observed for the tryptophan-containing ions; these are the products of cleaving the amide bond at the N-terminal of the tryptophan residue. In summary, having a methyl group at the α-carbon of the tryptophan residue results in only small changes in the dissociation pathways of these protonated peptides.

3.1.2 Fragmentation of the $[b_5]^+$ ions

The $[b_5]^+$ ions observed in the CID spectra of the protonated hexapeptides were isolated and subjected to further fragmentations (**Figure 3.2**). The dissociations of $[b_5]^+$ ions which are derived from α-methyltryptophan-containing hexapeptides can produce two different $[b_n]^+$ ions (n = 2-4), one containing the α-methyltryptophan residue which we will denote as $[b_n]^+$, and the other, without this residue, is labeled as $[b_n']^+$. As observed for the $[b_5]^+$ ions from peptides derived from tryptophan-containing hexapeptides (**Figure 3.3**),[59] the $[b_5]^+$ ions in **Figure 3.2** also showed very similar spectra, regardless of the original sequence. This indicates that the α-methyltryptophan-containing ions also cyclize to form a common intermediate prior to fragmentation.

In order to differentiate between the alanine residues, we label their positions relative to the α-methyltryptophan residue. As there is a greater loss of the α-methyltryptophan residue (*m/z* 285) than the alanine residue (*m/z* 414) from $[b_5]^+$ and, assuming that this occurs from an oxazolone ring at the C-terminus, then the structure $[AAAAW_{\alpha\text{-Me oxa}} + H]^+$ appears to be a dominant one in the fragmentation process and we have used this sequence as the basis for labeling. The following reference to each alanine residue relative to the hetero-residue will be used throughout this thesis.

$$\begin{array}{l} A^{i}\ A^{ii}\ A^{iii}A^{iv} \\ \downarrow\ \downarrow\ \downarrow\ \downarrow \\ [A\ A\ A\ A\ W_{\alpha\text{-Me oxa}} + H]^+ \end{array}$$

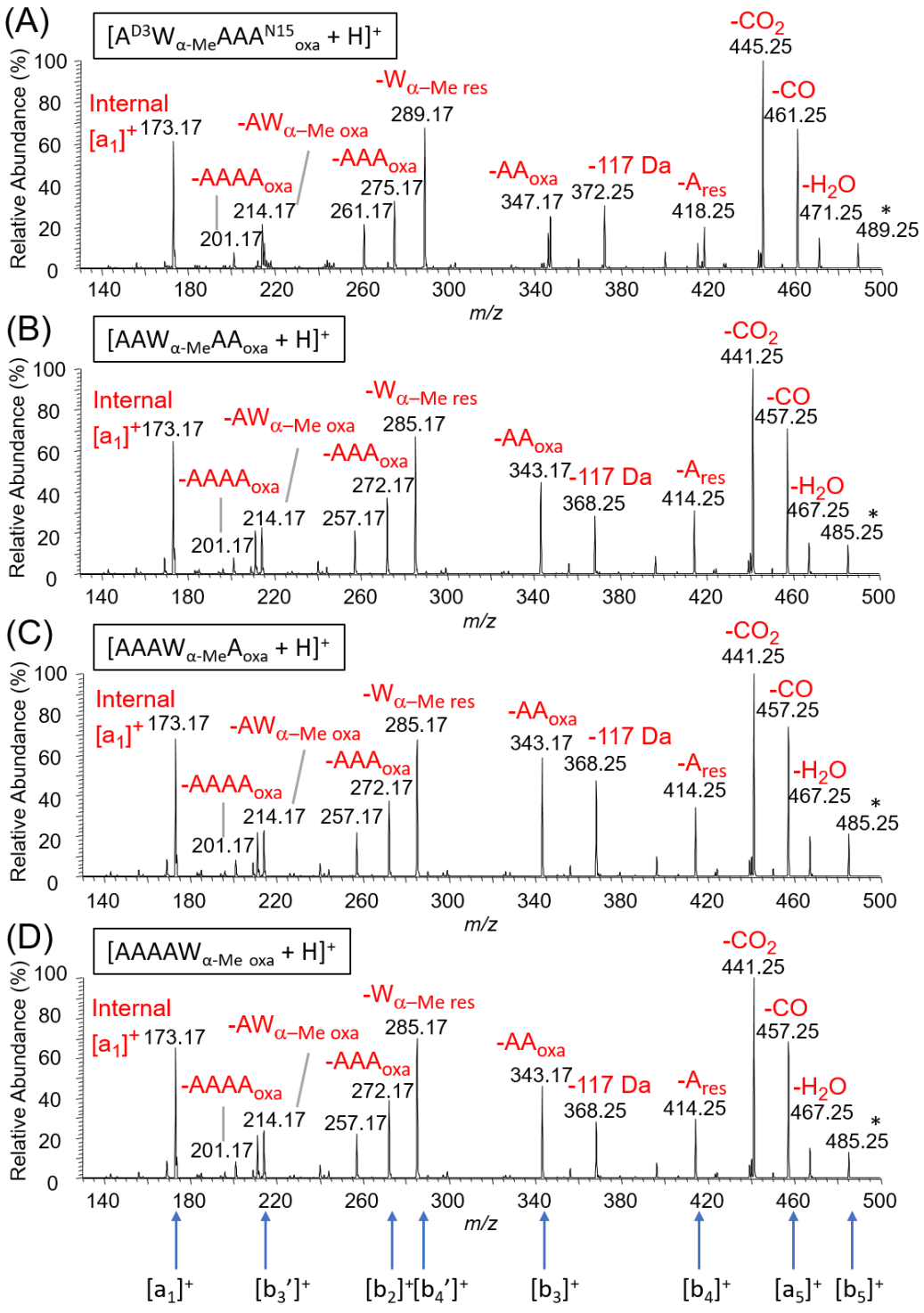

Figure 3.2 CID spectra of $[b_5]^+$ ions derived from α-methyltryptophan-containing hexapeptides, with the α-methyltryptophan residue at different positions.

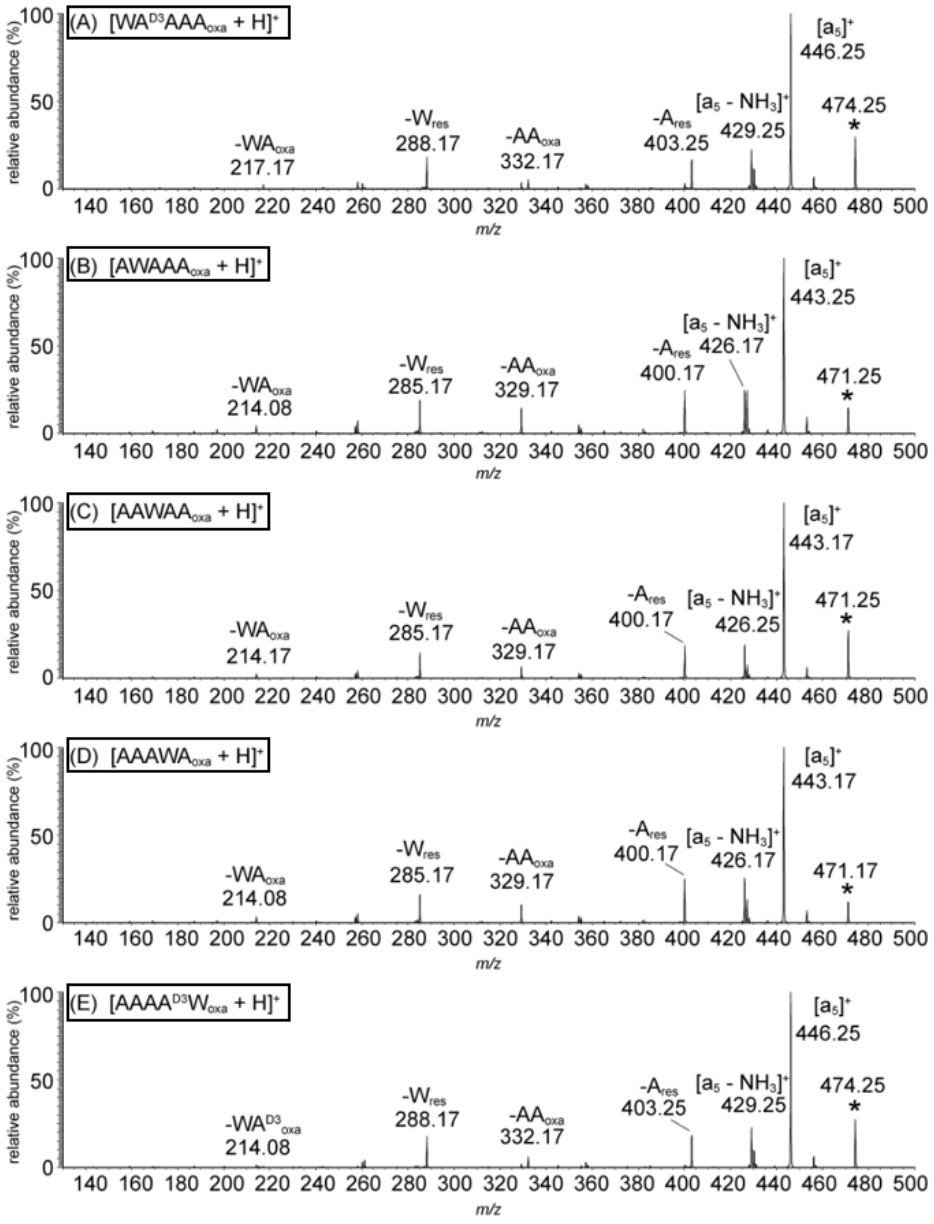

Figure 3.3 CID spectra of the $[b_5]^+$ ions derived from tryptophan-containing hexapeptides.[59]

The $[b_5]^+$ ions derived from both classes of protonated hexapeptides show the same progression of $[b_4]^+$, $[b_4']^+$, $[b_3]^+$and $[b_3']^+$ ions, but the relative abundances are quite different in the two series. Also, there are additional product ions in the CID spectra of the α-

methyltryptophan-containing ions. The differences and some of the unusual features observed for the α-methyltryptophan-containing $[b_5]^+$ are summarized below:

i) loss of CO_2 is observed and is the most abundant peak in all the spectra collected although it is not the lowest-energy fragmentation channel (*vide infra*). Such a loss is frequently observed in the CID spectra of open-shell radical cations,[60,52] but is unusual in the spectra of closed-shell $[b_5]^+$ ions derived from protonated peptides.

ii) a loss of 117 Da is observed. The high-resolution CID spectrum suggests that this loss does not correspond to the indole ring from the α-methyltryptophan side chain (C_8H_7N). Instead, the neutral being lost corresponds to ($C_4H_7NO_3$, **Figure 3.4**).

iii) the abundance of $[b_4']^+$ (*m/z* 285) is large and approximately twice that of the $[b_4]^+$ ion (*m/z* 414). This suggests that after macrocyclization and reopening, the $[b_5]^+$ ion with the α-methyltryptophan residue at the C-terminus is the most fragile and is the key intermediate leading to most of the fragmentations. By comparison, in the fragmentations of $[b_5]^+$ ions derived from $[AAAAW_{oxa}]^+$ (**Figure 3.3**), the abundances of $[b_4']^+$ and $[b_4]^+$ ions are approximately the same.

iv) the $[b_3]^+$ ion (*m/z* 343) resulting from the loss of two alanine residues (142 Da) is more abundant than the $[b_4]^+$ ion, the product of the loss of one alanine residue (71 Da). Also, the abundance of the $[b_2]^+$ (*m/z* 272) is comparable to that of the $[b_4]^+$ ion. By comparison in the dissociation of the $[b_5]^+$ ions with four alanine and one tryptophan residue, loss of one alanine residue is more abundant than the loss of two, and there is essentially no loss of additional alanine residues.

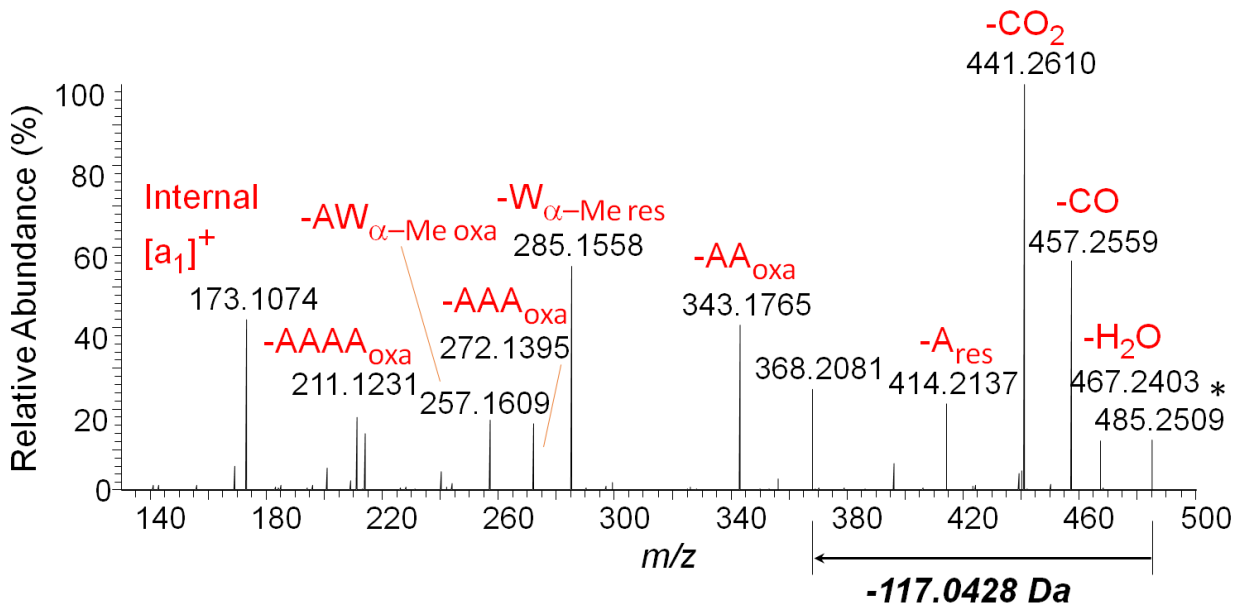

Chemical Formula: $C_4H_7NO_3$
Exact Mass: 117.04259

Chemical Formula: C_8H_7N
Exact Mass: 117.05785

Figure 3.4 CID spectrum of $[AAW_{\alpha\text{-}Me}AA_{oxa} + H]^+$ in high-resolution FTMS (240,000 FWHM). All observed mass values are within 1 ppm error from the theoretical mass values of the predicted structures. The observed mass of 368.2081 Da represents the ion $C_{20}H_{26}O_2N_5$ (0.27 ppm), a loss of $C_4H_7NO_3$; instead of the structure $C_{16}H_{26}O_5N_5$ (41.3 ppm), a loss of C_8H_7N (indole).

v) There is a high abundance of the 'internal' $[a_1]^+$ (*m/z* 173), the imine derived from α-methyltryptophan.

3.1.3 Structural information provided by isotopic labeling

The CID spectra of the $[b_5]^+$ ions of $[AAAW_{\alpha\text{-}Me}A_{oxa} + H]^+$ where one of the Ala residues has a CD_3 side chain (A^{D3}) (**Figure 3.5**) and an ^{18}O-labeled amide oxygen (A^{18O}) (**Figure 3.6**) are summarized, While **Figure 3.7** shows a different isomer $[AW_{\alpha\text{-}Me}AAA_{oxa} + H]^+$, with one Ala residue containing CD_3 and in another one having ^{15}N-labeled amide nitrogen (A^{15N}). These strategically located substitutions have enabled us to make conclusions about the structures of the ions undergoing cleavage.

Ion at m/z 414, loss of an alanine residue (71 Da).

Figure 3.5 and **Figure 3.6** show that in the loss of a single alanine residue from the $[b_5]^+$ ion, A^i is lost more easily than A^{ii} and that A^{iii} is not lost (**Figure 3.5 C**). Loss of residue A^{iv} is also possible, as exhibited by **Figures 3.6 C** and **Figure 3.7 B**. From these data we estimate that approximately 40% of the alanine loss comes from each of positions A^i and A^{iv} with the remaining 20% from position A^{ii}.

Ion at m/z 343, loss of two alanine residues (142 Da).

As noted earlier, the product of the loss of two alanine residues is more abundant than the loss of only one alanine. The spectra in **Figure 3.5 B** show that when the CD_3 is at position A^{ii} *only* labeled $A^{D3}A_{oxa}$ is lost; furthermore, when the CD_3 is at each of the adjacent positions (A^i and

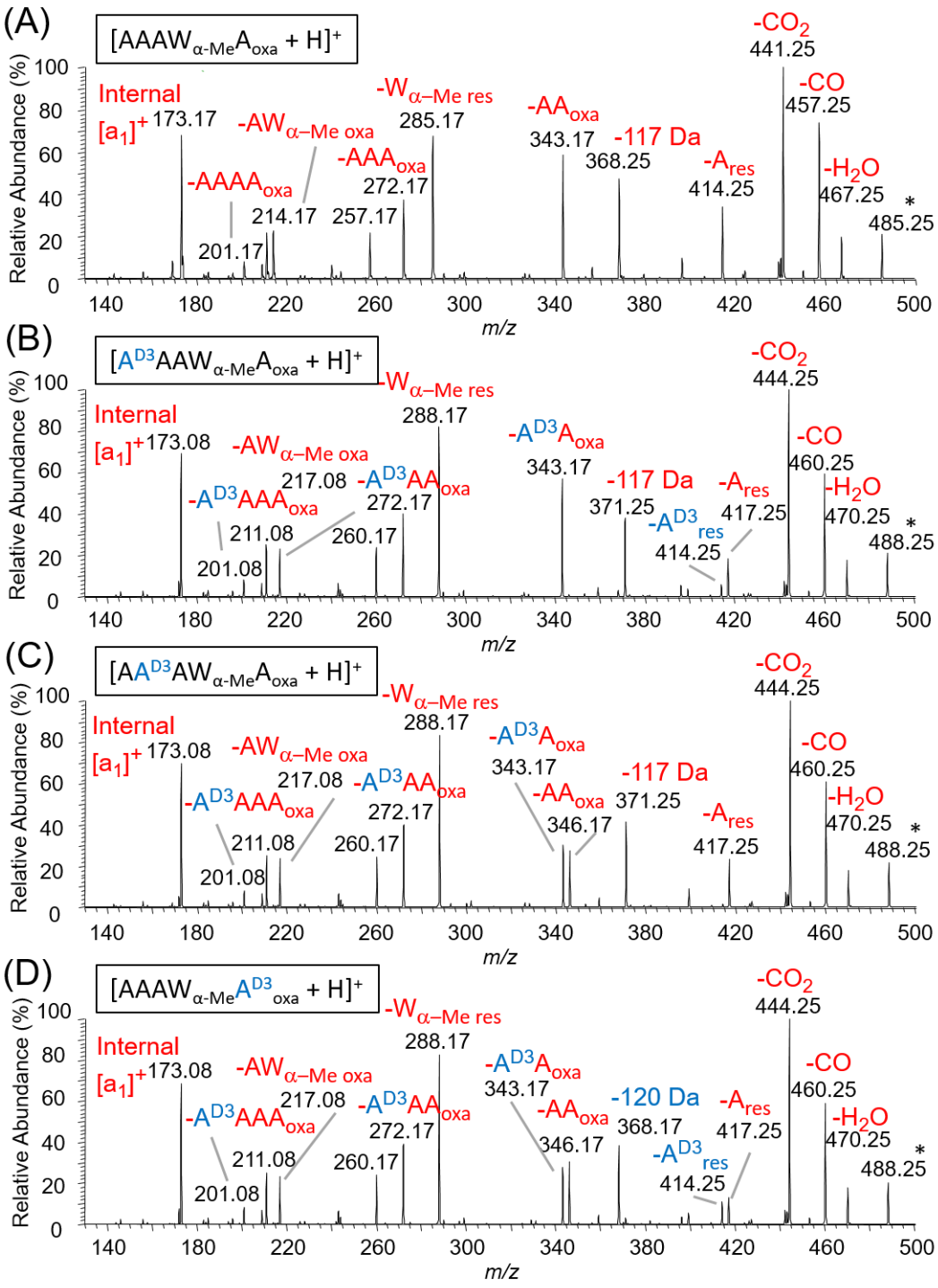

Figure 3.5 CID spectra of isotopomers of ion [AAAW$_{\alpha\text{-Me}}$A$_{oxa}$ + H]$^+$ **(A)**, with **(B) – (D)** having a CD_3 label at the first, second, or fifth residue respectively.

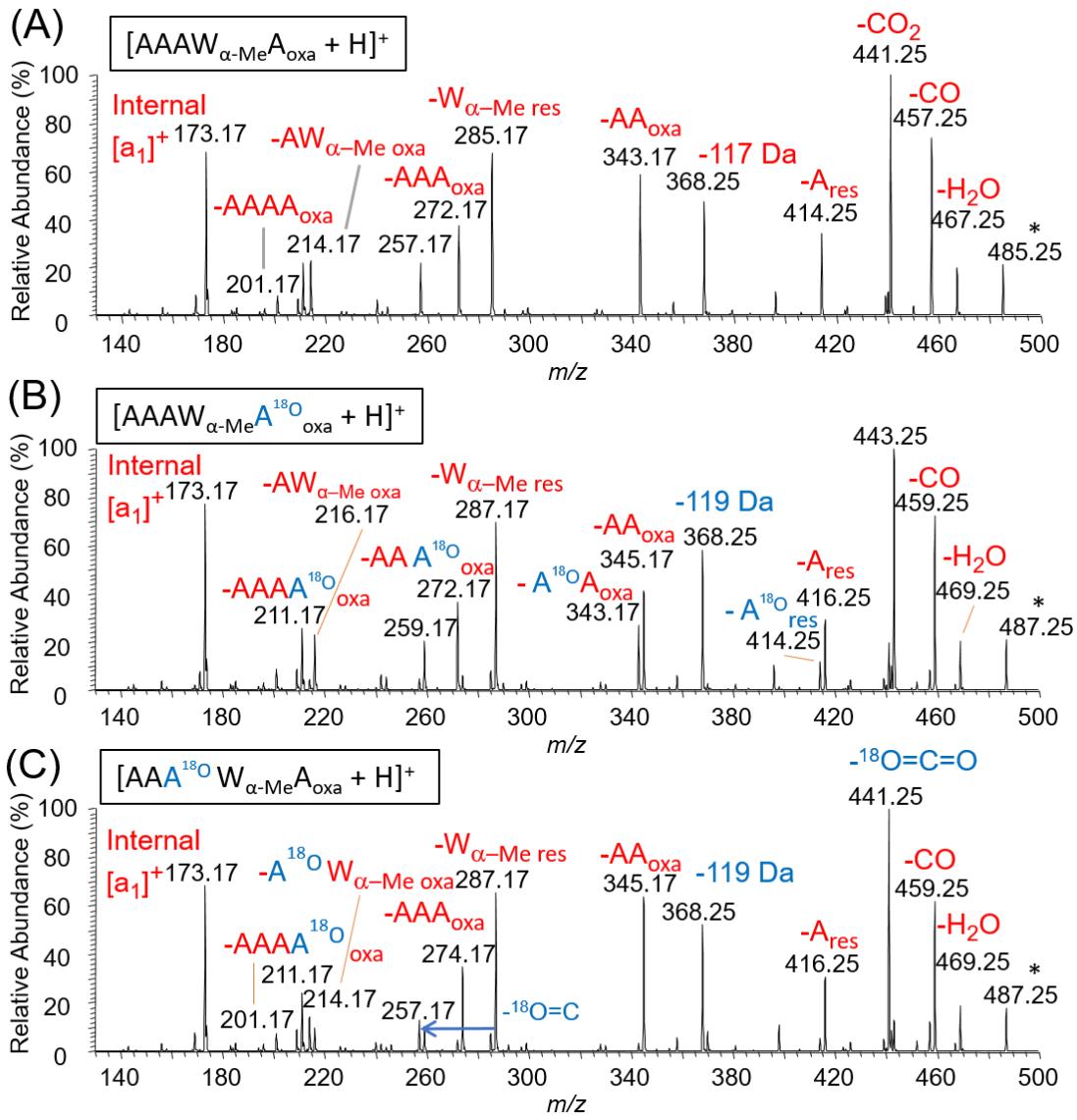

Figure 3.6 CID spectra of isotopomers of ion [AAAW$_{\alpha\text{-Me}}$A$_{oxa}$ + H]$^+$ **(A)**, with **(B)** and **(C)** having an ^{18}O label at the fifth and third residue respectively.

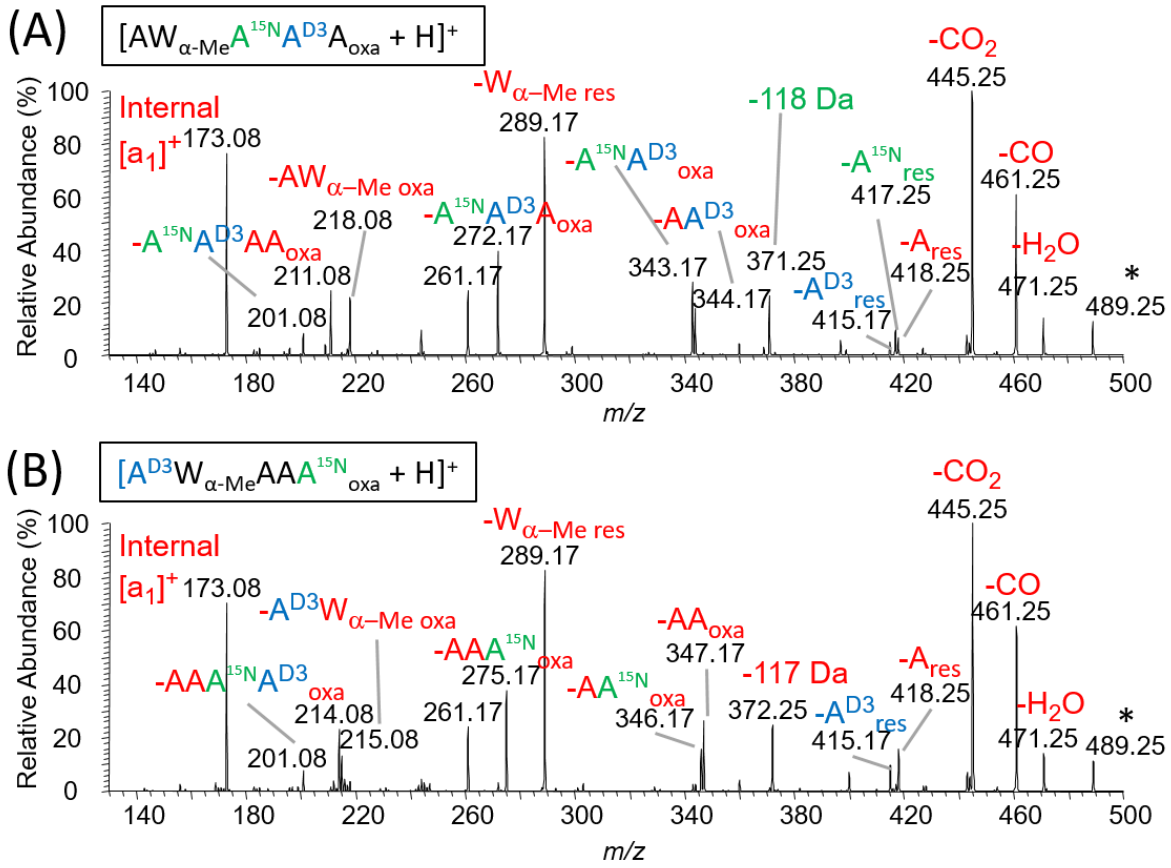

Figure 3.7 CID spectra of the ion $[AW_{\alpha\text{-Me}}AAA_{oxa} + H]^+$ with both ^{15}N label and CD_3 labels at different residues.

A^{iii}), approximately half the label is lost. Clearly, the loss of two alanine residues is either from residues A^{i} and A^{ii} or residues A^{ii} and A^{iii}. The spectra in **Figure 3.7** supports this analysis and suggests that there is slightly more loss of residue A^{i} than A^{iii}.

Ion at m/z 272, loss of three alanine residues (213 Da).

From **Figure 3.5 B, C** and **D**, there is no product ion at *m/z* 275, indicating that the CD_3-labeled alanine is always lost. This means that the product is the $[b_2]^+$ ion consisting of residue A^{iv} and the α-methyltryptophan residue, presumably $[AW_{\alpha\text{-Me oxa}} + H]^+$. This is consistent with the result of ^{15}N and CD_3 labeled peptide in **Figure 3.7** that the ions at *m/z* 272 and 275 correspond to the loss of three alanine residues at positions A^i, A^{ii}, and A^{iii} from the $[AWAAA_{oxa} + H]^+$ ion. Again, product ions at *m/z* 272 and 274 from the ^{18}O labeled $[b_5]^+$ ions of $[AAAW_{\alpha\text{-Me}}A^{18O} + H]_{oxa}^+$ and $[AAA^{18O}W_{\alpha\text{-Me}}A_{oxa} + H]^+$, respectively support this analysis. Note that in the losses of both two and three alanine residues, the amide bond between $A{-}W_{\alpha\text{-Me}}$ is never broken.

Ion at m/z 368, loss of ($C_4H_5NO_2 + H_2O$).

The accurate mass measurements showed that the loss of 117 Da corresponds to $C_4H_7NO_3$ (**Figure 3.4**). Further analysis suggests that the neutral loss consists of an oxazolone ring and a water molecule ($C_4H_5NO_2 + H_2O$). From **Figure 3.5 D**, the loss becomes 120 Da; here residue A^i contains the CD_3 side chain, thereby establishing that the oxazolone ring containig A^i is lost. This suggests that it is structure $[AAAW_{\alpha\text{-Me}}A_{oxa} + H]^+$ that dissociates. The corresponding loss from $[AW_{\alpha\text{-Me}}A^{15N}A^{CD3}A_{oxa} + H]^+$ is 118 Da (**Figure 3.7 A**) and this is consistent with losing the ^{15}N-alanine residue in position A^i; when residues A^{iii} and A^{iv} contain the heavy isotopes (**Figure 3.7 B**), then the loss is only 117 Da, again consistent with the A^i residue being lost.

The spectra for the ^{18}O-labeled structures in **Figure 3.6** provide the most definitive evidence for the structure of the ion that dissociates to give the *m/z* 368 ion. Substitution of the

oxygen atoms in either residue A^{i} or A^{iv} results in losses of 119 Da, implicating involvement of both residues. The removal of the oxazolone ring from the C-terminus of structure $[AAAW_{\alpha\text{-Me}}A_{oxa} + H]^+$ (formally creating an $[a_4]^+$ ion, product not observed) via the cleavage of C_α–C bond is assisted by the steric crowding at the α-carbon of the α-methyltryptophan residue. This is immediately followed by the loss of water from residue A^{iv}. A similar mechanism in which the C_α–C bond exocyclic to an oxazolone ring is cleaved has recently been proposed by Bythell and Harrison to explain the formation of $[a_1]^+$ ions *directly* from $[b_2]^+$ ions.[77]

Ion at m/z 441, the loss of CO_2.

The loss of CO_2 is one of the more interesting features of the $[b_5]^+$ ion in this study. To determine the mechanism for such a dissociation, residues A^{i} and A^{iv} were labeled separately with ^{18}O in the sequence $[AAAW_{\alpha\text{-Me}}A_{oxa} + H]^+$ (**Figures 3.6**). When residue A^{i} was labeled with ^{18}O, the product ion after the loss of CO_2 retained the label (*m/z* 443), indicating that residue A^{i} is not involved. Since the loss of CO_2 is mostly likely from the oxazolone ring, where there are two oxygen atoms bonded to a carbon, the loss of CO_2 in this system cannot come from ion $[AAAW_{\alpha\text{-Me}}A_{oxa} + H]^+$, where residue A^{i} is part of the oxazolone ring. Conversely, when the ^{18}O label was on residue A^{iv}, the label was lost in the CO_2 (*m/z* 441), indicating that *one of the oxygen atoms in the CO_2 comes from the amide oxygen of residue A^{iv}* This implies that the $[b_5]^+$ ion macrocyclizes and re-opens into either sequence $[AAAAW_{\alpha\text{-Me oxa}} + H]^+$ or $[W_{\alpha\text{-Me}}AAAA_{oxa} + H]^+$. As $[AAAAA_{oxa} + H]^+$ does not dissociate by loss of CO_2, it seems probable that it is the $[AAAAW_{\alpha\text{-Me oxa}} + H]^+$ structure that undergoes this loss.

3.1.4 Energy-resolved plot for dissociation of $[b_5]^+$ ion $[AAAAW_{\alpha\text{-Me oxa}} + H]^+$

The energy-resolved curves in **Figure 3.8** establish that the lowest energy dissociation pathway for $[AAAAW_{\alpha\text{-Me oxa}} + H]^+$ is loss of CO to form the $[a_5]^+$ ion. At a slightly higher collision energy the combination of the $[a_1]^+$ ion (*m/z* 173) and the $[b_4']^+$ ion (*m/z* 285) is generated;

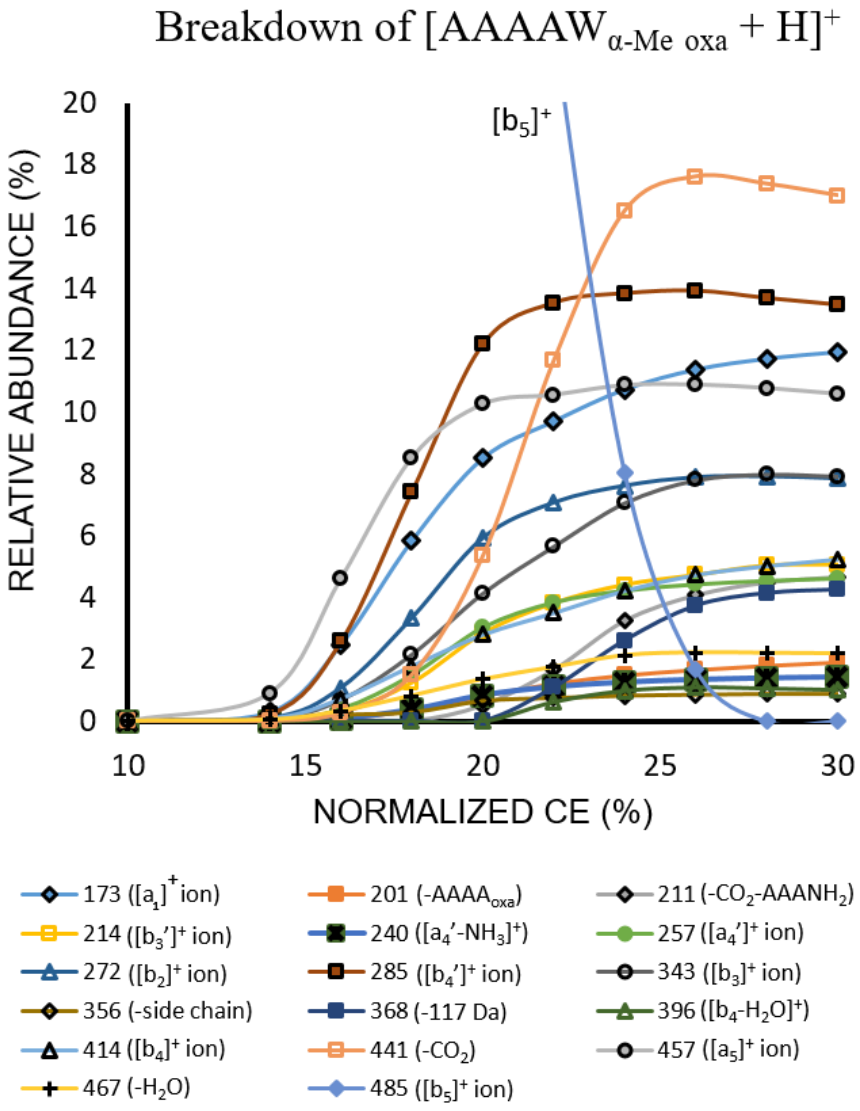

Figure 3.8 Energy-resolved breakdown diagram for $[AAAAW_{\alpha\text{-Me oxa}} + H]^+$ ion.

these are the complementary products of cleaving the amide bond of A−$W_{\alpha\text{-Me}}$ of an $[a_5]^+$ ion in which the α-methyltryptophan residue is at the C-terminus. The abundance of the $[a_1]^+$ ion continues to increase at higher collision energies, indicating that this ion has a very stable structure. In contrast, the abundance of the $[b_4']^+$ ion plateaus at intermediate collision energies showing it to be slightly less robust. At higher collision energies, where there are many products, the sum of the abundances of $[a_1]^+$ and $[b_4']^+$ ions is substantially higher than those of all other ions, with the exception of the *m/z* 441 ion which, on the basis of ^{18}O-labeling, we have deduced is also probably produced from isomer $[AAAAW_{\alpha\text{-Me oxa}} + H]^+$. Increasing the collision energy a little more results in formation of the complementary $[b_2]^+$ and $[b_3']^+$ ions (*m/z* 272 and 214 respectively), essentially at the same onset. As labeling established that the $[b_3']^+$ ion always contains residues A^i, A^{ii}, and, A^{iii}, this complementary pair are the products of cleaving a peptide bond in either $[AAAAW_{\alpha\text{-Me oxa}} + H]^+$ or $[AW_{\alpha\text{-Me}}AAA_{oxa} + H]^+$. The $[b_4]^+$ ion is another potential source of the $[b_3']^+$ ion. However, the abundance of the $[b_2]^+$ ion, the fragment that carries the α-methyltryptophan residue, is always approximately double that of the $[b_3']^+$ ion, suggesting that the $[b_2]^+$ and $[b_3']^+$ ions are formed in the same dissociation process.

Loss of only one alanine residue to create the $[b_4]^+$ ion at *m/z* 414 has a similar onset to formation of the $[b_2]^+/[b_3']^+$ combination. The labeling experiments showed that residues A^i and A^{iv} are each lost about 40% of the times, A^{ii} is lost 20% and A^{iii} is never lost. *Assuming* that these residues are lost from an oxazolone ring via a $[a_5]^+$ ion, then this indicates the participation of three different isomers and that there has been some sequence scrambling of the initial $[b_5]^+$ ion. Only the sequence $[AW_{\alpha\text{-Me}}AAA_{oxa} + H]^+$, where residue A^{iii} is at the C-terminus, is not implicated.

The channel for loss of water creating a $[b_5 - H_2O]^+$ ion at *m/z* 467 has a similar onset to those for formations of $[b_4]^+$, $[b_2]^+$ and $[b_3']^+$ ions. From the labeling experiments (**Figure 3.6**), this water is not lost from residues A^i and A^{iv}.

Dissociation to $[b_3]^+$ (*m/z* 343), involving loss of two alanine residues, has a slightly higher energy threshold than for losses of only one alanine or of three alanine residues. Labeling established that residue A^{ii} is always lost and that A^i and A^{iii} are lost in approximately the same amounts. This implies that more than one isomer of $[b_5]^+$ undergoes cleavage of a peptide bond. Only the isomer in which residue A^{ii} is in the central location, $[W_{\alpha\text{-Me}}AAAA_{oxa} + H]^+$, can be ruled out as a potential precursor .

As the $[b_4']^+$ curve flattens out at higher collision energies the $[a_4']^+$ (*m/z* 257) appears and almost simultaneously the $[b_3']^+$ (*m/z* 214) starts to grow. Loss of CO_2 (generating the ion at *m/z* 441), the channel that is dominant at the highest collision energies, has a higher onset energy than all the preceding channels. This ion subsequently loses trialanine amide, $AAANH_2$, to form an ion at *m/z* 211 that is very heavily stabilized by spreading the charge onto the indole ring (**Figure 3.9**).

The ions with the highest initial energy onsets are products at *m/z* 396 and 368. The former is very minor and is the $[b_4 - H_2O]^+$. The latter is the result of losses of the oxazolone ring and water and is most easily explained as originating from the rearranged structure, $[AAAW_{\alpha\text{-Me}}A_{oxa} + H]^+$. The energy-resolved curves for $[AAAW_{\alpha\text{-Me}}A_{oxa} + H]^+$, given in **Figure 3.10**, show some differences from those in **Figure 3.8**; this appears to be the result of incomplete scrambling. The product ions in both sets of curves and the onsets are the same but the abundances differ. Most notably, the *m/z* 368 ion is more abundant in **Figure 3.10** and, as isotopic substitution led us to

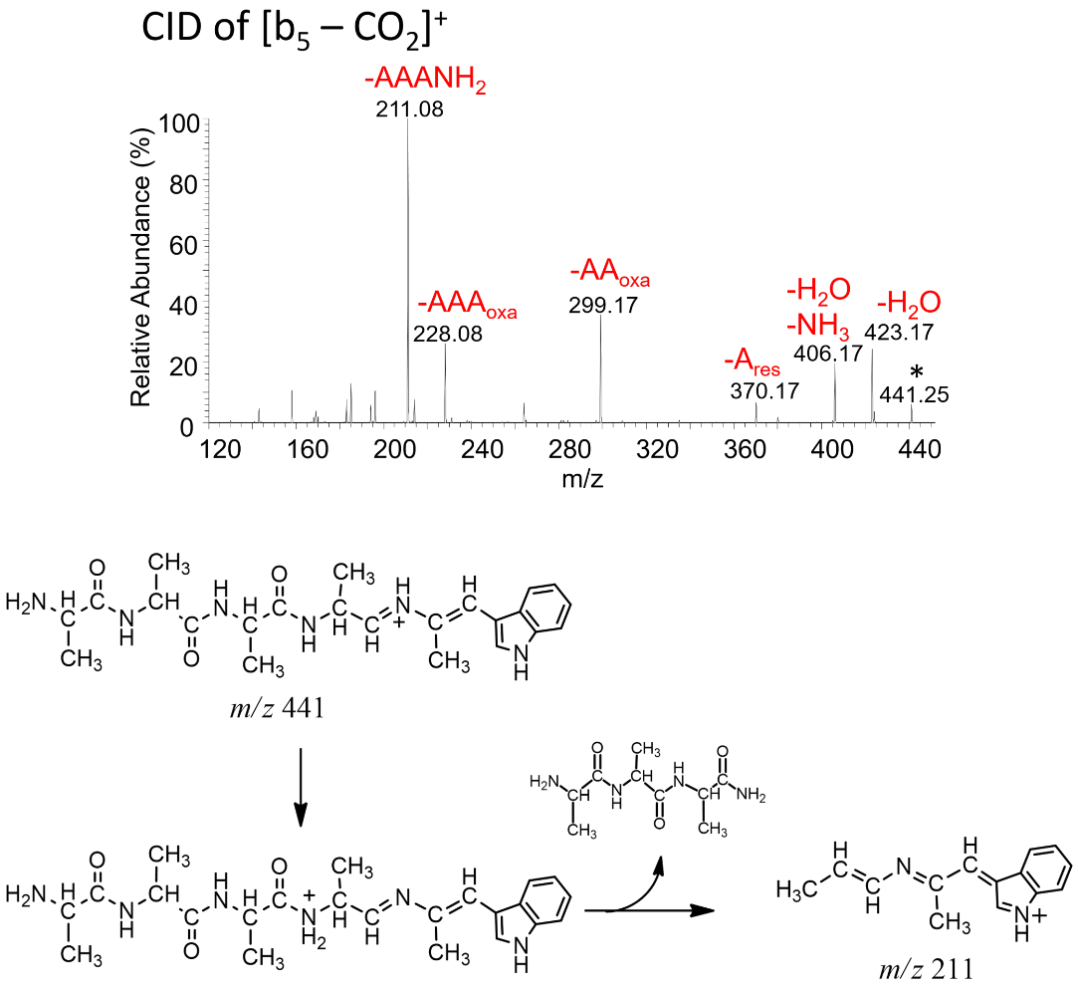

Figure 3.9 CID spectrum of ion at *m/z* 441, after loss of CO_2 from the $[b_5]^+$ ion.

conclude that this product comes from the $[AAAW_{\alpha\text{-}Me}A_{oxa} + H]^+$ ion, it appears that there is incomplete scrambling prior to dissociation. Here, we note that our theoretical studies give the barrier to formation of the macrocyclic ion, the proposed intermediate in the isomerization, is the largest for isomer $[AAAW_{\alpha\text{-}Me}A_{oxa} + H]^+$ (**Scheme 3.1**).

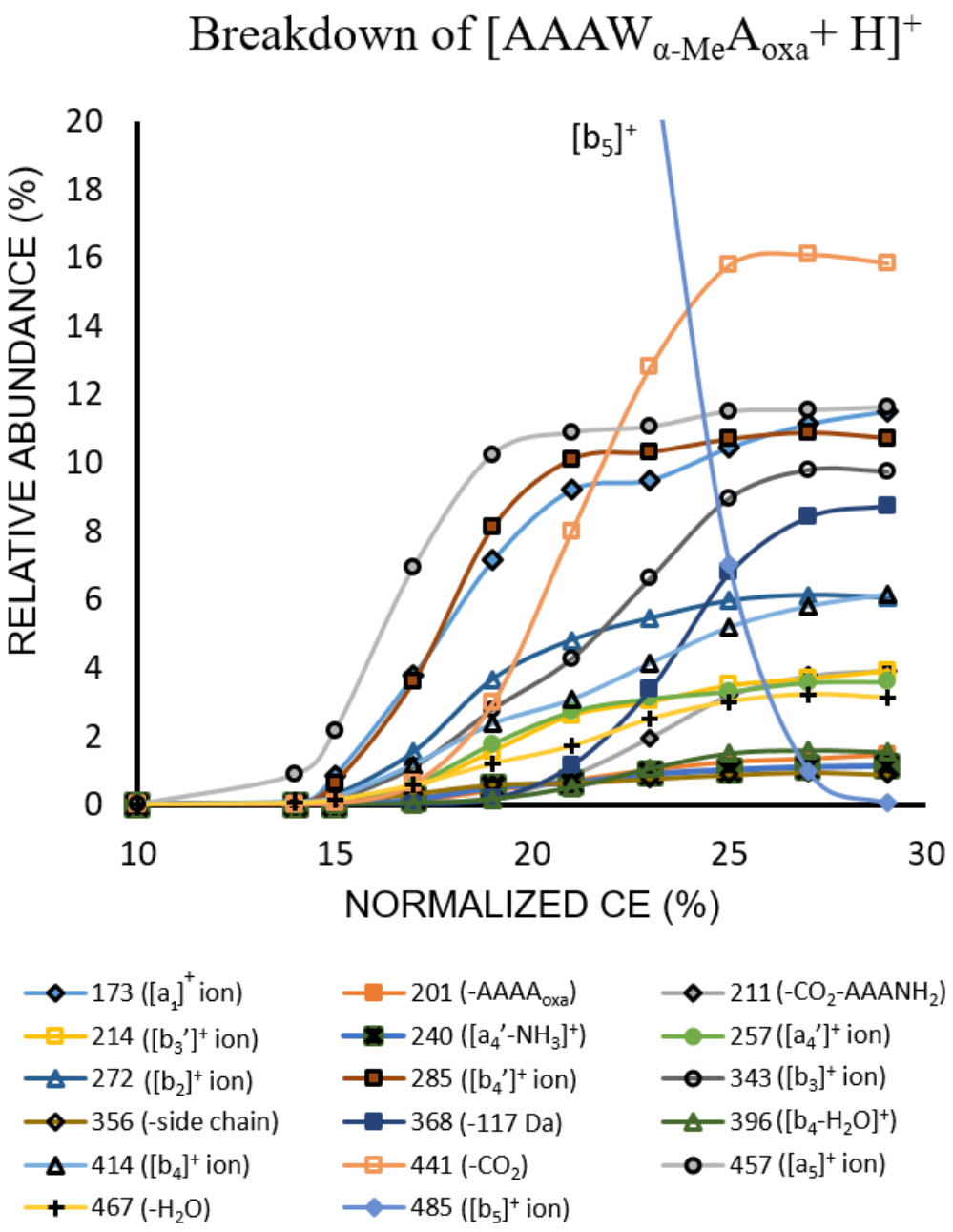

Figure 3.10 Energy-resolved breakdown diagram for [AAAW$_{\alpha\text{-Me}}$A$_{oxa}$ + H]$^+$ ion.

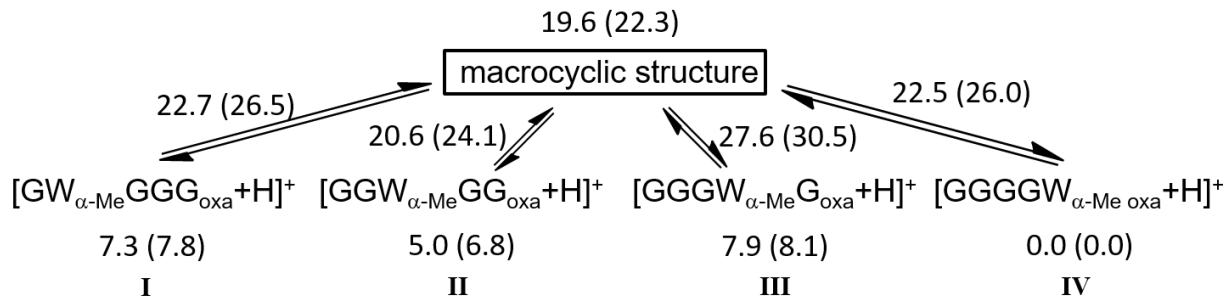

Scheme 3.1 Interconversion of the $[b_5]^+$ ions via cyclization into a common cyclic pentapeptide. The enthalpies (ΔH^o_0) and free energies (ΔG^o_{298} in parenthesis), both in kcal mol^{-1}, are relative to [AAAAW$_{\alpha\text{-Me oxa}}$ +H]$^+$, structure **IV**.

Another more minor difference in the two sets of breakdown curves is that the ratio $[b_3]^+$ / $[b_2]^+$, which is essentially 1 in the curves for [AAAAW$_{\alpha\text{-Me oxa}}$ + H]$^+$, is now closer to 2 for [AAAW$_{\alpha\text{-Me}}$A$_{oxa}$ + H]$^+$. Recalling that the isotopic labeling established that the A−W$_{\alpha\text{-Me}}$ amide bond is never broken in formation of both $[b_3]^+$ and $[b_2]^+$ ions, then having more of the product which does not necessitate prior rearrangement, the $[b_3]^+$ ion, again is consistent with a larger amount of dissociation from [AAAW$_{\alpha\text{-Me}}$A$_{oxa}$ + H]$^+$. Finally, the abundance of $[a_5]^+$ ion (*m/z* 457) is slightly higher from [AAAW$_{\alpha\text{-Me}}$A$_{oxa}$ + H]$^+$ and this probably reflects that $[a_5]^+$ ions having the remnants of an alanine residue at the C-terminus are more robust than the one that has the α-methyltryptophan at that location.

3.2 Theoretical investigations

From the energy-resolved curves the lowest energy dissociation channel is for the loss of CO forming an $[a_5]^+$ ion, followed by cleavage of the A−$W_{\alpha\text{-Me}}$ amide bond to create the $[b_4']^+$ / $[a_1]^+$ combination of ions. Formation of the latter products requires the intermediacy of an $[a_5]^+$ ion derived from $[AAAAW_{\alpha\text{-Me oxa}} + H]^+$, i.e. the α-methyltryptophan residue is located at the C-terminus (**Figure 3.11**). Here, DFT calculations are used to examine interconversion between

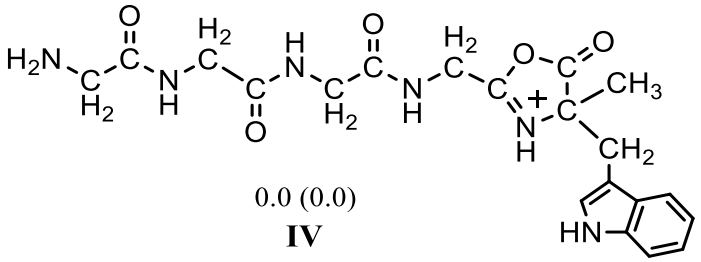

Figure 3.11 The proposed structure of the $[b_5]^+$ ion used for DFT calculations after rearrangement.

different $[b_5]^+$ isomers via the macrocyclic structure along with possible dissociation pathways from the lowest energy isomer. Note that for computational simplicity we have opted to use four glycyl residues rather than the slightly larger alanyl residues that we examined experimentally, *i.e.* the theoretical study is for the dissociation channels of $[G_4W_{\alpha\text{-Me oxa}} + H]^+$.

3.2.1 Method of calculations

Geometry optimizations and calculations of harmonic vibrational frequencies were performed using the Gaussian 09 suite of programs (Revision D.01)[78] with the B3LYP functional based on Becke's three-parameter exchange potential [79,80] and the Lee, Yang and Parr correlation functional.[81] The standard Pople 6-31++G(d,p) basis set was used for all calculations.[82,83] All structures were characterized by harmonic frequency calculations; intrinsic reaction coordinate calculations were used to determine the two minima associated with each transition state structure.[84] Throughout the text the relative energies quoted are enthalpies at 0 K (ΔH^{o}_{0} values).

3.2.2 Isomers of $[b_5]^+$

Scheme 3.1 summarizes the relative energies of four different $[b_5]^+$ ions, as well as the energy barriers for head-to-tail cyclization for each isomer. Isomer $[GGGGW_{\alpha\text{-Me oxa}}+H]^+$, structure **IV** (**Figure 3.11**), has the lowest energy among all the $[b_5]^+$ ions and the barriers to interconversion via a macrocyclic structure are in the range 20-28 kcal mol^{-1}. The macrocyclic ion has the highest energy and lies 19.6 kcal mol^{-1} above **IV**.

3.2.3 Dissociation pathways

The proposed mechanism for loss of CO is described in pathway A in **Scheme 3.2**. It has a barrier of 30.5 kcal mol^{-1} leading to an $[a_5]^+$ ion. This is slightly higher than the barriers to interconversion between isomers of the $[b_5]^+$ ion. Subsequent dissociation of the $[a_5]^+$ ion has a higher energy (33.1 kcal mol^{-1}) to produce an ion-molecule complex (**VI**) which dissociates to give the $[b_4']^+$ and $[a_1]^+$ ions; formation of the $[a_1]^+$ ions is the thermodynamically favored product.

Pathway A

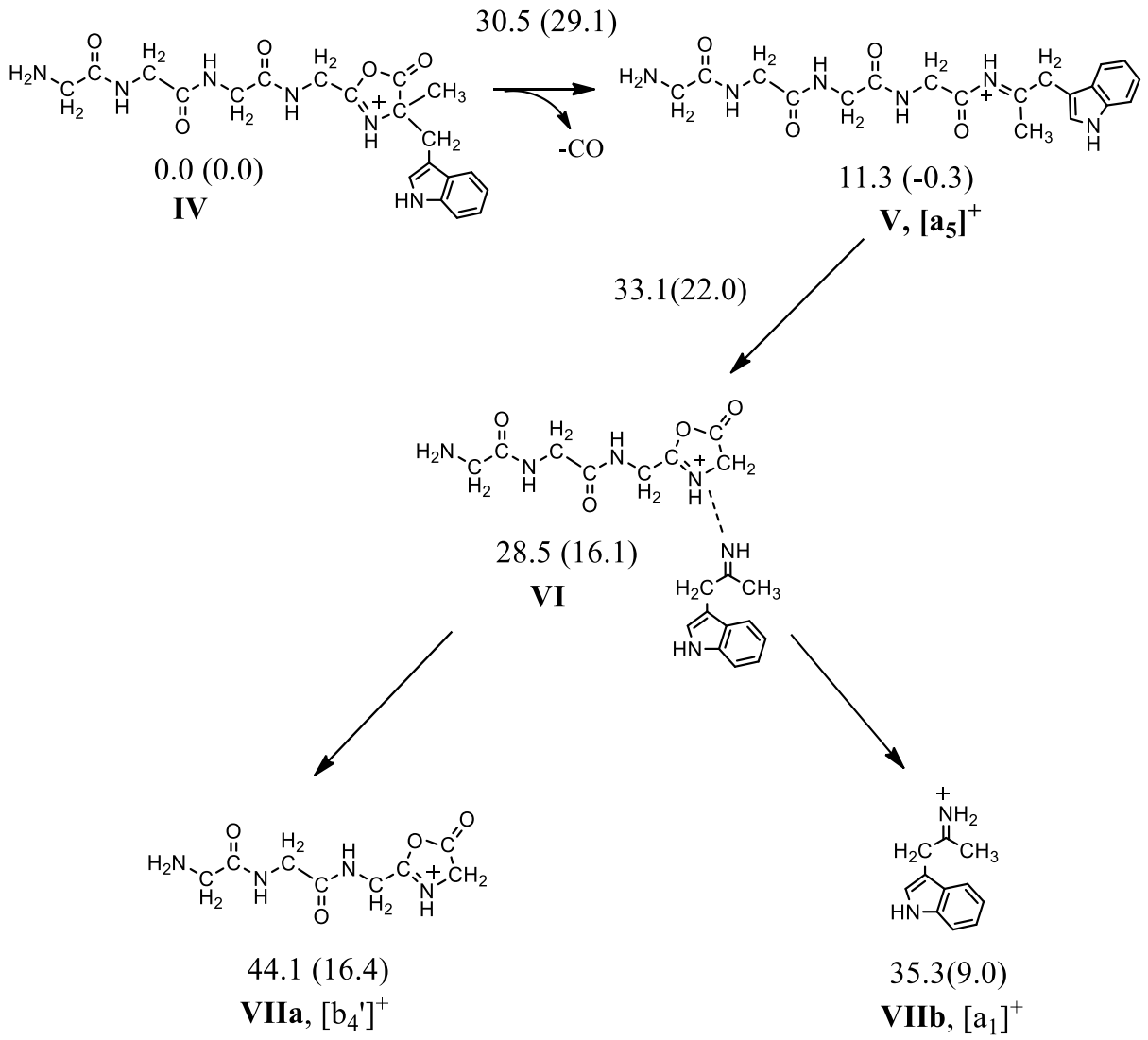

Scheme 3.2 Proposed mechanism for the loss of CO, which further dissociates to become $[a_1]^+$ ion of α-methyltryptophan and the $[b_4']^+$ ion.

Pathway B

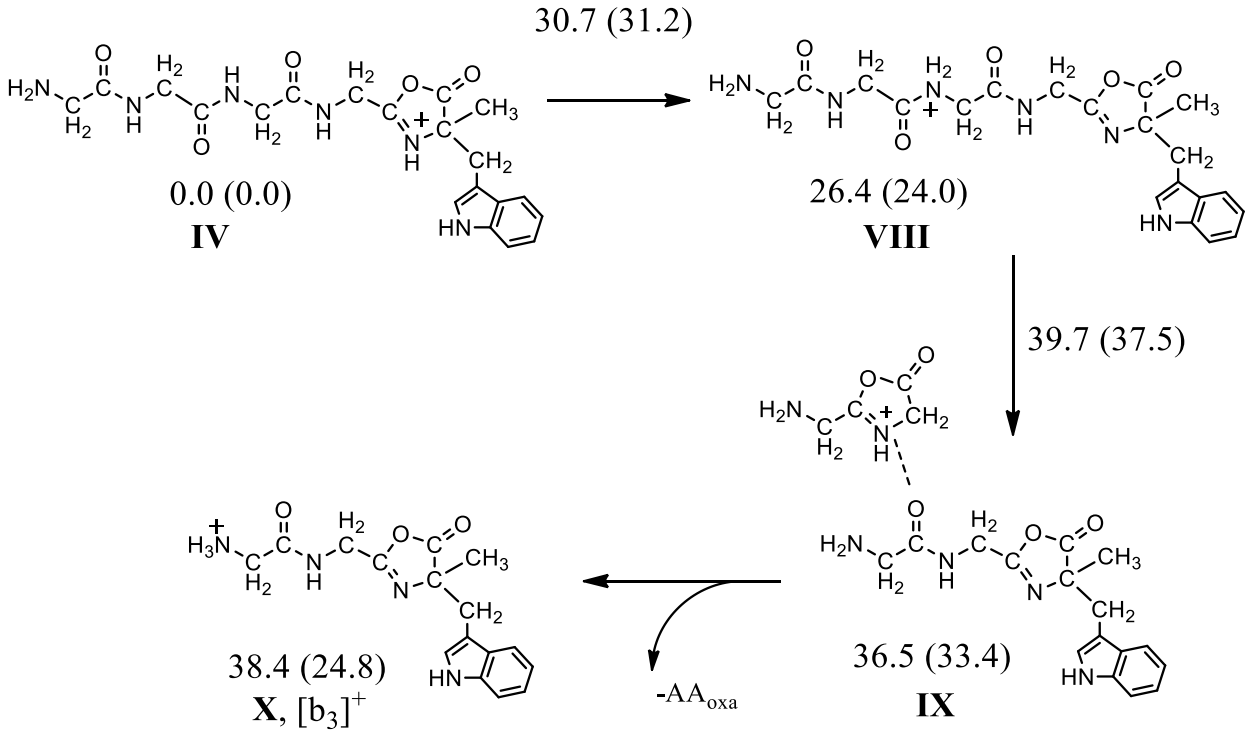

Scheme 3.3 Proposed mechanism for the loss of AA_{oxa} from the N-terminus of the $[b_5]^+$ ion.

Scheme 3.3 describes cleavage of the second protonated amide bond producing the $[b_3]^+$ ion and neutral AA_{oxa} via a solvated complex. Here the barrier to the formation of the solvated complex has the highest barrier, 39.7 kcal mol^{-1}. Similarly, cleavage of the third protonated peptide bond gives the $[b_2]^+$ and $[b_3']^+$ ions with the former favored with an endothermicity of 41.3 kcal mol^{-1}(**Scheme 3.4**). Both products were observed experimentally with the $[b_2]^+$ ion in higher abundance at all collision energies. Note that Pathways B and C have similar endothermicities and were found to have similar onset energies (**Figure 3.8**).

Pathway C

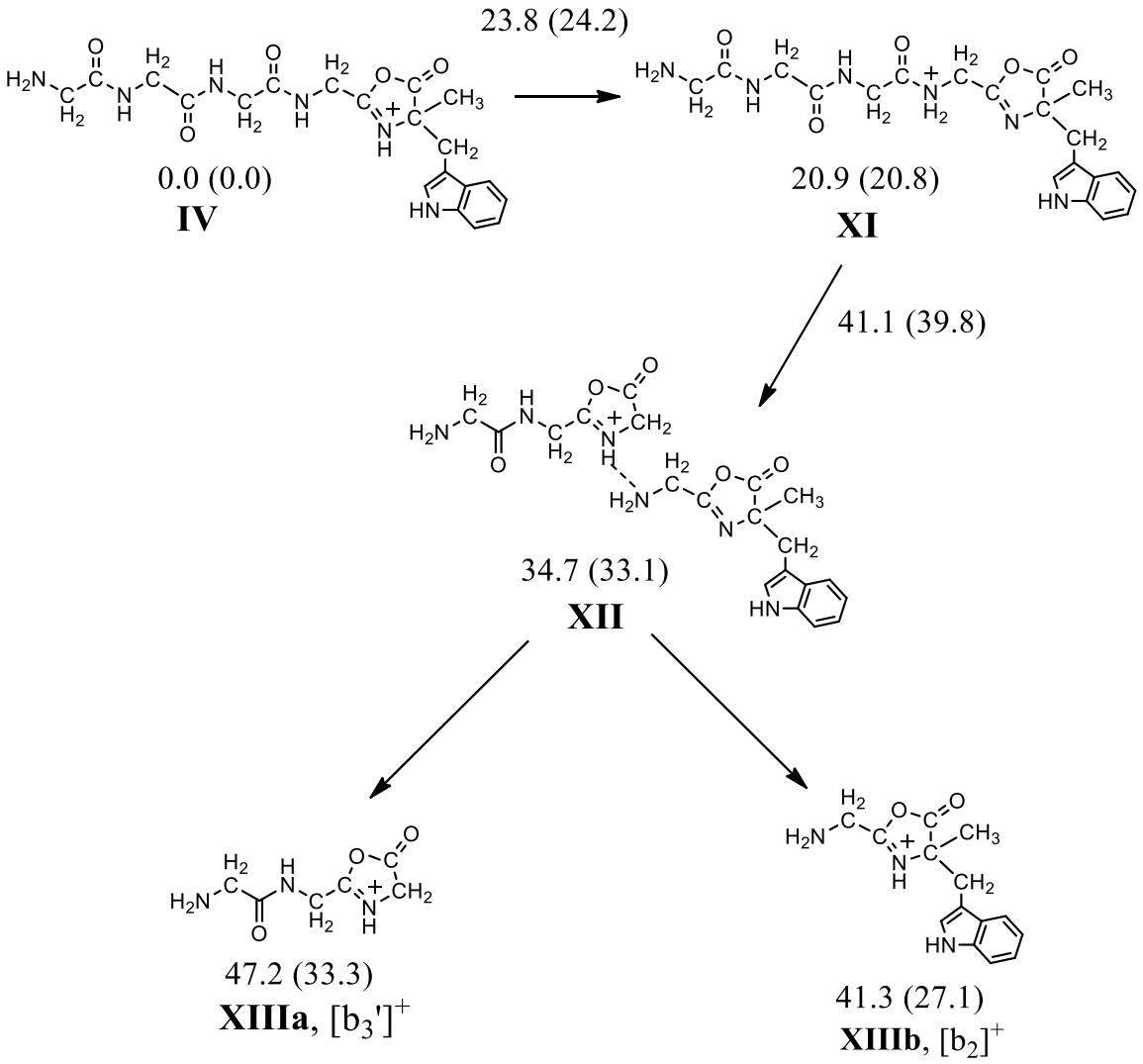

Scheme 3.4 Proposed mechanism for the formation of the $[b_3']^+$ and $[b_2]^+$ ions

In the first step to the loss of CO_2 (**Scheme 3.5**, **Pathway D**), a hydride from the β-carbon of the side chain of the α-methyltryptophan residue migrates to a carbon in the oxazolone ring, thereby formally transferring the charge onto the side chain (**XIV**). Cleavages of the C_α–C and

Pathway D

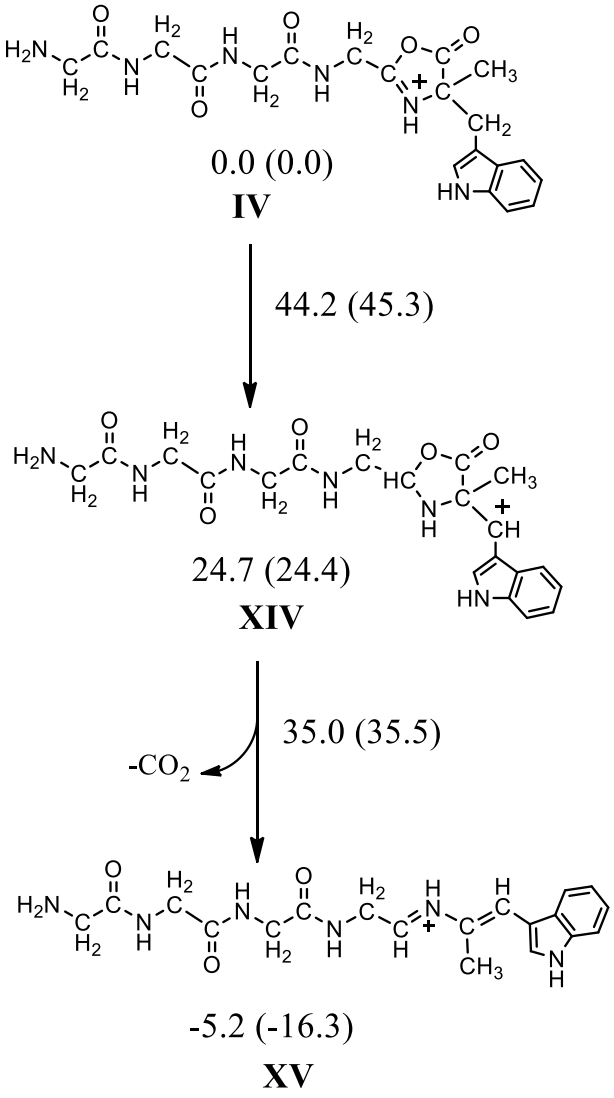

Scheme 3.5 Proposed mechanism for the loss of CO_2.

C−O bonds simultaneously in the oxazolone ring lead to the loss of CO_2. The barrier for this reaction is 44.2 kcal mol^{-1} for the hydride transfer and is slightly higher than the other pathways

for the dissociation of $[GGGGW_{\alpha\text{-Me oxa}} + H]^+$, consistent with the higher onset energy in the energy-resolved diagram (**Figure 3.8**).

The ion at *m/z* 368 is a result of the loss of an oxazolone ring containing residue A^i and a water molecule containing an oxygen from residue A^{iv}; these products are most easily rationalized as coming from $[AAAW_{\alpha\text{-Me}}A_{oxa} + H]^+$. The mechanism for this dissociation using the analogous glycyl system, ion **III** (**Figure 3.12**), is summarized in Pathway E (**Scheme 3.6**). First, the C_α–C bond of the α-methyltryptophan residue breaks and forms a complex with an $[a_4]^+$ ion hydrogen bonded to the oxazolone (**XVI**). This cleavage is analogous to the dissociation of $[b_2]^+$ ions into

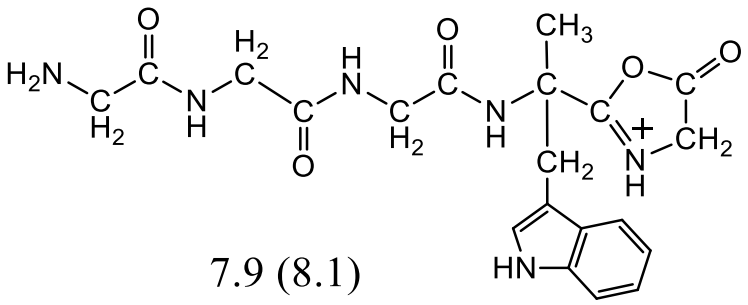

Figure 3.12 Structure of $[GGGW_{\alpha\text{-Me}}G_{oxa}]^+$ used for calculation for the loss of an oxazolone ring and a water molecule.

Pathway E

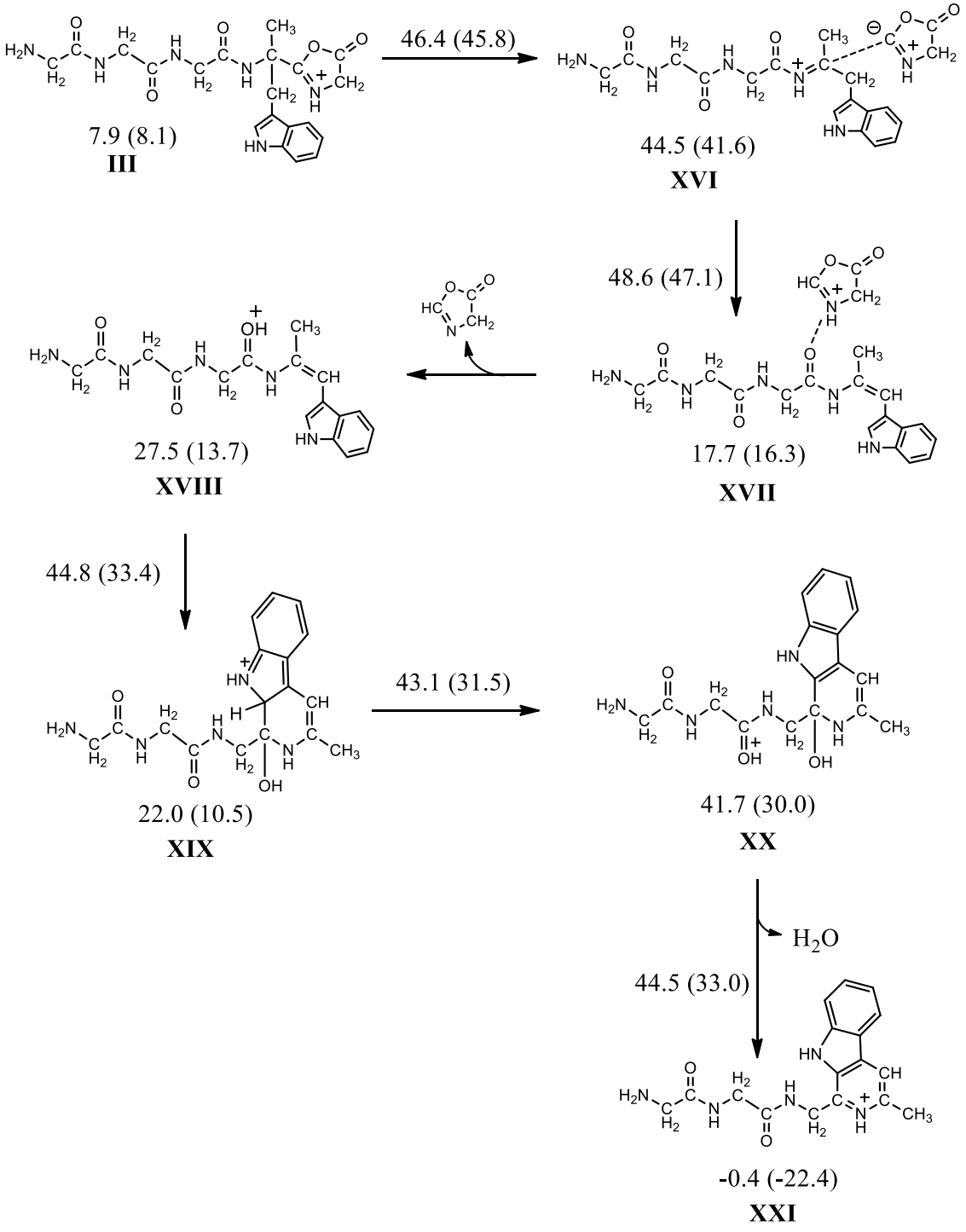

Scheme 3.6 Proposed mechanism for the loss of an oxazolone ring and a water molecule.

$[a_1]^+$ ions recently reported.[52] In the highest energy step in **Scheme 3.6** a β-proton from the side chain of the α-methyltryptophan residue is then transferred to the oxazolone, forming an ion-molecule complex at much lower energy (17.7 kcal mol^{-1}). Proton transfer from the protonated oxazolone followed by separation leads to the formation of structure **XVIII.** Nucleophilic attack by the indole on the carbon of the protonated amide, followed by two proton transfer steps leads to the loss of water. The final product, ion **XXI**, has an additional aromatic ring and the extra stabilization afforded by this results in the overall reaction being slightly exothermic. All the steps in the loss of water have lower energies than the second step in the loss of oxazolone (**XVI→XVII**, 48.6 $kcal^{-1}$); consequently, the losses of oxazolone and water are concomitant.

3.3 Summary

Comparable fragmentation patterns were observed for a series of protonated hexapeptides, both with and without an α-methyl group on the tryptophan residue, with the formation of $[b_5]^+$ ions being the most abundant product for every peptide. This indicates that substituting a methyl group onto the α-carbon of the tryptophan residue does not affect the dissociation mechanisms, despite the additional steric crowding introduced at the α-carbon.

The fragmentations of the two types of $[b_5]^+$ ions are very different. The CID spectra of the $[b_5]^+$ ions containing an α-methyltryptophan residue are more complicated than those of $[b_5]^+$ with

a ‘normal’ tryptophan residue. Both series of $[b_5]^+$ ions undergo head-to-tail macrocyclizations prior to dissociation, as reflected by isomers having very similar CID spectra. Common to both classes of $[b_5]^+$ ions are losses of CO (giving $[a_5]^+$ ions), and a single amino acid residue (giving $[b_4]^+$ ions).

The energy-resolved curves for two sequences, ions $[AAAW_{\alpha\text{-Me}}A_{oxa} + H]^+$ and $[AAAAW_{\alpha\text{-Me oxa}} + H]^+$ are similar, but not identical, indicating that scrambling is not complete. Loss of CO is the lowest energy dissociation pathway, with subsequent cleavage to form the imine derived from α-methyltryptophan, an internal $[a_1]^+$ ion along with the complementary $[b_4']^+$ occurring at slightly higher collision energies. The formation of the latter implies that $[AAAW_{\alpha\text{-Me}}A_{oxa} + H]^+$ has rearranged to $[AAAAW_{\alpha\text{-Me oxa}} + H]^+$ prior to dissociation.

The spectra of α-methyltryptophan-containing ions have high abundances of the internal $[a_1]^+$ ion, and in this respect differ from the spectra of the $[b_5]^+$ ions containing ‘normal’ tryptophan (Figure S1), showing the stabilizing effect of the α-methyl group. At higher collision energies loss of CO_2 becomes the dominant pathway and ^{18}O labeling showed that this involves residue A^{iv} and is most easily understood in terms of loss from $[AAAAW_{\alpha\text{-Me oxa}} + H]^+$. Another higher energy dissociation pathway involves the loss of neutrals with a combined mass of 117 Da. Labeling and accurate mass measurements established that the neutral products lost were water (from residue A^{iv}) and the oxazolone ring incorporating residue A^{i}. These losses are concomitant and appear to come from ion $[AAAW_{\alpha\text{-Me}}A_{oxa} + H]^+$.

CHAPTER 4: Fragmentation of Radical Peptide Cations of α-methyltryptophan-containing Hexapeptides and Their $[b_5 - H]^{\bullet+}$ Ions

4.1 Results and discussions

4.1.1 Fragmentation of the hexapeptide radical cations

The CID spectra of hexapeptides containing an α-methyltryptophan residue are simpler than those of the corresponding peptides in which hetero-residue is a tryptophan, and the abundances of $[b_5 - H]^{\bullet+}$ ions are low, except in the dissociation of $[AAAAW_{\alpha\text{-Me}}G]^{\bullet+}$ (**Figure 4.1**).[85] For each hexapeptide radical cation, all the major products are the results of bond cleavages around the α-carbon of the α-methyltryptophan residue, a consequence of steric crowding. For $[AW_{\alpha\text{-Me}}AAAG]^{\bullet+}$ the $[z_5 - H]^{\bullet+}$ ion is the major product and is a result of cleaving the N-C_α bond of the $W_{\alpha\text{-Me}}$ residue. Similarly, $[z_m - H]^{\bullet+}$ ions are in high abundance in the spectra of the other peptide radical cations. Note that in **Figure 4.1 d)**, the CID spectrum of $[AAAAW_{\alpha\text{-Me}}G]^{\bullet+}$, it is the complementary ion $[c_4 + 2H]^+$ at *m/z* 302 that is the more abundant than the $[z_2 - H]^{\bullet+}$ ion.

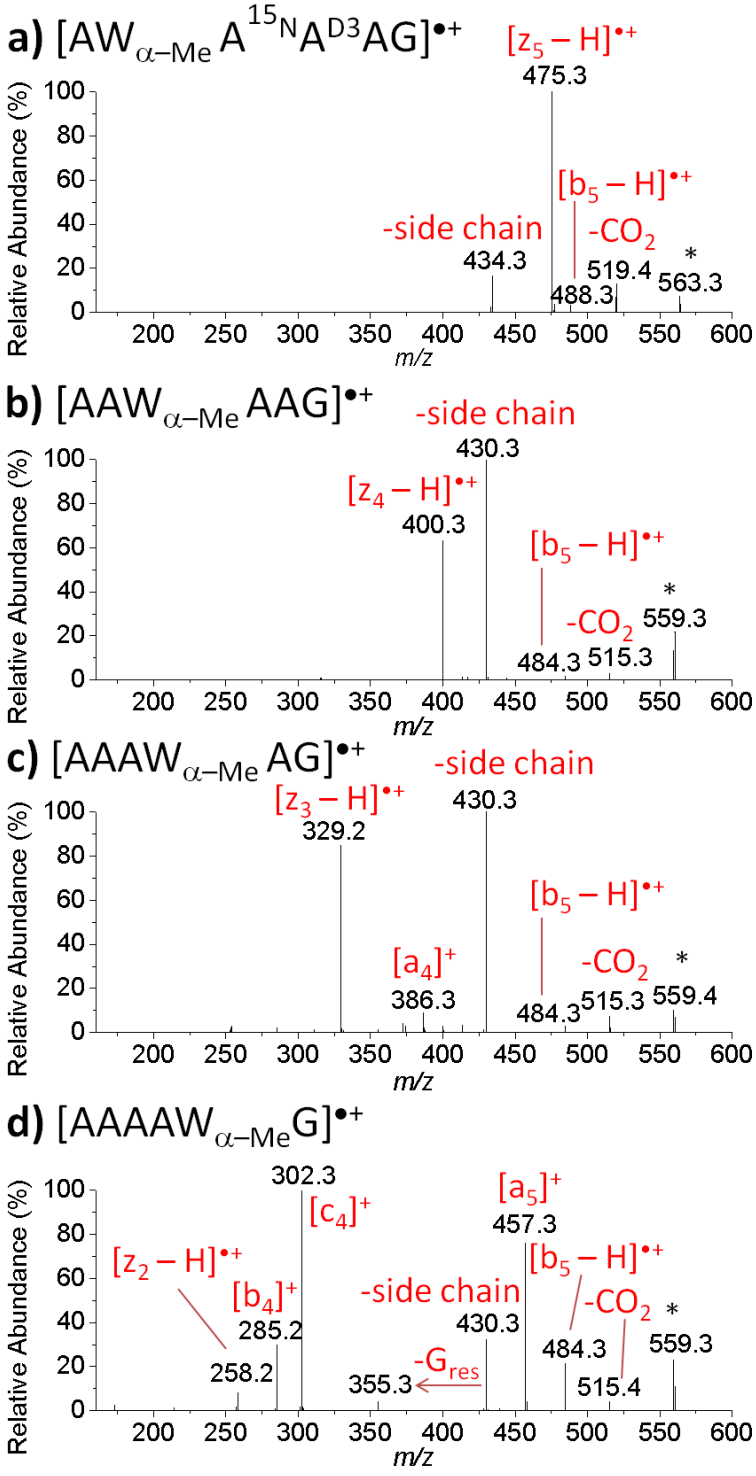

Figure 4.1 CID spectra of peptide radical cations from α-methyltryptophan-containing hexapeptides, with the hetero-residue at different positions of the peptide.

Cleavage of the C_α–C_β bond of the side chain of the α-methyltryptophan residue as 3-methyleneindolenine (loss of 129 Da) provides the base peak for $[AAW_{\alpha\text{-}Me}AAG]^{\bullet+}$ and $[AAAW_{\alpha\text{-}Me}AG]^{\bullet+}$ and is present for the other two peptides.

The spectrum of $[AAAAW_{\alpha\text{-}Me}G]^{\bullet+}$ has one product, an $[a_5]^+$ ion; and its dissociation product, a $[b_4]^+$ ion. This involves the homolytic cleavage of the C_α–C bond of the α-methyltryptophan residue, formally losing the radical $C^{\bullet}ONHCH_2COOH$.

4.1.2 Fragmentation of $[b_5 - H]^{\bullet+}$ ions

The CID spectra of the four $[b_5 - H]^{\bullet+}$ ions composed of one α-methyltryptophan residue and four alanine residues (**Figure 4.2**) are very different from each other, indicating that *there is no sequence scrambling in this set of ions*. This is in marked contrast with the spectra of the various $[A_4W_{oxa}]^{\bullet+}$ ions, where there was complete scrambling and only the isomer with the tryptophan at the C-terminus dissociated. Despite the differences in the spectra in **Figure 4.2** there are some observable patterns:

- All spectra show the corresponding $[b_4 - H]^{\bullet+}$ ion. The loss of the alanine residue (71 Da) occurs from three of the ions and the α-methyltryptophan residue is lost from $[AAAAW_{\alpha\text{-}Me\ oxa}]^{\bullet+}$. The spectra of the isotopically labeled $[b_5 - H]^{\bullet+}$ in **Figure 4.3** establishes that for $[AAAW_{\alpha\text{-}Me}A_{oxa}]^{\bullet+}$ the alanine residue at the C-terminus is the one that is lost. These data are consistent with the $[b_5 - H]^{\bullet+}$ ions having unrearranged oxazolone structures.

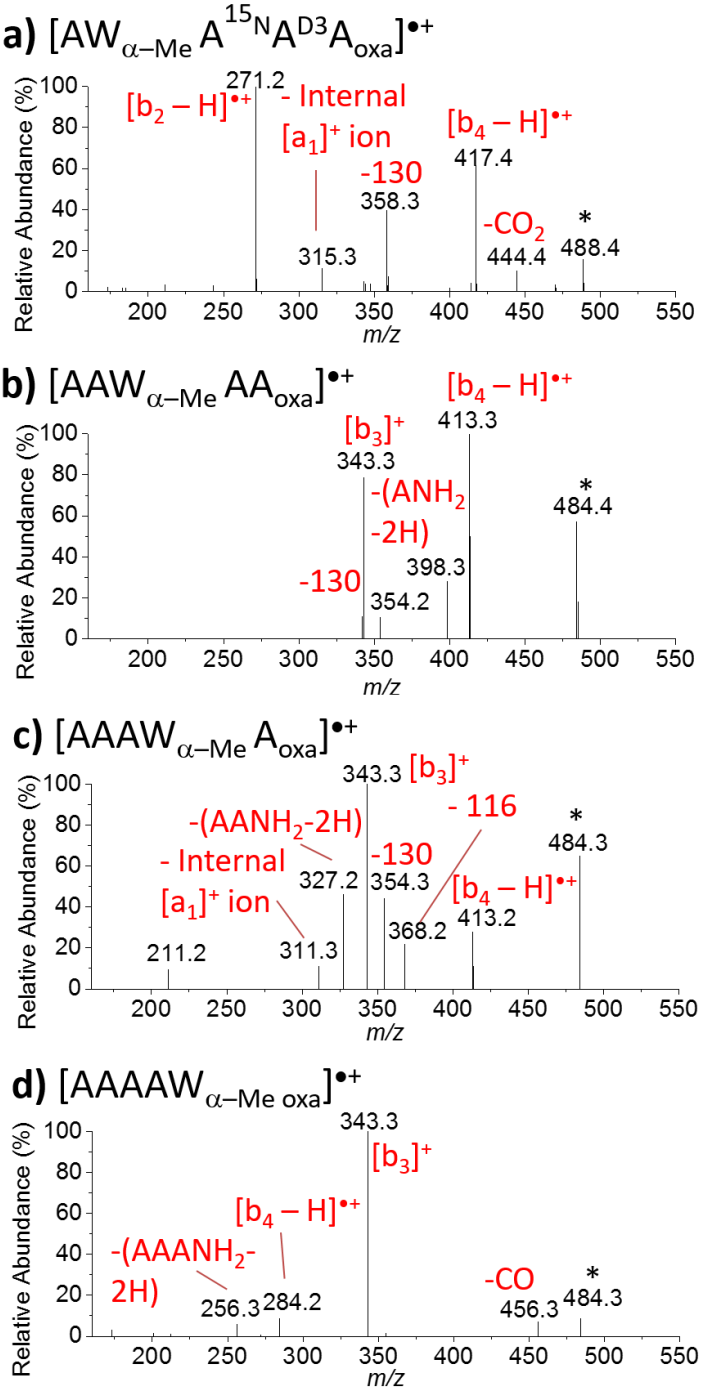

Figure 4.2 CID spectra of the $[A_4W_{\alpha\text{-Me oxa}}]^{\bullet+}$ ions, with the α-methyltryptophan located at different positions.

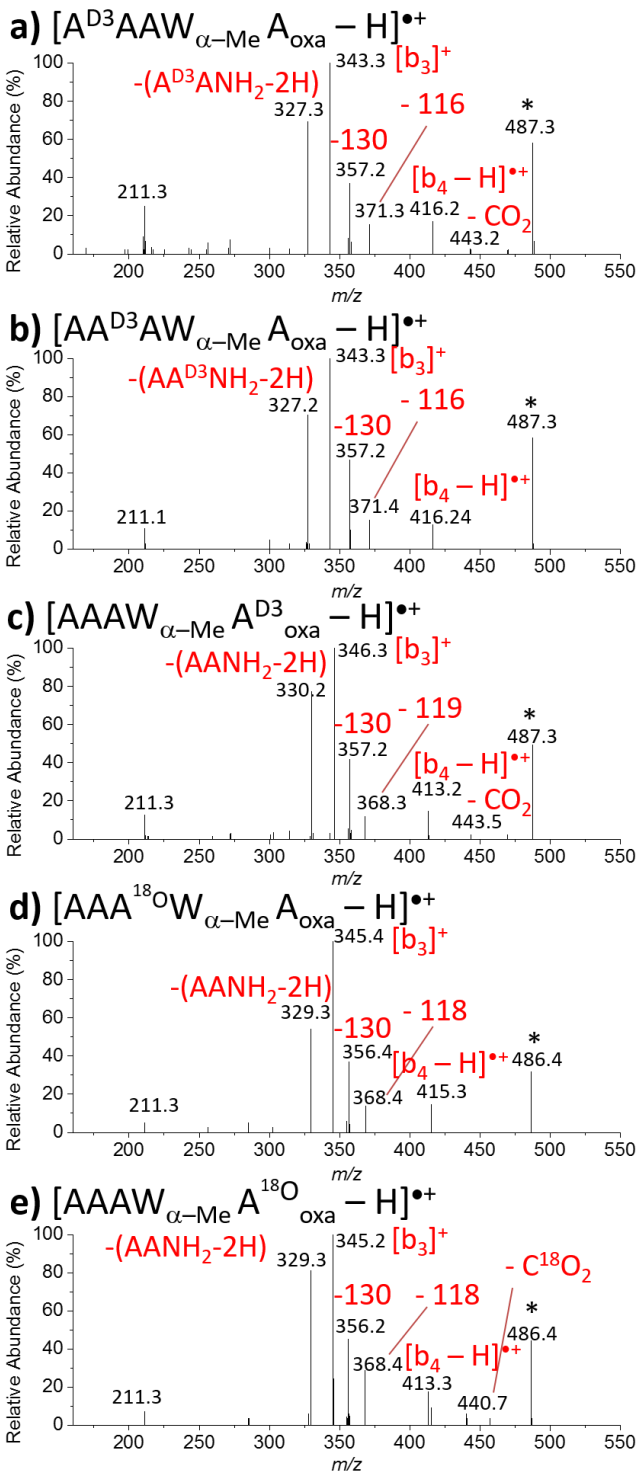

Figure 4.3 CID of $[AAAW_{\alpha\text{-}Me}A_{oxa}]^{\bullet+}$ ions, **a), b), c)** with CD_3 labels and **d), e)** with ^{18}O labels, at different alanine residues.

- Loss of the side chain as a radical (130 Da) occurs from the first three ions in **Figure 4.2**, but not from $[AAAAW_{\alpha\text{-Me oxa}}]^{\bullet+}$, where the α-methyltryptophan residue would be in the oxazolone ring and loss of the side chain would create an improbable structure in which there are two double bonds attached to the nitrogen. Loss of the side chain is most easily rationalized as being homolytic cleavage of the C_α–C_β of the π-radical cation isomer. Such loss was not observed from $[b_5 - H]^{\bullet+}$ ions that contain a tryptophan residue without the α-methyl group.
- Three of the spectra have a product ion at *m/z* 343, corresponding to the loss of dialanine radical (141 Da), forming $[b_3]^+$ ion. The exception is in the spectrum of $[AW_{\alpha\text{-Me}}AAA_{oxa}]^{\bullet+}$, where there is only one alanine residue at the N-terminus. Isotopic labeling (**Figure 4.3**) established unambiguously that it is the two residues from the N-terminus of $[AAAW_{\alpha\text{-Me}}A_{oxa}]^{\bullet+}$ that are lost. The N-terminal captodative structure is a likely precursor to this channel.

- Three of the spectra show losses of (A_mNH_2-2H), an imine-amide structure, $HN{=}C(CH_3)(CONHC(CH_3))_{(m-1)}CONH_2$, where m is 1 in **4.2 b)**, 2 in **4.2 c)**, and 3 in **4.2 d)**. These products are the result of cleavage of the N–C_α bond of the alanine residue on the N-side of the α-methyltryptophan residue. Isotopic labeling in **Figure 4.3**, where m is 2, establish that it is the first two residues of $[AAAW_{\alpha\text{-Me}}A_{oxa}]^{\bullet+}$ that are lost. The unsaturation at the N-terminus of the imine-amide is most easily rationalized in terms of loss from the N-terminal captodative structure.

- Losses of CO and CO_2 occur but the products are in very low abundances. Similar behavior was noted for the $[b_5 - H]^{\bullet+}$ ions derived from tryptophan-containing hexapeptides.[59] By contrast, the closed-shell $[b_5]^+$ ions containing an α-methyltryptophan lose both CO and CO_2 in high abundance, with the CO loss occurring at lower onset energies than the loss of CO_2.

There are some features of the spectra that are unique to individual isomers. These include:

- A loss of 116 Da from $[AAAW_{\alpha\text{-}Me}A_{oxa}]^{\bullet+}$. One possibility here was that this might be the loss of an indole radical as has previously been observed in the dissociation of peptide radical cations containing a tryptophan residue,[2] but isotopic labeling (**Figure 4.3)** showed that both the carbonyl oxygens in alanine residues adjacent to the α-methyltryptophan residue are lost. This corresponds to a loss of an oxazolone radical, $(C_4H_4O_2N)^{\bullet}$ plus H_2O. A loss of 117 Da was observed in the fragmentations of the analogous $[b_5]^+$ ions and these were attributed to dissociation of $[AAAWA_{oxa}+H]^+$ ions (**Scheme 3.6**).

- In the spectrum of $[AAAW_{\alpha\text{-}Me}A_{oxa}]^{\bullet+}$ there is a minor product at *m/z* 211 and this is present in all the spectra in **Figure 4.3**, showing that none of the heavy isotopes in these different isotopomers is retained. One of the most abundant products in the CID of $[AAAW_{\alpha\text{-}Me}A_{oxa}]^{\bullet+}$ is the ion at *m/z* 327 and a subsequent CID of this ion gave only the ion at *m/z* 211, again a loss of 116 Da.

- Isomer $[AW_{\alpha\text{-}Me}AAA_{oxa}]^{\bullet+}$ is the only ion that showed a simultaneous loss of three alanine residues (217 Da), creating the $[b_2 - H]^{\bullet+}$, the dominant product. Formation of this ion would be facilitated by cleaving the second amide bond of the N-terminal captodative radical. This $[b_2 - H]^{\bullet+}$ ion would be heavily stabilized by the captodative effect as it has a powerful electron donor (the NH_2 group) and a strongly electron-withdrawing group, the protonated oxazolone.

4.1.3 Energy-resolved plot for dissociation of the ion $[AAAW_{\alpha\text{-}Me}A^{D3}{}_{oxa}]^{\bullet+}$

The energy-resolved breakdown diagram generated for the ion $[AAAW_{\alpha\text{-}Me}A^{D3}{}_{oxa}]^{\bullet+}$ indicated that the loss of the side chain as a radical (130 Da) and the loss of dialanine radical (141 Da) are the most easily formed fragment ions, and the loss of the side chain radical dominates at higher energy (**Figure 4.4**). The next lowest barrier is for the loss of the imine-amide, which is the loss of $(AANH_2 - 2H)$ from this ion. We should note that this ion reaches its maximum abundance at mid-range collision energies, then begins to decrease in abundance at higher energies. In contrast to this ion, the ion at *m/z* 211, which is a further loss of 116 Da after the loss of imine-amide, increases rapidly at high energies. This is a good indication that the ion at *m/z* 211 is a dissociation product from the ion after the loss of the imine-amide.

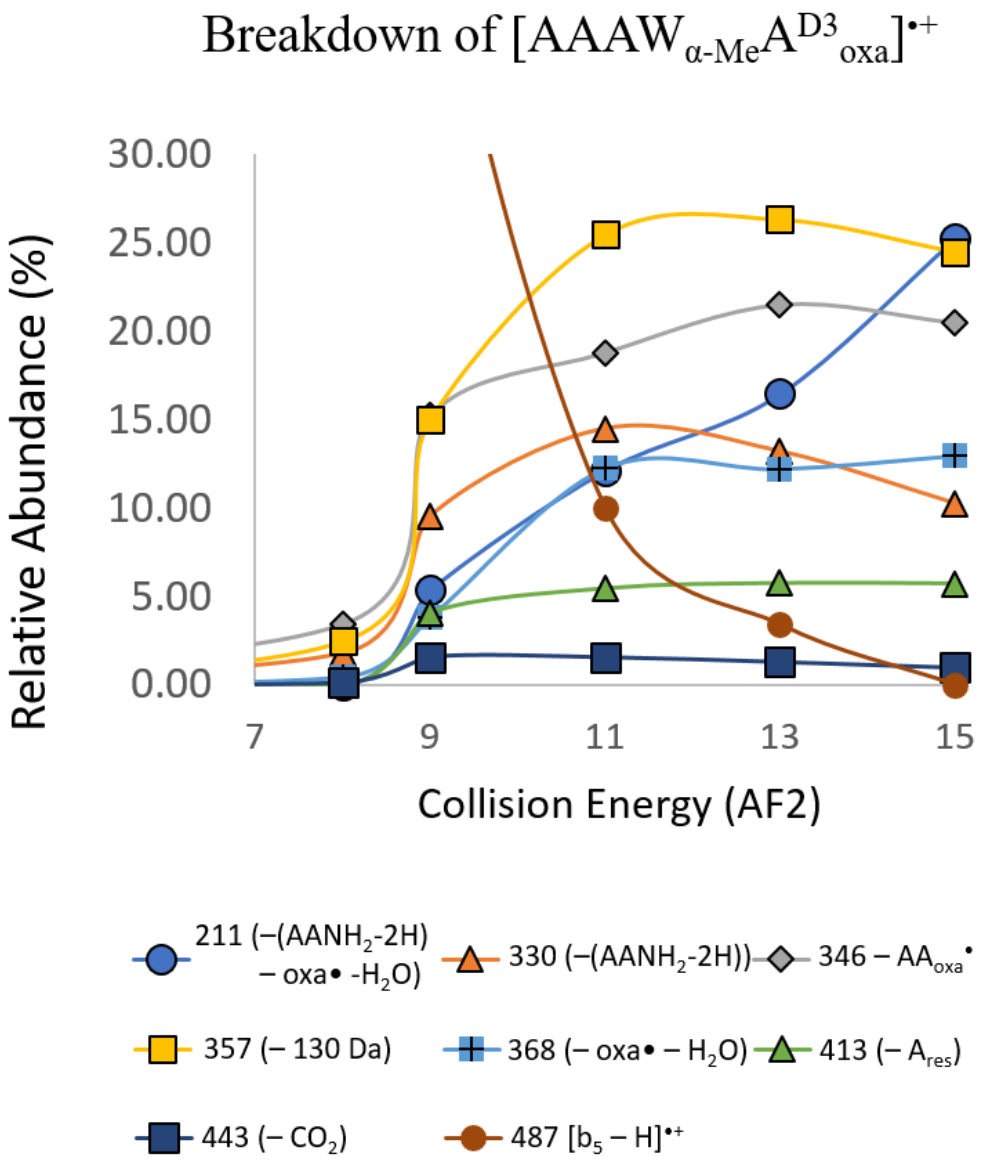

Figure 4.4 Energy-resolved breakdown diagram for dissociation of the ion [AAAW$_{\alpha\text{-Me}}$A$^{D3}_{oxa}$]$^{\bullet r+}$. "-130 Da" refers to a loss of the tryptophan side chain as a radical.

4.2 Proposed dissociation pathways

4.2.1 Isomers of the $[AAAW_{\alpha\text{-}Me}A_{oxa}]^{\bullet+}$ ion

The CID spectra in **Figure 4.2** clearly show that there is no isomerization between the four isomeric $[b_5 - H]^{\bullet+}$ ions. Our most extensive isotopic labeling studies have been on isomer $[AAAW_{\alpha\text{-}Me}A_{oxa}]^{\bullet+}$ and for this reason we have limited our computational work to this isomer.

In previous study on the $[b_5 - H]^{\bullet+}$ ions derived from tryptophan-containing hexapeptides, the ions macrocyclize and are able to rearrange into different isomers. DFT calculations found that the isomer $[AAAAW_{oxa}]^{\bullet+}$ with the radical located at the α-carbon of the tryptophan residue is at the global minimum of all isomers. In this study, the same α-carbon is blocked by a methyl group, which inhibited the event of sequence scrambling by requiring an alternative location for the radical. Our best interests was to investigate the new location of the radical, and investigate how it prevents sequence scrambling of the ion.

Based on DFT calculations, the best structure for the $[b_5 - H]^{\bullet+}$ ions has the radical center located at the α-carbon of the N-terminal residue (**Figure 4.5 (**I)), compared to the structure with a β-radical (**Figure 4.5 (II)**) or the canonical structure (**Figure 4.5 (III)**). The radical in this structure is stabilized by the electron-donating nitrogen and the electron-withdrawing protonated oxygen next to it. Such a captodative structure delocalizes the charge at the N-terminus, making the N-terminus less nucleophilic. At the same time, the oxazolone at the C-terminus is less electrophilic without the charge. Hence, forming the captodative structure for the $[b_5 - H]^{\bullet+}$ ion prevents macrocyclization and inhibits sequence scrambling.

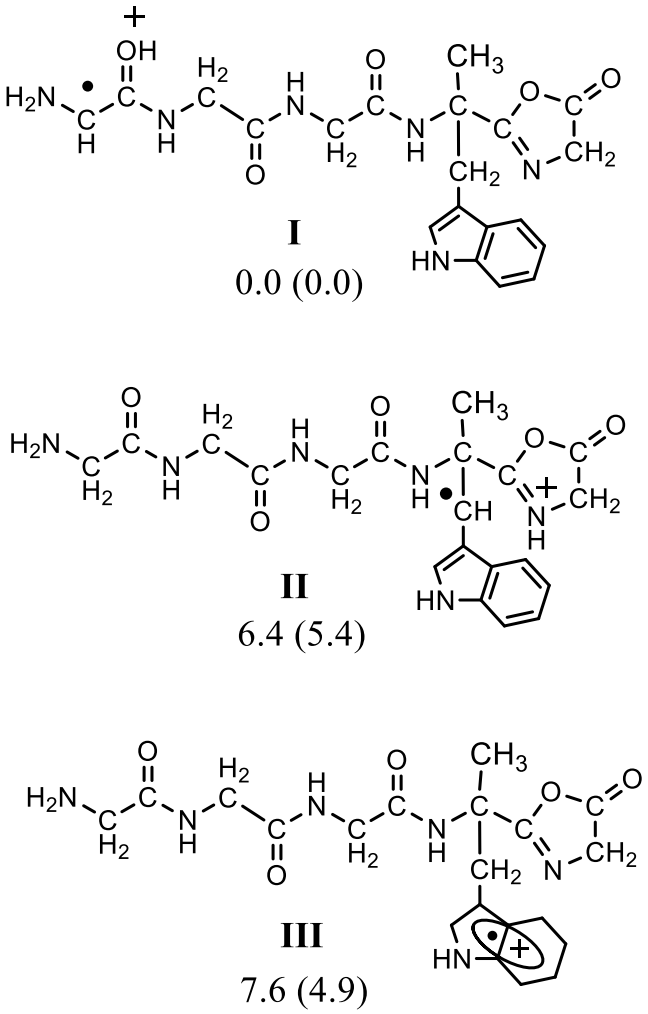

Figure 4.5. Possible structures for the $[A_4W_{\alpha\text{-Me oxa}}]^{\bullet+}$ ions, with relative energies. The enthalpies (ΔH^o_0) and free energies (ΔG^o_{298} in parenthesis), both in kcal mol^{-1}, are relative to structure **I.**

4.2.2 Loss of one residue from C-terminus

As described previously, the losses of one residue from the $[b_5 - H]^{\bullet+}$ ions are observed to come from the C-terminus of the original sequence without scrambling. It would be logical to

suggest that the mechanism for such loss follows the conventional mechanisms for gas-phase protonated peptide fragmentation, by first losing a CO from the oxazolone ring at the C-terminus which gives the $[a_5 - H]^{\bullet+}$ ion, followed by the further loss of the amine. Such mechanism is shown in **Scheme 4.1** as pathway A.

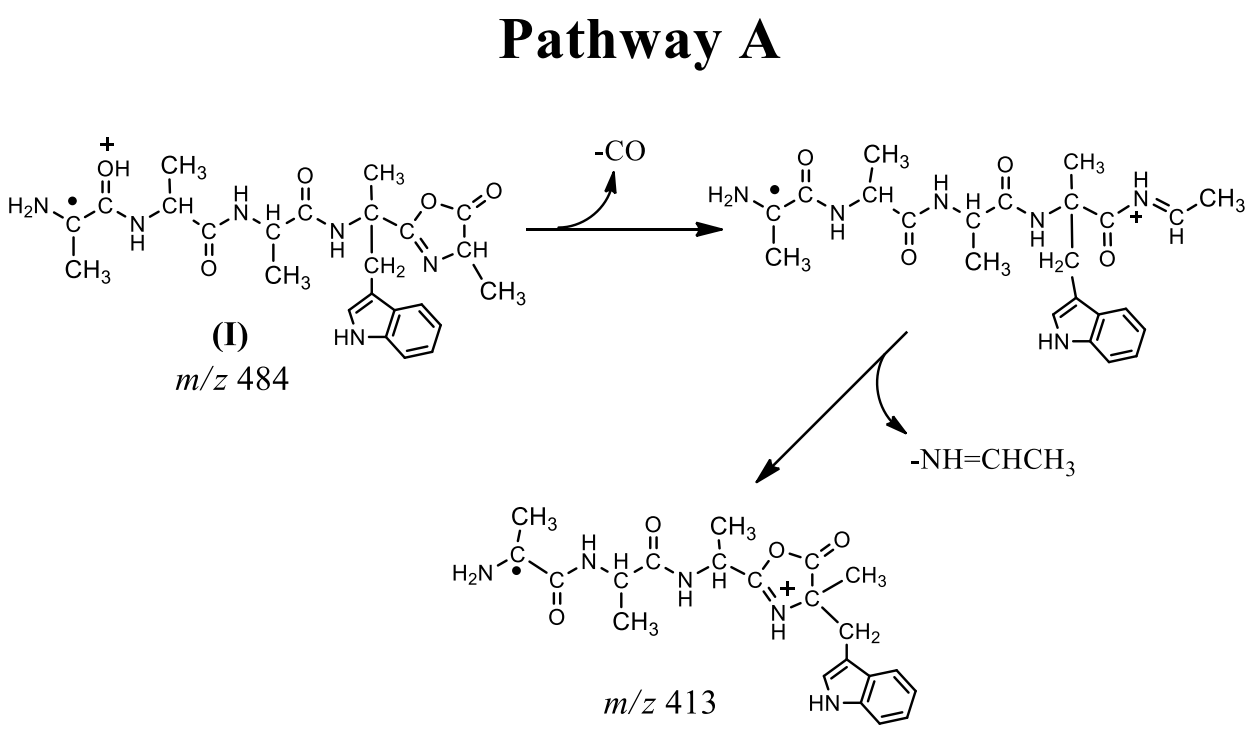

Scheme 4.1 Proposed mechanism for the loss of one residue from the C-terminus for the $[A_4W_{\alpha\text{-}Me}]^{\bullet+}$ ions.

4.2.3 Loss of oxazolone with a radical and water

The $[b_5 - H]^{\bullet+}$ ion showed a loss of 116 Da only when the α-methyltryptophan is at the fourth position, which corresponds to a loss of the oxazolone ring with a radical and a water molecule. This is analogous to the loss of 117 Da from the $[b_5]^+$ ions containing α-methyltryptophan. Thus, we propose similar mechanism for the loss of 106 Da from the ion $[AAAW_{\alpha\text{-Me}}A_{oxa}]^{\bullet+}$, which is described as pathway B in **Figure 4.2**. Starting from the captodative structure **(I)**, HAT from the β-carbon of the α-methyltryptophan side chain changes the radical center to be a β-radical. Then, a homolytic cleavage of the C_α-C bond between the α-methyltryptophan residue and the oxazolone ring results in a loss of the oxazolone ring with a radical (98 Da), contrasts to the closed-shell structure (99 Da) being lost from the $[b_5]^+$ ion in its loss of 117 Da. A six-membered ring is formed via nucleophilic attack by the indole ring to the closest carbonyl carbon, where the carbonyl oxygen is protonated. After proton transfer, a water molecule is quickly lost, and a conjugated three-ring system is formed. The final product is the same ion at *m/z* 368 that has been observed in CID of the closed-shell $[A_4W_{\alpha\text{-Me oxa}} + H]^+$ ions after a loss of 117 Da.

Pathway B

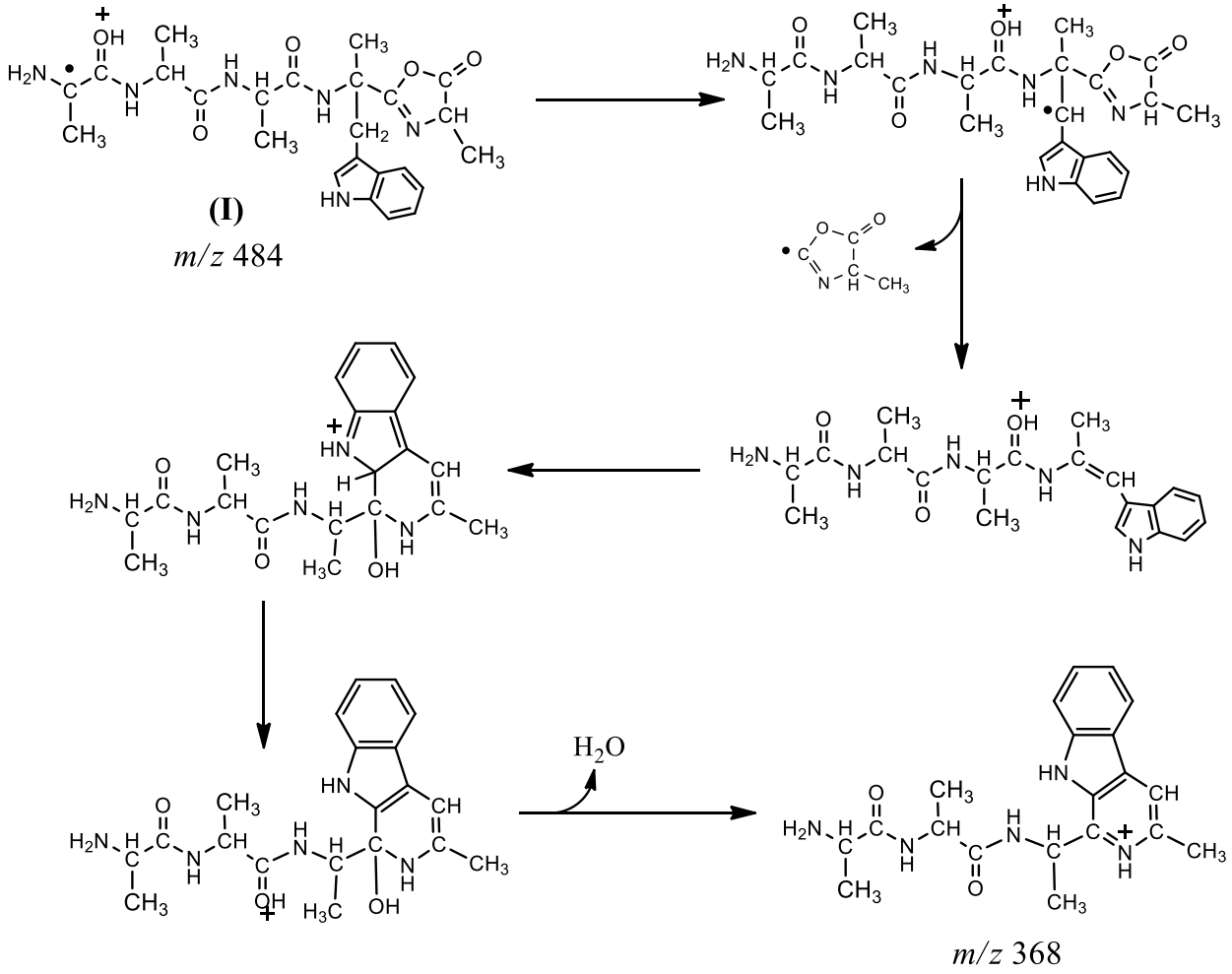

Scheme 4.2 Proposed mechanism for the loss of 116 Da, which is a loss of the oxazolone ring radical and a water molecule, from $[AAAWA_{oxa}]^{\bullet+}$ ion.

4.2.4 Loss of side chain as a radical

The side chain loss from the CID of the $[b_5 - H]^{\bullet+}$ ions is the loss of an open-shell fragment with the radical (130 Da), contrasts to the loss of a closed-shell fragment (129 Da) from CID of the peptide radical cation. Proposed mechanism for this loss is described in pathway C (**Scheme 4.3**). The $[b_5 - H]^{\bullet+}$ first migrates both the charge and the radical to the indole ring. Then, the C_α-C_β bond is cleaved, and the side chain with the radical is lost. This produces the ion at *m/z* 354 with a protonated imine on the backbone.

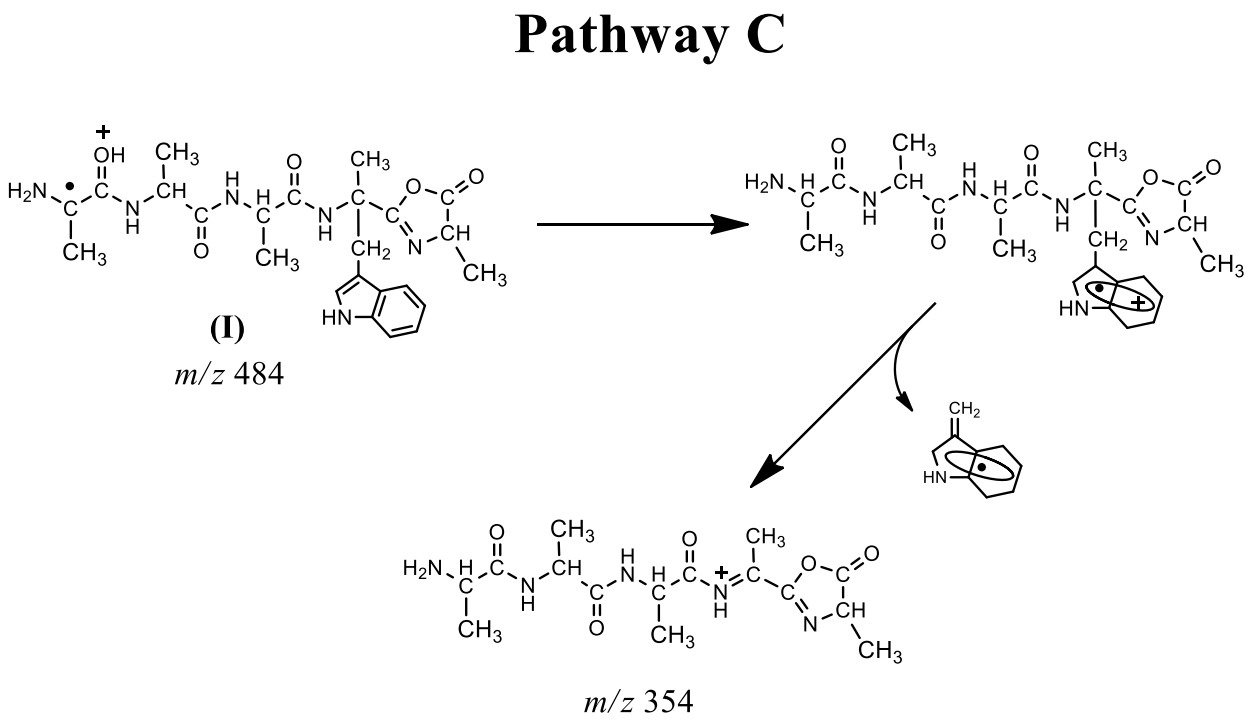

Scheme 4.3 Proposed mechanism for the loss of the side chain radical from the $[A_4W_{\alpha\text{-Me oxa}}]^{\bullet+}$ ions.

4.2.5 Loss of dialanine oxazolone with a radical

Isotopically-labeled $[AAAW_{\alpha\text{-}Me}A_{oxa}]^{\bullet+}$ ions clearly indicated that the loss of dialanine with a radical (141 Da) is from the N-terminus, and forms the most dominant peak in the spectrum. This is also one of the reasons that led us to believe that the radical center of the $[b_5 - H]^{\bullet+}$ ion before dissociation is located at the N-terminus. The proposed pathway D begins with the captodative structure **(I)** (**Scheme 4.4**). Then, a cleavage of the second amide bond initially creates two oxazolone structures in a solvated complex. Next, a proton transfer to the C-terminal fragment occurs due to the higher proton affinity of the α-methyltryptophan residue, followed by dissociation of the complex. The final product shown in the spectra would be a $[b_3]^+$ ion from the C-terminus of the original sequence, which corresponds to a loss of dialanine radical from the N-terminus.

Pathway D

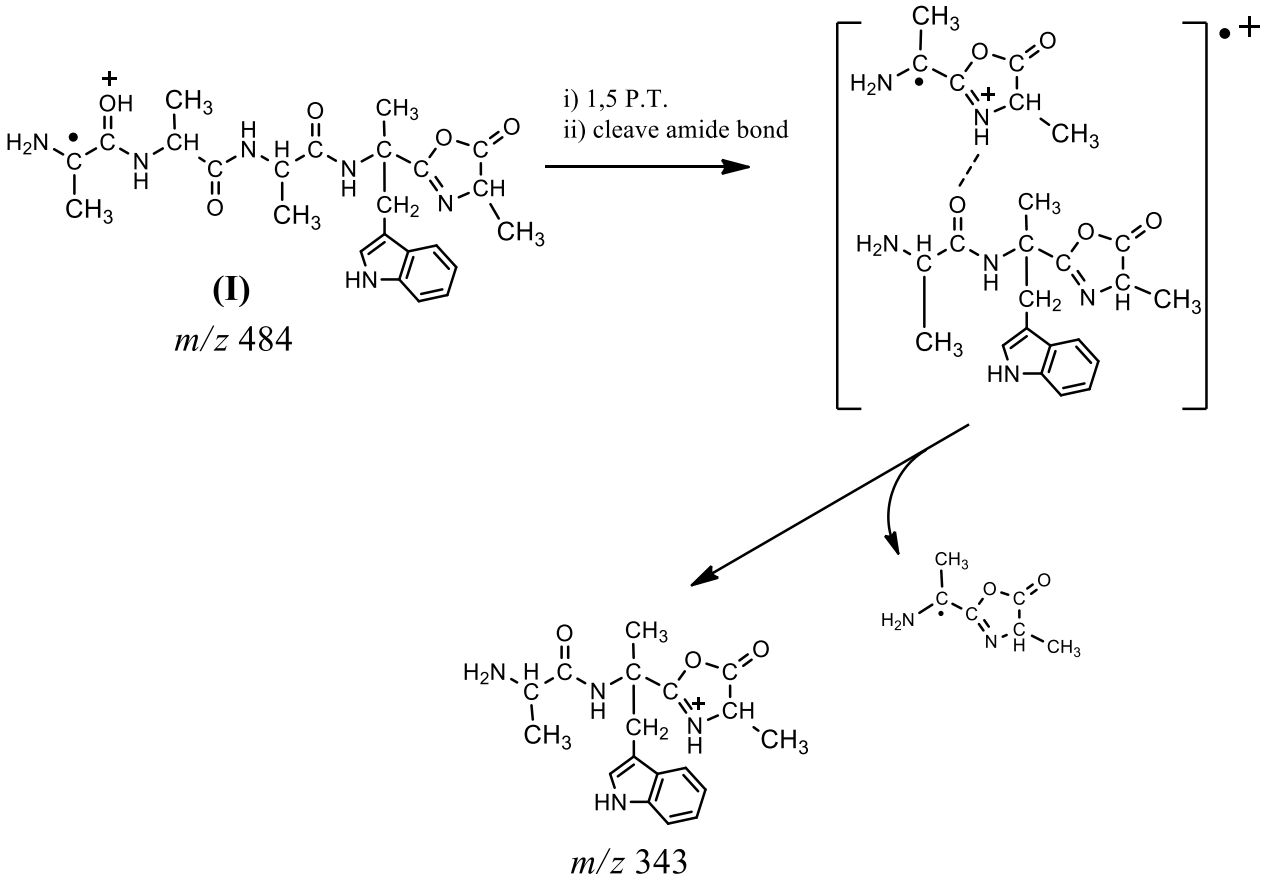

Scheme 4.4 Proposed mechanism for the loss of dialanine radical from the N-terminus of the $[A_4W_{\alpha\text{-}Me}]^{\bullet+}$ ions.

4.2.6 Loss of imine-amides

Loss of an imine-amide by cleavage of the N-C_α bond of the residue at the N-side of the α-methyltryptophan residue is another pattern in the CID of the $[A_4W_{\alpha\text{-Me oxa}}]^{\bullet+}$ ions. Such dissociation pattern is novel in CID of b-type ions, which implies that the α-methyltryptophan residue may play a role in the dissociation mechanism. A proposed mechanism for the loss of imine-amides is described in **Scheme 4.5** as pathway E. Structure **(I)** first forms a solvated complex of two fragments, after a homolytic cleavage of the N-C_α bond of the residue at the N-side of the α-methyltryptophan residue. This initially forms a charged fragment from the N-terminus, and the C-terminal fragment with a radical located at the α-carbon of the alanine residue on the N-terminus of the α-methyltryptophan residue. Next, in the C-terminal fragment, a HAT occurs from the β-carbon of the α-methyltryptophan residue to the α-carbon of the alanine residue at the N-terminus, migrating the radical center to the β-carbon. This is followed by a proton transfer from the N-terminal fragment to the C-terminal fragment, and produces the ion at *m/z* 327 shown in the CID spectra.

The next part is a further loss of 116 Da from the ion at *m/z* 327, which follows the mechanism described previously. Homolytic cleavage of the C_α-C bond results in the loss of the oxazolone ring with the radical (98 Da). This is immediately followed by a six-membered ring formation and a loss of a water molecule. The resulting product is a stable three-ring structure at *m/z* 211.

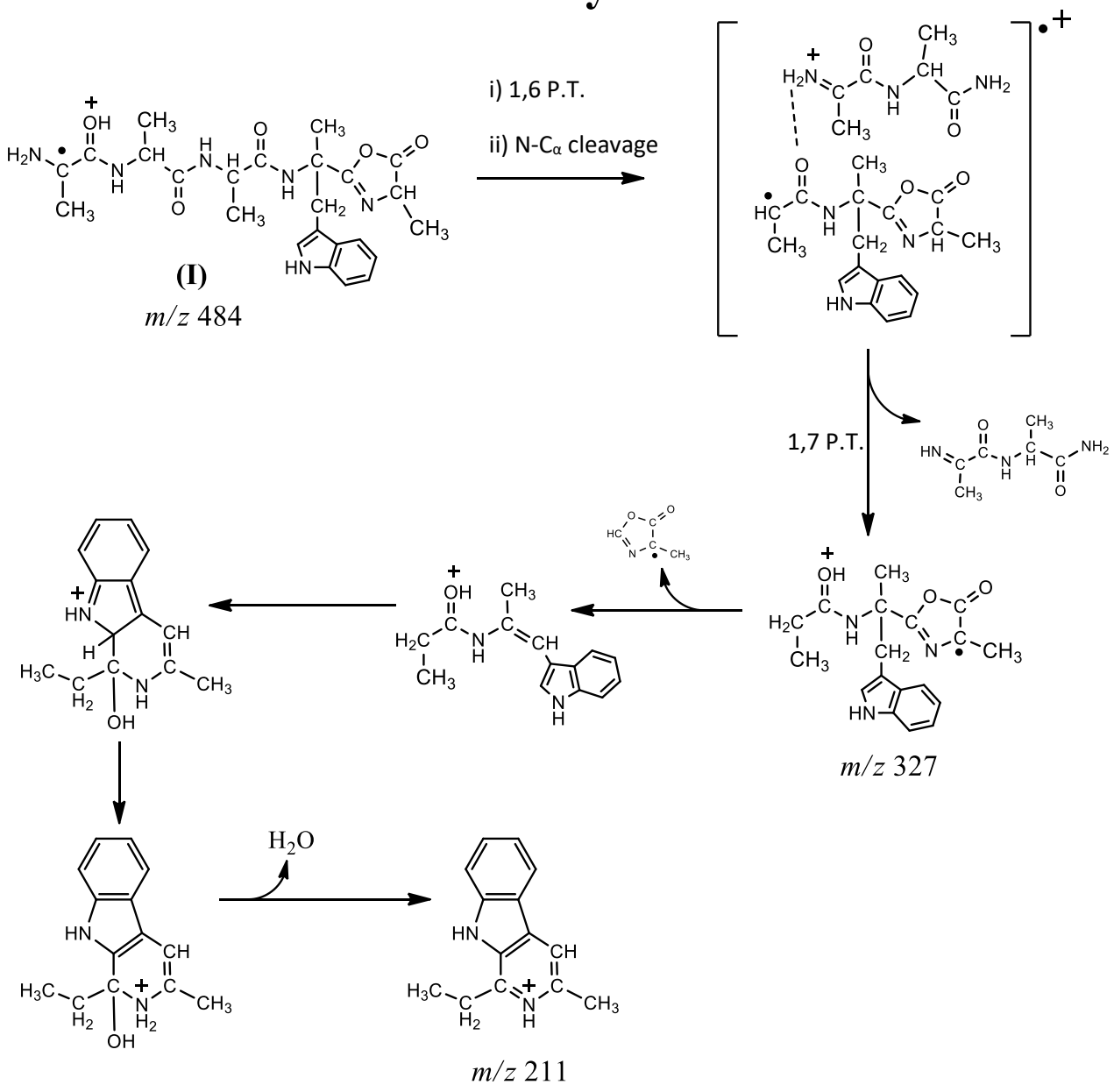

Scheme 4.5 Proposed mechanism for the loss of imine-amides from the N-terminus of the $[A_4W_{\alpha\text{-}Me}]^{\bullet+}$ ions, followed by a further loss of 116 Da.

4.3 Summary

We have learned that the fragmentation of α-methyltryptophan-containing hexapeptides results from cleavages of the bonds around the α-carbon of the α-methyltryptophan residue, due to steric crowding. As a result, these peptide radical cations mainly produces a series of $[z_m - H]^{\bullet+}$ ions, and a loss of the 129 Da closed-shell fragment of the tryptophan side chain. The $[b_5 - H]^{\bullet+}$ ions generated in the CID spectra of these peptide radical cations are in very low abundance.

The marked difference for the dissociation of the $[b_5 - H]^{\bullet+}$ ions derived from α-methyltryptophan-containing peptides is that there is no sequence scrambling. This means that CID of the $[b_5 - H]^{\bullet+}$ ions with the hetero-residue at different positions produce non-identical spectra, and fragment ions shown in these spectra have characteristic information from the original sequence, as indicated from isotopically-labeled peptides. For example, loss of one residue is unambiguously from the C-terminus of the original sequence. Energy-resolved breakdown curve of the ion suggested that loss of dialanine radical and loss of the tryptophan side chain radical have the lowest energy barriers. It also indicated that the after the $[AAAW_{\alpha\text{-}Me}A_{oxa}]^{\bullet+}$ ion loses an imine-amide from the N-terminus, it can further lose 116 Da, which is the loss oxazolone ring as a radical and a water molecule.

The loss of 116 Da is also present in the CID spectra of the $[b_5 - H]^{\bullet+}$, but only form the sequence $[AAAW_{\alpha\text{-}Me}A_{oxa}]^{\bullet+}$. This is analogous to the loss of 117 Da from the analogous closed-shell $[b_5]^+$ ions. The fact that the loss of 116 Da is only present in CID of the sequence $[AAAW_{\alpha\text{-}Me}A_{oxa}]^{\bullet+}$ further supported that the proposed mechanism for the loss of 117 Da from the analogous closed-shell $[b_5]^+$ ions begins with the ion $[AAAW_{\alpha\text{-}Me}A_{oxa} + H]^+$ after sequence scrambling.

CHAPTER 5: Fragmentations of $[b_5 - H]^{\bullet+}$ Ions Containing Tyrosine or Methionine Residues

5.1 Dissociation of $[b_5 - H]^{\bullet+}$ radical cations

In the ongoing study of sequence scrambling in $[b_5 - H]^{\bullet+}$ ions, we have learned that ions derived from tryptophan-containing hexapeptides ($[A_4W_{oxa}]^{\bullet+}$) demonstrate complete sequence scrambling, with one resulting sequence ($[AAAAW_{oxa}]^{\bullet+}$) that dissociates (**Figure 3.3**).[59] The ion $[AAAAW_{oxa}]^{\bullet+}$ is proposed to have the radical center located at the α-carbon of the tryptophan residue in the oxazolone ring, which induces fragmentations. In this thesis, we have explored the $[b_5 - H]^{\bullet+}$ ion in the same way, but with a methyl group located at the α-carbon of the tryptophan residue. Here, we noticed the opposite behavior. The CID spectra of isomers of $[A_4W_{\alpha\text{-Me oxa}}]^{\bullet+}$ are non-identical, and clearly showed no evidence of rearrangements from the fragments based on isotopic labeling experiments. This is due to the captodative radical located at the N-terminus of the ion, which reduces the nucleophilicity of the N-terminal nitrogen and prevents the ion from undergoing head-to-tail macrocyclization. The $[A_4W_{oxa}]^{\bullet+}$ and $[A_4W_{\alpha\text{-Me oxa}}]^{\bullet+}$ ions provided consistent results that explain when and why $[b_5 - H]^{\bullet+}$ ions scramble.

On the other hand, there is a previous study on the $[A_4G_{oxa}]^{\bullet+}$ ions, generated by cleavage of the side chain from $[A_5W]^{\bullet+}$ ions followed by further CID, which initially generated a radical at the α-carbon of the glycine residue (**Figure 5.1**).[51] However, this system did not follow either one of the trends mentioned above, and showed both evidences for isomerization and for no isomerization, based on CID of the different sequences and isotopically-labeled peptides. In addition, we further studied the $[A_4Y_{oxa}]^{\bullet+}$ and $[A_4M_{oxa}]^{\bullet+}$ ions to further explore $[b_5 - H]^{\bullet+}$ ions in

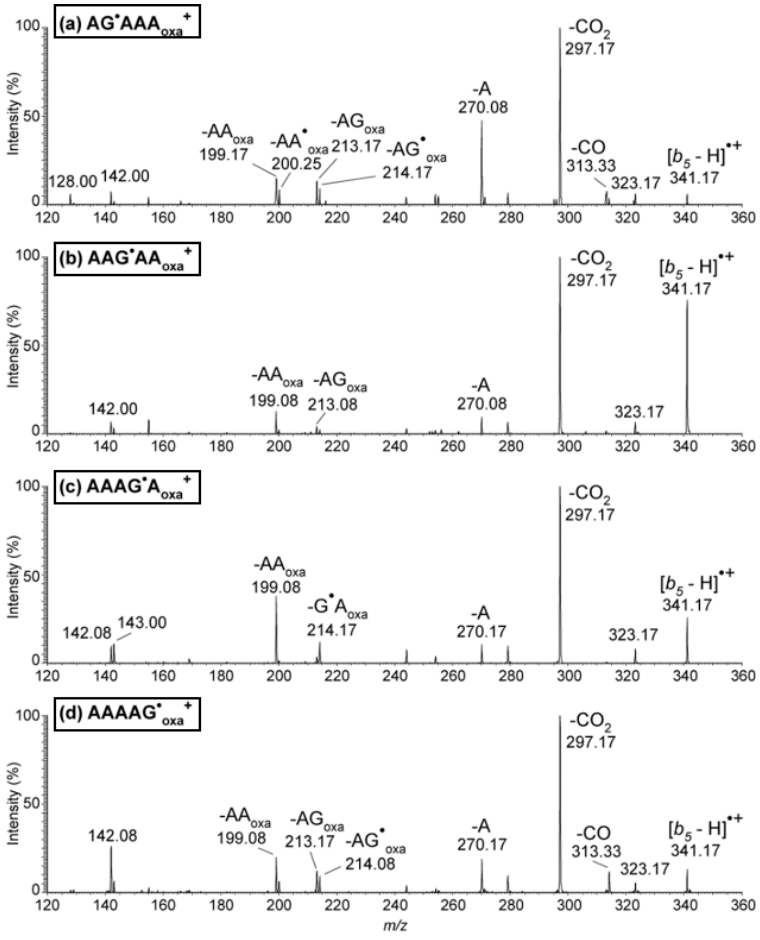

Figure 5.1 CID spectra of the $[A_4G_{oxa}]^{\bullet+}$ ions, with the glycine residue at different positions. Figure adapted from Lau et. al.[51]

different systems, looking for similarities between the different systems. The $[A_4Y_{oxa}]^{\bullet+}$ ions were generated by CID of the hexapeptide radical cations, which was generated as described in earlier studies (**Figure 5.2**).[85] We note that the $[A_4M_{oxa}]^{\bullet+}$ ions were generated directly from CID of [hexapeptide + Cu(II) + (18-crown-6)]$^{\bullet 2+}$ complex instead of from the hexapeptide radical cation $[A_4MG]^{\bullet+}$, due to the absence of the peptide radical cation in the CID of the complex shown in **Figure 5.3**. Also note that for additional confirmation of the $[b_5 - H]^{\bullet+}$ ion, the peptide used in **Figure 5.3 d)** has a methylated alanine residue at the C-terminus, in contrast to the glycine residue for other peptides used in **Figure 5.3 a)**, **b)**, and **c)**, while the $[b_5 - H]^{\bullet+}$ ion with the same *m/z* 415 was still observed and isolated.

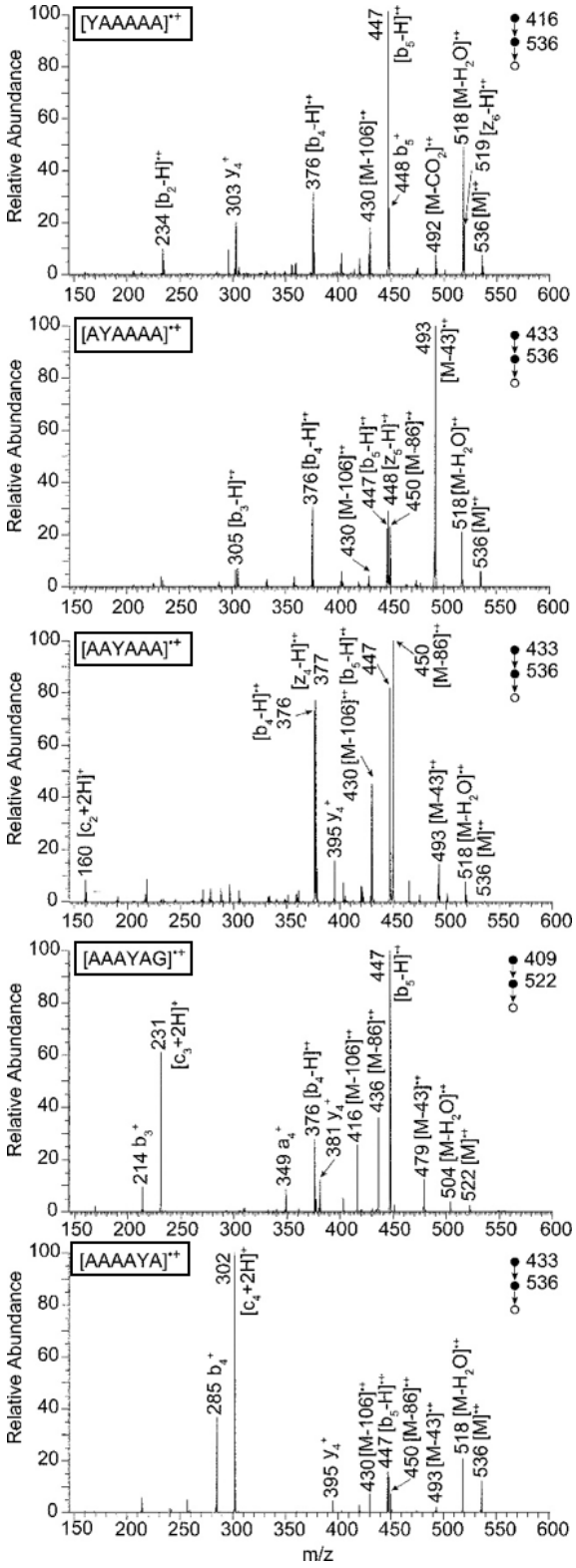

Figure 5.2 CID spectra of tyrosine-containing hexapeptides. Figure adapted from Mädler et. al.[85]

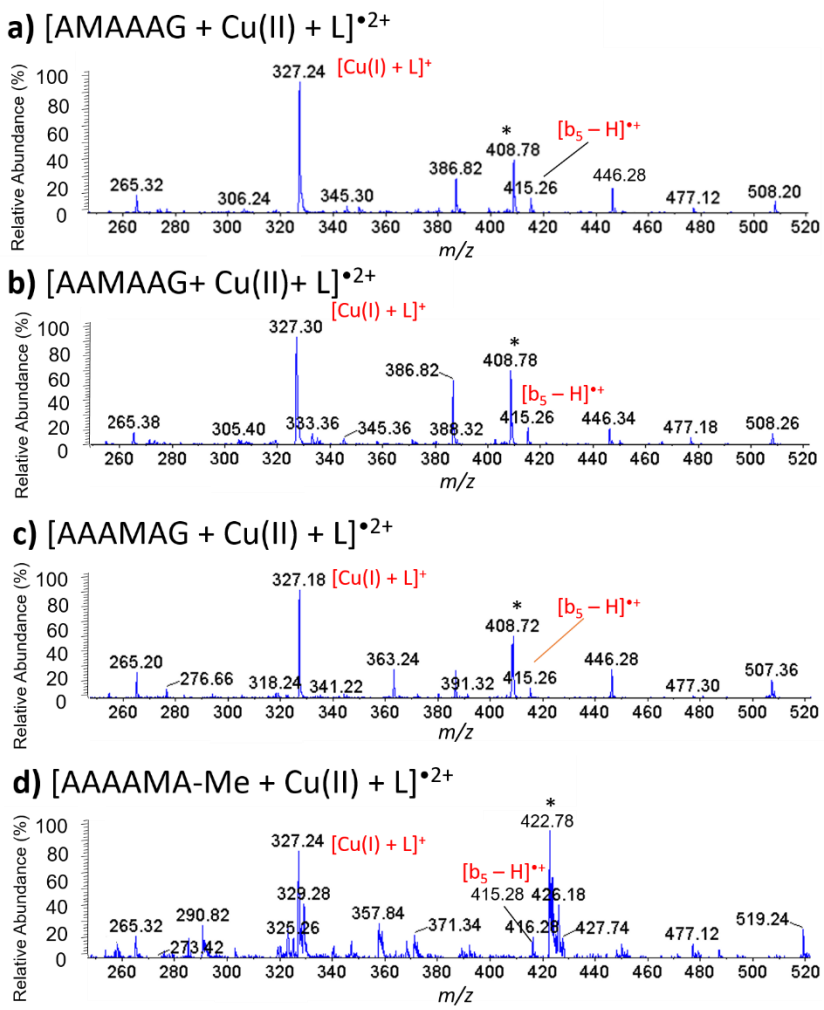

Figure 5.3 CID spectra of the [pep + Cu(II) + L]$^{\bullet+}$ complexes, where "L" refers to the ligand used, 18 crown 6; and hexapeptides refers to "pep" refers to hexapeptides with the methionine residue at varying positions.

CID spectra of $[A_4Y_{oxa}]^{\bullet+}$ ions are given in **Figure 5.4**. In contrast to the CID of the closed-shell $[b_5]^+$ ions of $[A_4Y_{oxa}]^+$, which exhibited complete scrambling, the $[b_5 - H]^{\bullet+}$ radical cations showed similarities across different sequences, but are non-identical.[54] The spectra consist of the

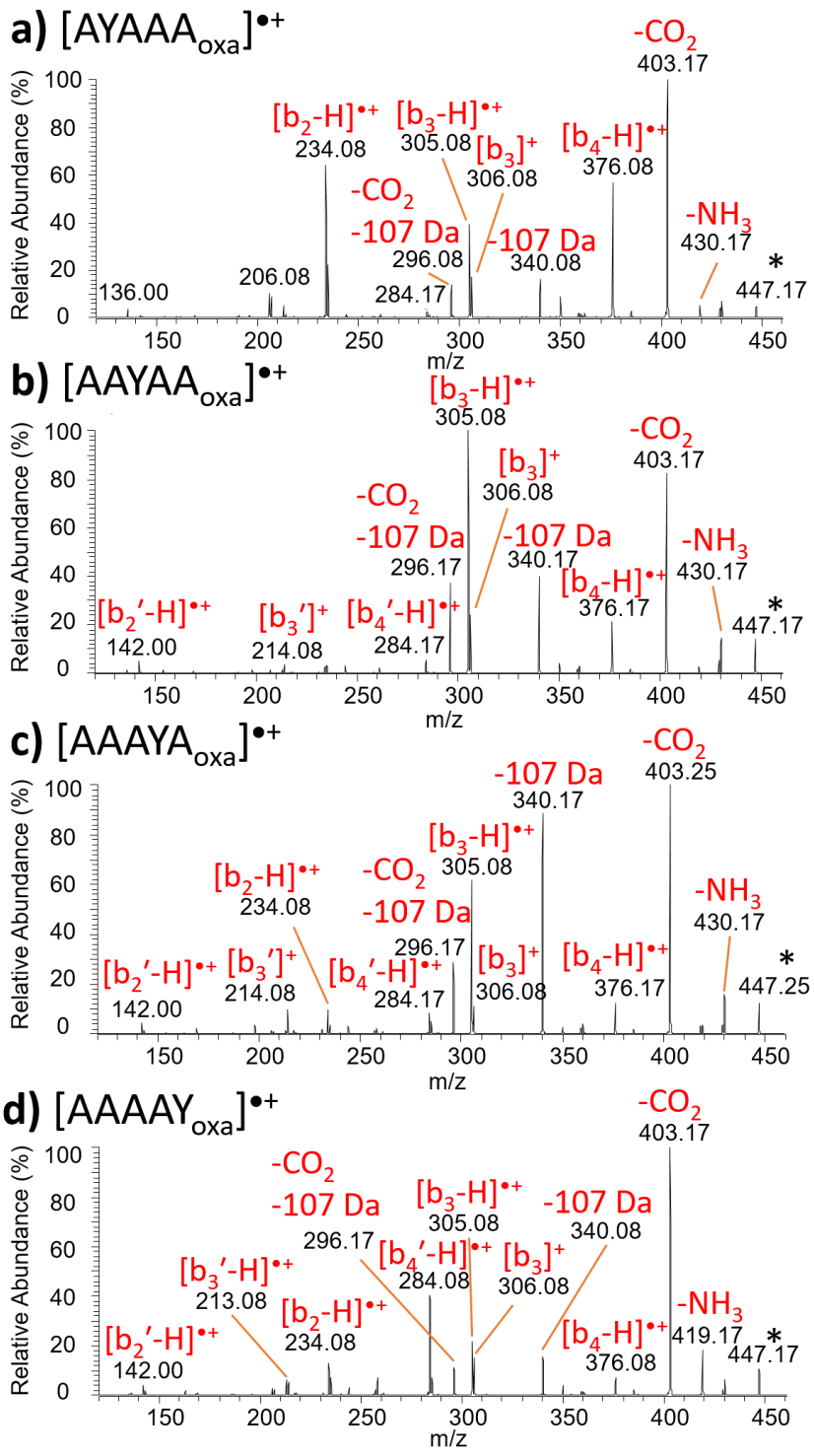

Figure 5.4 CID spectra of the $[A_4Y_{oxa}]^{\bullet+}$ ions, with the tyrosine residue at different positions. "107 Da" corresponds to the radical structure of the tyrosine side chain.

same fragment ions across different sequences, but relative abundances of certain ions differ drastically between different sequences. For example, the $[b_2 - H]^{\bullet+}$ ion resulting from a loss of three alanine residues at *m/z* 234 is at around 60% relative abundance in the CID of $[AYAAA_{oxa}]^{\bullet+}$ ion, while the same ion in the CID spectrum of $[AAYAA_{oxa}]^{\bullet+}$ or $[AAAYA_{oxa}]^{\bullet+}$ ion is at less than 1% abundance. The $[b_4' - H]^{\bullet+}$ ion resulting from a loss of the tyrosine residue (*m/z* 284) is present in all spectra, but at different abundances, which suggests that some rearrangement occurred before dissociation.

The loss of CO_2 (*m/z* 403) is a dominant peak in most of the spectra. This observation is consistent with CO_2 loss in the spectra of the $[A_4G_{oxa}]^{\bullet+}$ ions; it differs from the spectra of both the $[A_4W_{oxa}]^{\bullet+}$ ions and $[A_4W_{\alpha\text{-Me oxa}}]^{\bullet+}$ ions, where CO_2 loss is always in negligible abundance. In addition to the dominant loss of CO_2, other fragments include the loss of one, two, and three alanine residues, which becomes the $[b_4 - H]^{\bullet+}$ (*m/z* 376) , $[b_3 - H]^{\bullet+}$ (*m/z* 305), and $[b_2 - H]^{\bullet+}$ ions (*m/z* 234). A $[b_3]^+$ ion from a loss of dialanine radical (*m/z* 306) is also present in all spectra, with the complementary $[b_2' - H]^{\bullet+}$ ion (*m/z* 142). There is a loss of 107 Da in all spectra (*m/z* 340), which corresponds to the loss of the tyrosine side chain radical. The complementary ion of the $[b_2 - H]^{\bullet+}$ ion, which is the $[b_3']^+$ ion from losing one tyrosine and one alanine residue with the radical (*m/z* 214) is also present at low abundance in some of the spectra.

CID spectra of $[A_4M_{oxa}]^{\bullet+}$ ions are summarized in **Figure 5.5**. The CID of these ions also have the same fragment ions across different sequences, but again the relative abundances of the fragment ions are different, making the spectra non-identical. As the $[A_4Y_{oxa}]^{\bullet+}$ ions, loss of CO_2 in the CID of $[A_4M_{oxa}]^{\bullet+}$ ions is also the dominant peak in all spectra. Losses of alanine residues, which form the series of $[b_n - H]^{\bullet+}$ ions (n = 4,3 and 2) are also present. Analogous to the $[A_4Y_{oxa}]^{\bullet+}$ ions, the complementary pair of $[b_2' - H]^{\bullet+}$ (*m/z* 142) and $[b_3]^+$ ions (*m/z* 274) are present in the

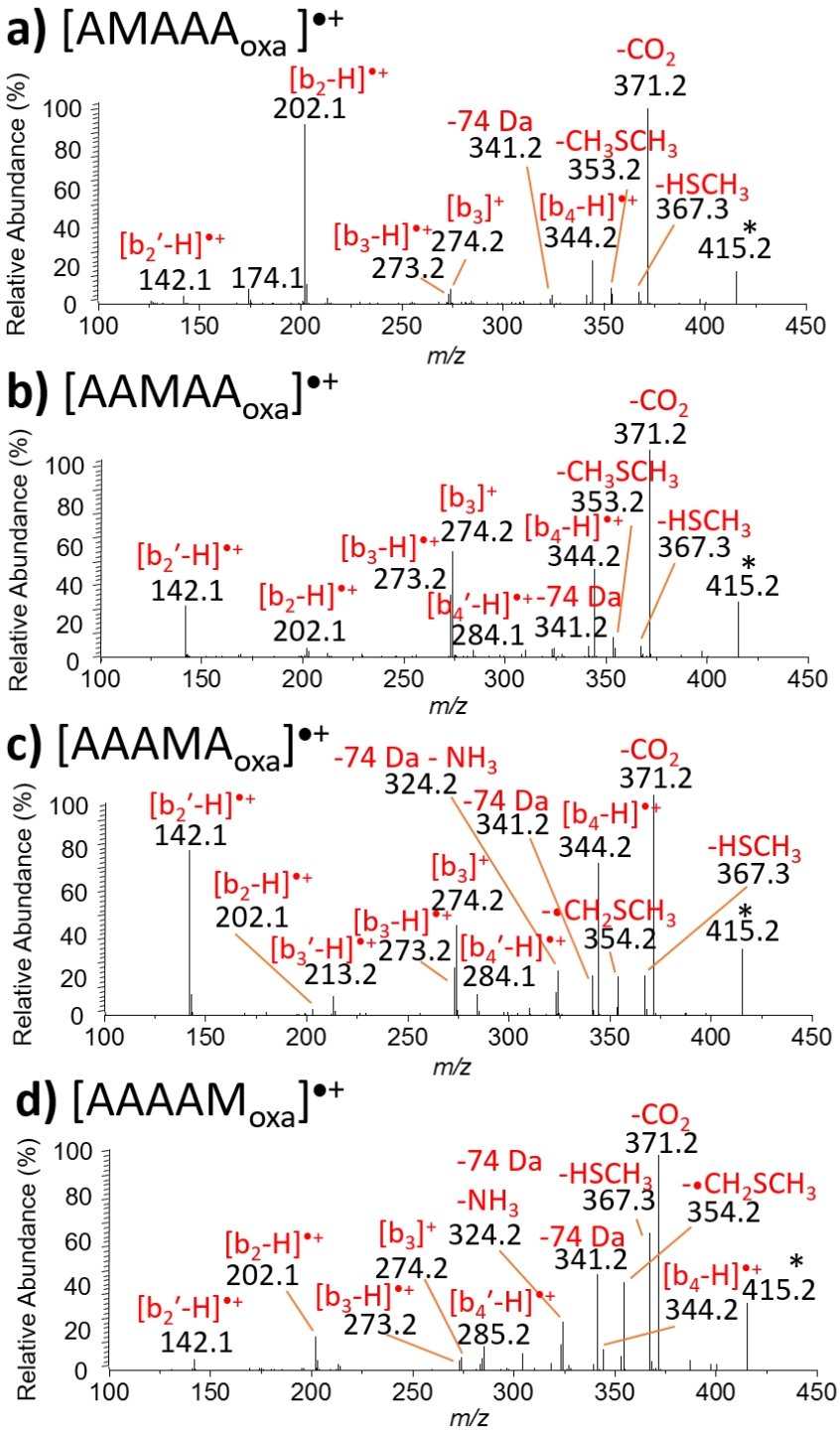

Figure 5.5 CID spectra of the $[A_4M_{oxa}]^{\bullet+}$ ions, with the methionine residue at different positions.

CID of the $[A_4M_{oxa}]^{\bullet+}$ ions. Also, the corresponding $[b_4' - H]^{\bullet+}$ ion (*m/z* 284) and $[b_3' - H]^{\bullet+}$ ion (*m/z* 213) are also present at small abundance. The $[A_4M_{oxa}]^{\bullet+}$ ions showed a loss of a closed-shell side chain fragment of 74 Da (*m/z* 341), $H_3SCH{=}CH_2$. In addition, $[AMAAA_{oxa}]^{\bullet+}$ and $[AAMAA_{oxa}]^{\bullet+}$ also lose CH_3SCH_3 (giving an ion at *m/z* 353), while $[AAAMA_{oxa}]^{\bullet+}$ and $[AAAAM_{oxa}]^{\bullet+}$ showed a loss of $\bullet CH_2SCH_3$ (giving an ion at *m/z* 354).There is also a loss of $HSCH_3$ (giving an ion at *m/z* 367) from all sequences.

5.2 Information provided by isotopic labeling and breakdown diagram

5.2.1 CID of ^{18}O-labeled $[AAAYA_{oxa}]^{\bullet+}$ ions

The sequence AAAYAG was chosen to put ^{18}O label on all four different positions of alanine residues, and the CID spectra of the labeled $[AAAYA_{oxa}]^{\bullet+}$ ions, *m/z* 449, are summarized in **Figure 5.6**. The most notable observation here is the loss of CO_2. In all four spectra, the CO_2 lost consists of a mixture of the labeled and the unlabeled oxygen. When the label is on the first, second, or third residue, loss of CO_2 without the label is the dominant peak, followed by a minor loss of the labeled $^{18}O{=}C{=}O$ (~10% relative abundance) (**Figure 5.6 a), b), and c)**). When the label is on the fifth residue, the opposite is true, with the loss of $^{18}O{=}C{=}O$ being the dominant (**Figure 5.6 d)**). This suggests that there are some rearrangements of the $[b_5 - H]^{\bullet+}$ ions, and there is more than one structure that dissociates to give the CID spectra, at least for the loss of CO_2. However, the majority of fragment ions originate from the original sequence.

The *m/z* of the $[b_4 - H]^{\bullet+}$ ions showed loss of an unlabeled alanine residue had occurred when the label is on the first, second, or third residue. When the label is on the fifth residue, the loss is a

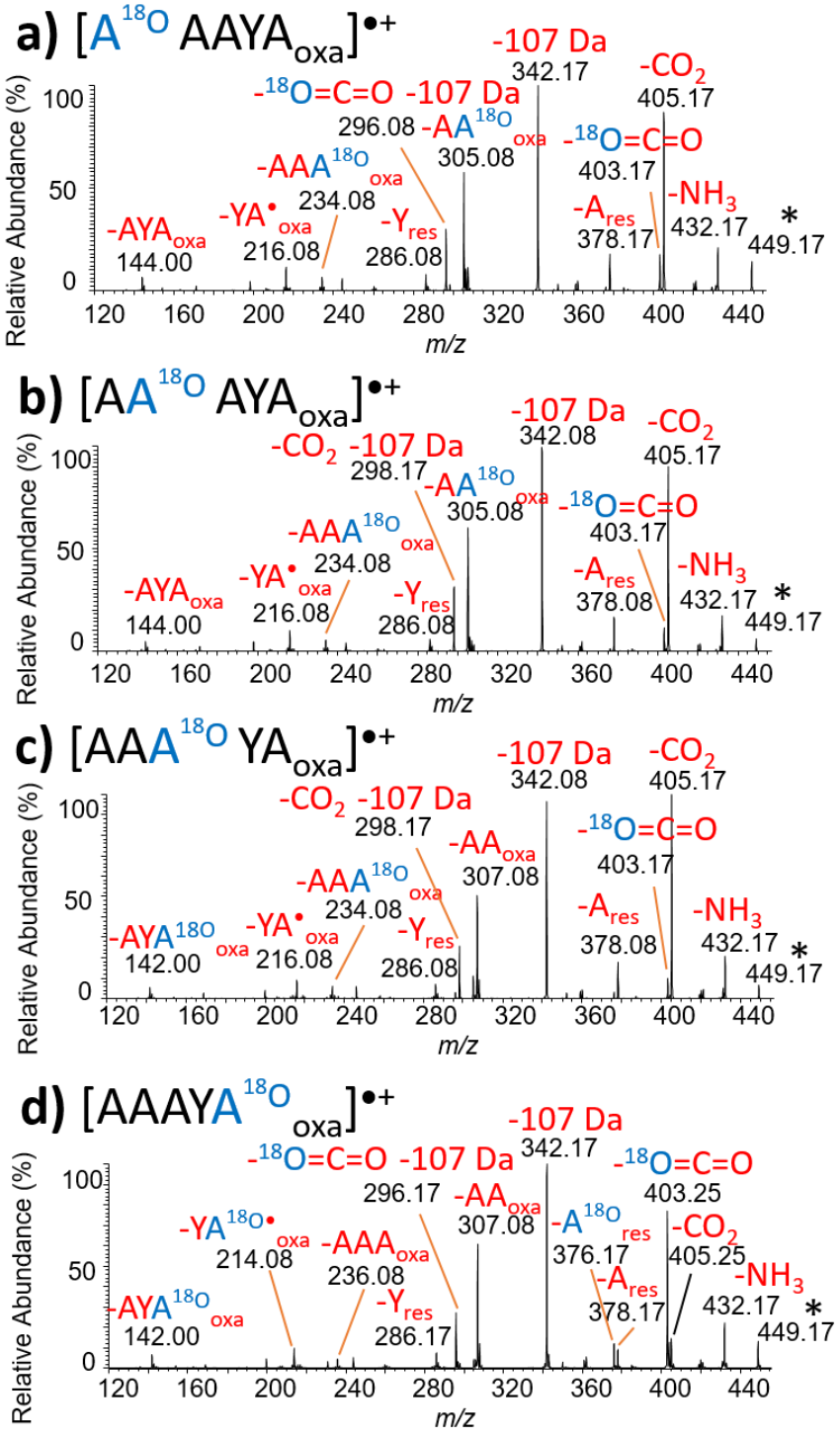

Figure 5.6 CID spectra of $[AAAYA_{oxa}]^{\bullet+}$ with ^{18}O label on different positions.

mixture of both the labeled and the unlabeled alanine, in approximately the same abundance (**Figure 5.5 d)**). This suggests that at least half of the $[b_4 - H]^{\bullet+}$ ions is from the original sequence. The $[b_3 - H]^{\bullet+}$ ion does not retain the label when the label is on the first or second residue, and retains the label when it is on the third or fifth residue. However, a minor mixture of the opposite (~10% relative abundance) is present in the spectra of $[A^{18O}AAYA_{oxa}]^{\bullet+}$ and $[AA^{18O}AYA_{oxa}]^{\bullet+}$. We can conclude that the majority of the two alanine residues being lost here are the first and second alanine residues from the N-terminus; with also a minor loss of the second and the third residues. The $[b_2 - H]^{\bullet+}$ ion only retained the label when it is on the fifth residue; as well, the complementary $[b_3']^{+}$ ion has lost the label only when the fifth residue is labeled. The spectra of the $[b_2' - H]^{\bullet+}$ ions showed that the label is retained when it is on the first or second residue from the N-terminus. Since the relative abundance of these two fragment ions are both very low (< 5%), any minor mixture of these ions would be in negligible abundance.

The fragment ions after the dominant loss of CO_2 from $[AAAYA_{oxa}]^{\bullet+}$ were further selected for CID, and the spectra were given in **Figure 5.7**. The ion can further lose two or three alanine residues, as well as the side chain, but the most dominant fragment from this ion is the loss of dialanine amide. Based on the spectra, when the first or second residue was labeled, the label was lost with the loss of dialanine amide (*m/z* 244). The ion selected from $[AAAYA^{18O}_{oxa}]^{\bullet+}$ has lost the label from the initial loss of CO_2 (**Figure 5.7 d)**). Only the fragment ion from $[AAA^{18O}YA_{oxa} - CO_2]^{\bullet+}$ retained the label (*m/z* 246) after the loss of dialanine amide (**Figure 5.7 c)**). This indicates that, after the loss of CO_2 from $[AAAYA_{oxa}]^{\bullet+}$, it further loses dialanine amide from the N-terminus, by cleavage of the N-C_α bond between the second and the third residue.

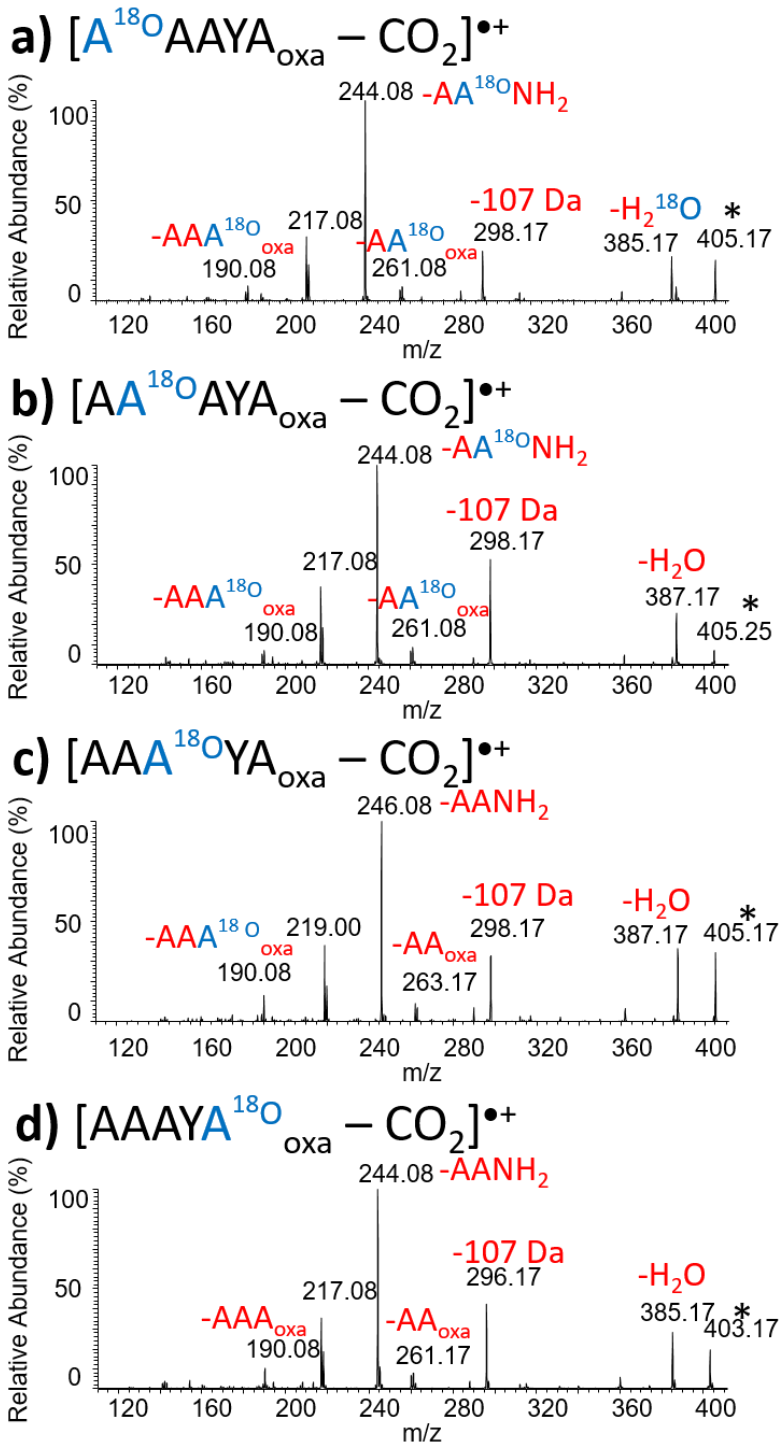

Figure 5.7 CID spectra of $[AAAYA_{oxa} - CO_2]^{\bullet+}$, with ^{18}O label on different positions. Note that the parent ion selected for **d)** has already lost the ^{18}O label from the initial CO_2 loss.

5.2.2 CID of CD_3- and ^{15}N-labeled $[AAAMA_{oxa}]^{\bullet+}$ ions

CD_3 and ^{15}N labels were both put on the sequence AAAMAG. Two peptides were synthesized, with the CD_3 and ^{15}N label on different positions as described in **Figure 5.8**, which covered all four alanine residues. Based on the spectra in **Figure 5.8**, it can be concluded that the loss of one alanine residue is from the C-terminus, and the loss of two alanine residues is from the N-terminus, from the original sequence of the $[AAAMA_{oxa}]^{\bullet+}$ ion. There are also minor evidences indicating loss of one or two alanine residues from the sequence $[AAMAA_{oxa}]^{\bullet+}$: a minor peak for loss of an ^{15}N-labeled alanine residue exists in CID of $[A^{15N}A^{D3}AMA_{oxa}]^{\bullet+}$ ion (**Figure 5.8 b)**); and there is also a minor peak for the loss of dialanine oxazolone with the ^{15N}N label from CID of $[AAA^{N15}MA^{D3}{}_{oxa}]^{\bullet+}$ ion (**Figure 5.8 c)**). The complementary pair of the $[b_2' - H]^{\bullet+}$ ion and the $[b_3]^+$ ion are unambiguously the results of a cleavage between the second and third residue from the N-terminus of $[AAAMA_{oxa}]^{\bullet+}$. The loss of three alanine residues ($[b_2 - H]^{\bullet+}$ ion) and the loss of a methionine residue and an alanine residue ($[b_3' - H]^{\bullet+}$ ion) both showed a mixture of peaks and are at very small abundance, thus cannot be used to draw conclusions.

The ions after loss of CO_2 from the two labeled $[AAAMA_{oxa}]^{\bullet+}$ ions have also been isolated for further fragmentation, and the CID spectra are given in **Figure 5.9**. CID of these ions revealed that the most dominant fragment is the loss of $\bullet CH_2SCH_3$ from the side chain (*m/z* 314). The only significant difference between the CID spectra of the two ions with labels on different positions

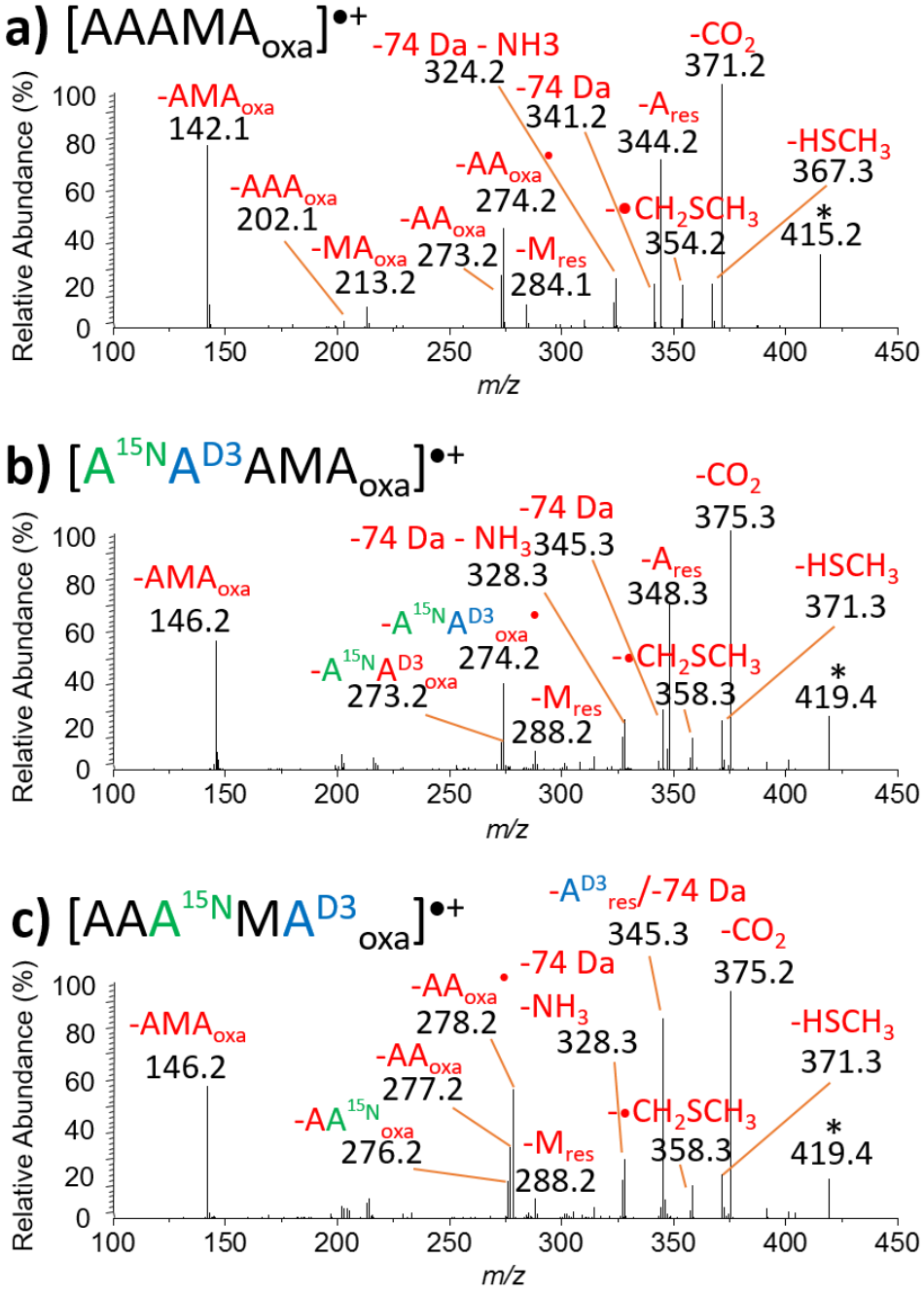

Figure 5.8 CID spectra of [AAAMA$_{oxa}$]$^{\bullet+}$, and the same sequence with CD_3 and ^{15}N label on different positions. "-74 Da" refers to loss of the closed-shell side chain fragment (CH_2CHSCH_3). Note that in **c)** the loss of CD_3-labeled alanine residue is isobaric with the loss of CH_2CHSCH_3.

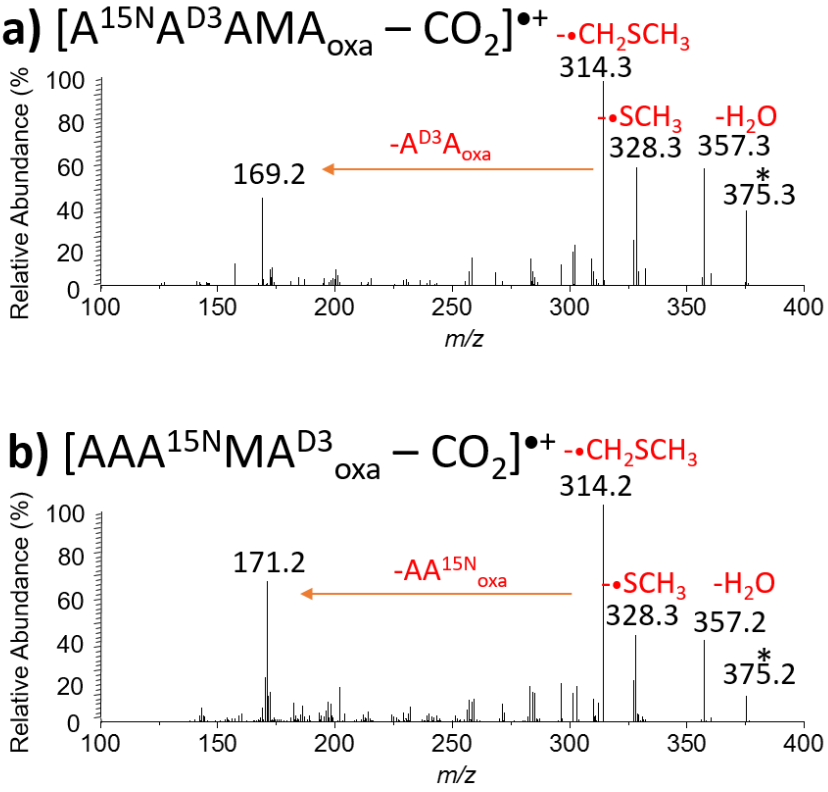

Figure 5.9 CID spectra of the ion $[AAAMA_{oxa} - CO_2]^{\bullet+}$ from the labeled peptides.

is the ion at *m/z* 169 from $[A^{15N}A^{D3}AMA_{oxa} - CO_2]^{\bullet+}$, versus the ion at *m/z* 171 from $[AAA^{15N}MA^{D3}{}_{oxa} - CO_2]^{\bullet+}$. This species was generated from dissociation of the most abundant ion in the spectrum, $[A_4M_{oxa} - CO_2 - \bullet CH_2SCH_3]^+$ (*m/z* 314), as illustrated by further isolation and CID of the ion (**Figure 5.10**). The former can be translated to a loss of two alanine residues with one CD_3 label (145 Da) from $[A_4M_{oxa} - CO_2 - \bullet CH_2SCH_3]^+$, while the latter is a loss of two alanine residues with one ^{15}N label (143 Da). From here, we can conclude that after the loss of CO_2 from $[A_4M_{oxa}]^{\bullet+}$, the ion most easily dissociates by losing $\bullet CH_2SCH_3$ from the side chain, and then further lose two alanine residues from the second and the third residue. The proposed mechanism

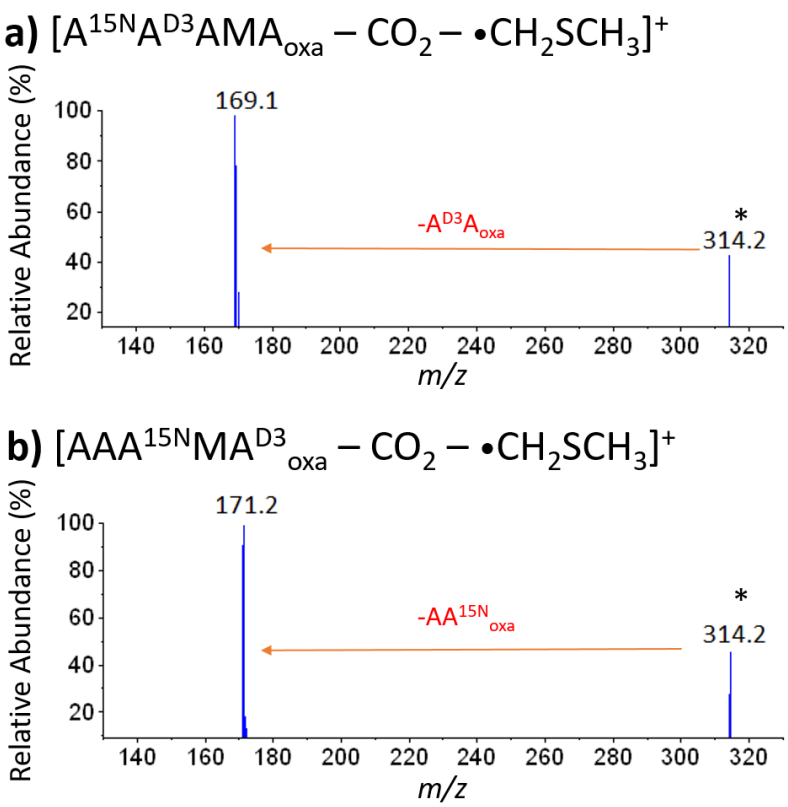

Figure 5.10 CID of the ion [AAAMA$_{oxa}$ – CO$_2$ - •CH$_2$SCH$_3$]$^+$ from the labeled peptides.

for this pathway is that loss of CO$_2$ from the [b$_5$ – H]$^{•+}$ ion is followed by a HAT, to generate a structure with the radical center at the N-terminal α-carbon (**Scheme 5.1**). This radical then attacks the beta-carbon of the methionine, which forms a macrocyclic structure and displaces the •CH$_2$SCH$_3$ fragment from the side chain via homolytic cleavage. This macrocyclic structure then re-opens at the N-terminal of the methionine residue, which exposes the two alanine residues that were originally in the middle of the ion [AAAMA$_{oxa}$]$^{•+}$ to the C-terminus. Finally, a stable six-member ring structure is formed by nucleophilic attack by the nitrogen atom from the N-terminus, and the two alanine residues that are now at the C-terminus are lost.

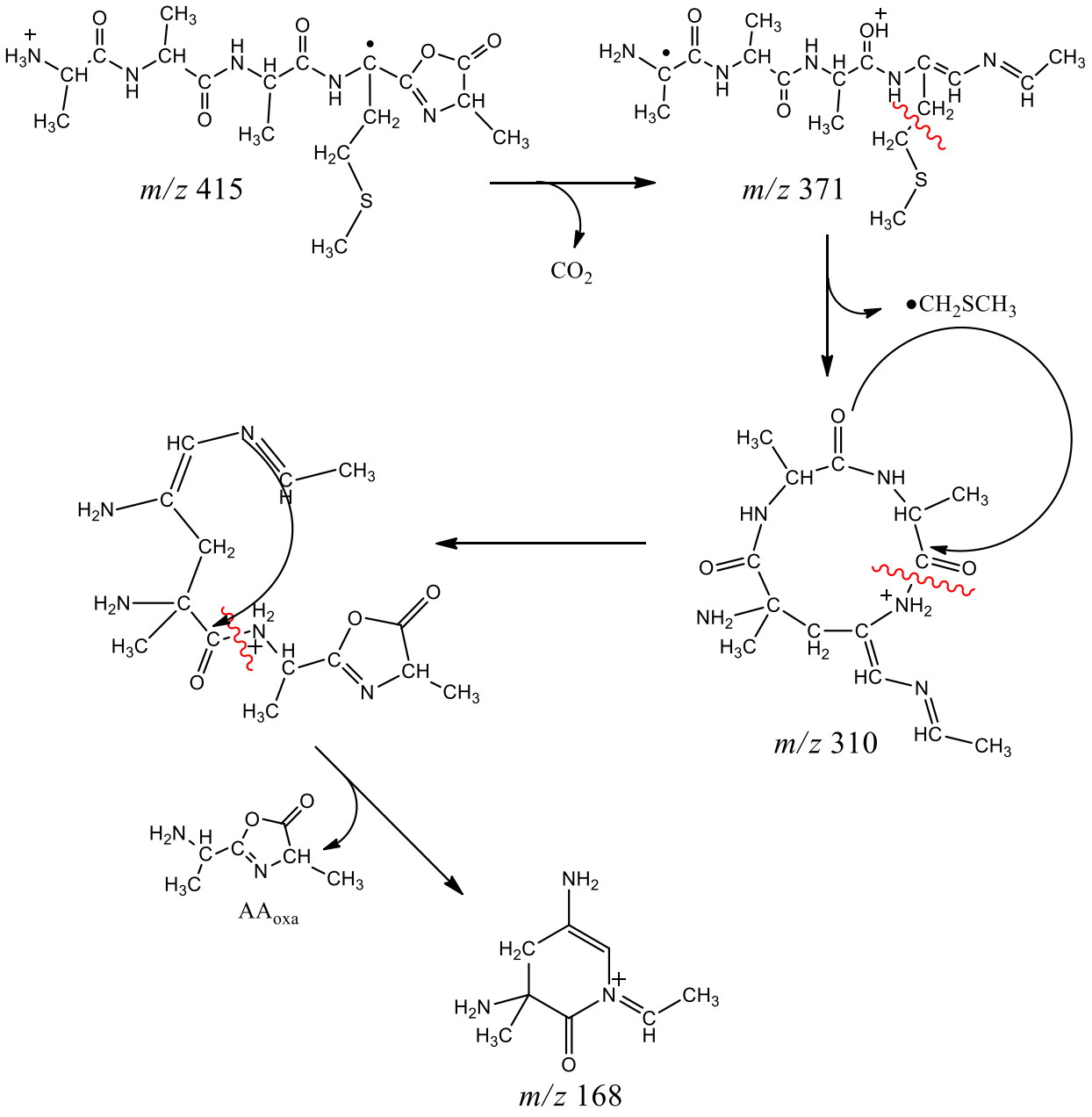

Scheme 5.1 Proposed mechanism for dissociation pathway after loss of CO_2 from $[A_4M_{oxa}]^{\bullet+}$.

5.2.3 Energy-resolved diagram of ion $[A^{15N}A^{D3}AMA_{oxa}]^{\bullet+}$

An energy-resolved breakdown diagram of the ion $[A^{15N}A^{D3}AMA_{oxa}]^{\bullet+}$ was generated and shown in **Figure 5.11**. The curve indicates that the loss of CO_2 has the lowest energy barrier, and is the most dominant fragment at all collision energies. At higher collision energies, the relative abundance for the loss of CO_2 begins to drop, and other fragments that require higher energy starts to increase.

The next most abundant fragment ions are the $[b_4 - H]^{\bullet+}$ ion and the $[b_2' - H]^{\bullet+}$ ion, which share similar abundance across all energies. However, the complementary ion for the $[b_2' - H]^{\bullet+}$ ion, which is the $[b_3]^+$ ion, lies below as the next most abundant ion. This indicates that the $AA_{oxa}^{\bullet}$ fragment must have a slightly higher proton affinity than the AMA_{oxa} fragment. The $[b_3 - H]^{\bullet+}$ ion has a relatively high onset energy compared to other fragment ions, but quickly increases in abundance at higher collision energy. From this particular breakdown diagram, the energy barrier for the loss of two alanine residues that produces the $[b_3 - H]^{\bullet+}$ ion is greater than that for the loss of one alanine residue, at all energies.

Below the $[b_3]^+$ ion, next most abundant ion, especially at lower collision energies, is the loss of the closed-shell side chain fragment, CH_2CHSCH_3 (74 Da). At higher energies, the fragment from a loss of CH_2CHSCH_3 plus NH_3 (91 Da) starts to increase rapidly. This possibly suggests that the mechanism leading to the loss of CH_2CHSCH_3 will lead to a further loss of an NH_3 at higher energy.

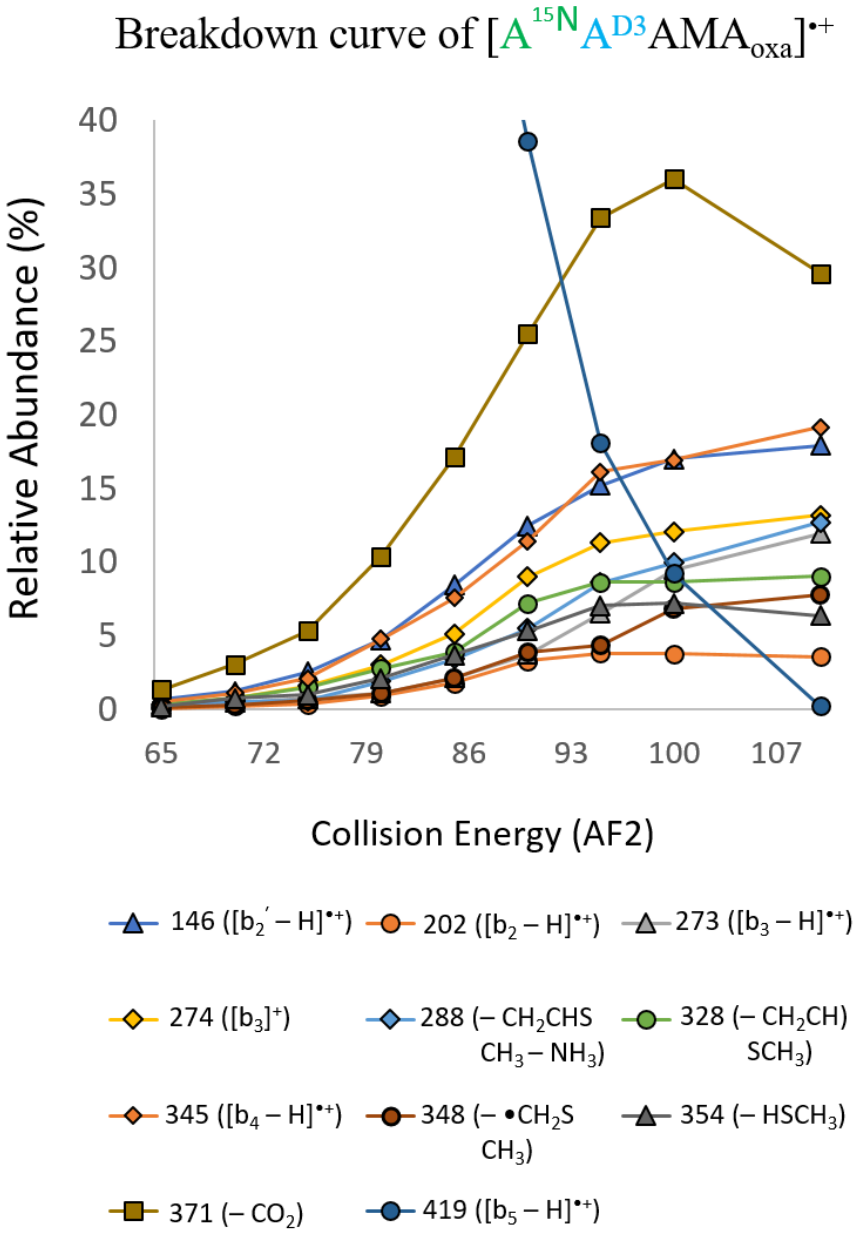

Figure 5.11 Energy-resolved breakdown diagram of the ion $[A^{15N}A^{D3}AMA_{oxa}]^{\bullet+}$;the CID spectrum is given in Figure 5.6 (b).

5.3 Discussions

Based on the CID spectra of $[A_4Y_{oxa}]^{\bullet+}$ and $[A_4M_{oxa}]^{\bullet+}$ ions, we noticed similarities in the two different series of $[b_5 - H]^{\bullet+}$ ions. These similarities can also be linked to the CID spectra of $[A_4G_{oxa}]^{\bullet+}$ ions that have been studied. In all of the three series, CID spectra produced from the $[b_5 - H]^{\bullet+}$ ion with the hetero-residue at different position are non-identical, with the same fragment ions but at different relative abundance. Labeling experiments have been done for each series. They all suggested that there is some of rearrangement, and that there is more than one structure undergoing dissociation when producing the CID spectra. This behavior is different from the $[A_4W_{oxa}]^{\bullet+}$ ions that fully rearranged into one common sequence before dissociation, and the $[A_4W_{\alpha\text{-Me oxa}}]^{\bullet+}$ ions that exhibit no rearrangements and dissociate from the original structure. Here we summarize the similarities and differences between the CID of $[A_4Y_{oxa}]^{\bullet+}$, $[A_4M_{oxa}]^{\bullet+}$, and $[A_4G_{oxa}]^{\bullet+}$, to conclude some general dissociation patterns in $[b_5 - H]^{\bullet+}$ ions.

5.3.1 The most dominant peak: loss of CO_2

In all of the $[A_4Y_{oxa}]^{\bullet+}$, $[A_4M_{oxa}]^{\bullet+}$, and $[A_4G_{oxa}]^{\bullet+}$ ions, the most dominant fragment ion from the CID of the $[b_5 - H]^{\bullet+}$ ion is frequently the loss of CO_2. This is the major characteristic shared between the three series. It is also a marked difference that distinguishes these three series from the $[A_4W_{oxa}]^{\bullet+}$ ions or the $[A_4W_{\alpha\text{-Me oxa}}]^{\bullet+}$ ions, where loss of CO_2 is negligible. From the study of the $[A_4G_{oxa}]^{\bullet+}$ ions, we have learned that the loss of CO_2 is facilitated by an α-radical

located next to the oxazolone ring (**Scheme 5.2**). We have also learned that for the ions $[AG^{\bullet}AAA_{oxa}]^{+}$, $[AAG^{\bullet}AA_{oxa}]^{+}$, and $[AAAG^{\bullet}A_{oxa}]^{+}$, the energy barrier to macrocyclization is lower than the barrier for HAT and subsequent loss of CO_2, while ion $[AAAAG^{\bullet}_{oxa}]^{+}$ is the most easily formed ion from ring-opening of the macrocyclic structure (**Scheme 5.3**). A subsequent 1-13 HAT in this ion, followed by formation of a second macrocyclic structure and ring-opening, results in the ion $[AAGA^{\bullet}A_{oxa}]^{+}$, which has the lowest barrier for CO_2 loss of all isomers.

Since CO_2 loss is also the most dominant peak in the CID spectra of $[A_4Y_{oxa}]^{\bullet+}$and $[A_4M_{oxa}]^{\bullet+}$ ions, and they share similarities in fragmentation patterns, we may suggest similar dissociation mechanisms for the loss of CO_2 in these ions. Based on the ^{18}O-labeled $[AAAYA_{oxa}]^{\bullet+}$, CO_2 loss is from more than one structure, but majority of the ion is from a CO_2 loss from the ion $[AAAYA^{18O}_{oxa}]^{\bullet+}$. It is reasonable to propose that the radical center in this ion is at the α-carbon of the tyrosine residue, which is next to the oxazolone ring, and is sufficiently stabilized by the tyrosine side chain. This may facilitate CO_2 loss, with mechanisms similar to that for the $[A_4G_{oxa}]^{\bullet+}$ ions. Whether the $[A_4Y_{oxa}]^{\bullet+}$ ions rearrange and isomerize into the ion $[AAAY^{\bullet}A_{oxa}]^{+}$ before CO_2 loss or such loss occurs from the original structure is unclear, as the ion $[AAAYA_{oxa}]^{\bullet+}$ is the only sequence selected for ^{18}O-labeling and no theoretical calculations have yet been done. For the $[A_4M_{oxa}]^{\bullet+}$ ions, although CO_2 loss is also the most dominant peak in all CID spectra, no ^{18}O-labeling work has been done to reveal information about the loss of CO_2.

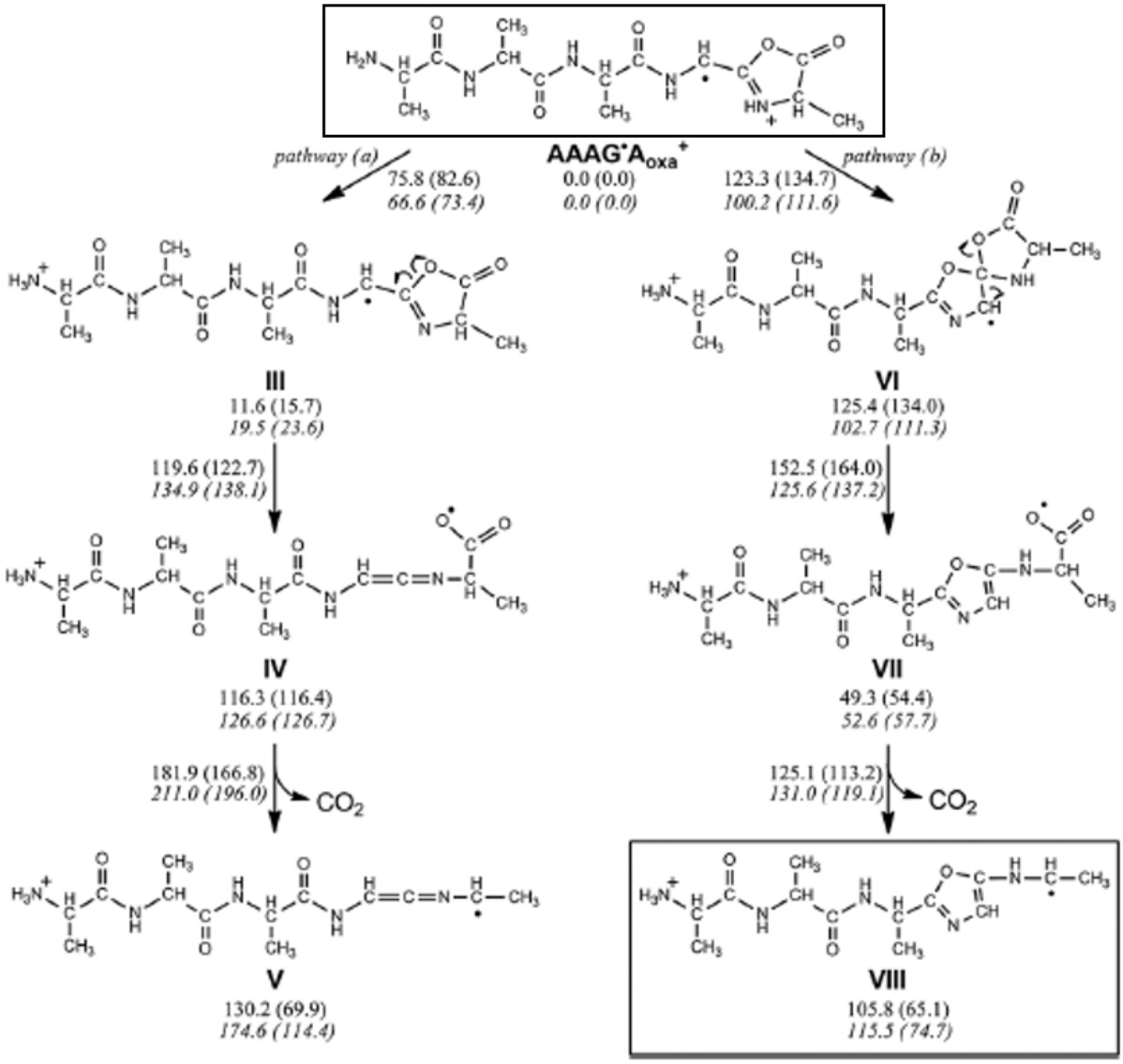

Scheme 5.2 Mechanism for loss of CO_2 from AAAG$^{\bullet}$A$_{oxa}$$^+$. The enthalpies ($\Delta H^o_0$) and free energies ($\Delta G^o_{298}$, in parentheses) in kJ mol^{-1} are relative to isomer AAAG$^{\bullet}$A$_{oxa}$$^+$ and were calculated at the B3LYP/6-31++G(d,p) level (regular fonts). Single-point energies at the M06-2X/6-311++G(d,p) level (in italic fonts) were calculated on selected systems for comparisons. Figure adapted from Lau et. al.[2]

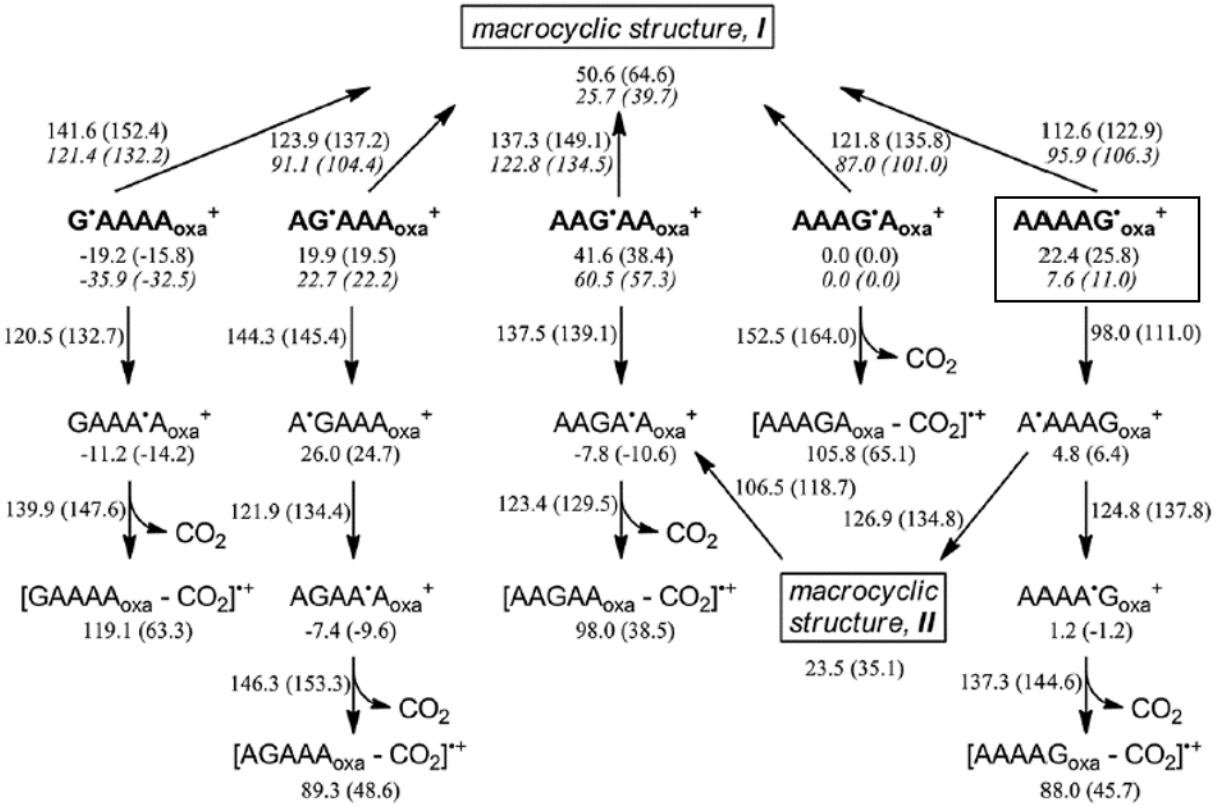

Scheme 5.3 Isomerization of $[A_4G_{oxa}]^{\bullet+}$ ions via macrocyclization and HAT, to produce structures with radical center at the α-carbon next to the oxazolone ring, followed by the loss of CO_2. The enthalpies (ΔH^o_0) and free energies (ΔG^o_{298}, in parentheses) in kJ mol^{-1} are relative to isomer $AAAG^{\bullet}A_{oxa}^{+}$ and were calculated at the B3LYP/6-31++G(d,p) level (regular fonts). Single-point energies at the M06-2X/6-311++G(d,p) level (in italic fonts) were calculated on selected systems for comparisons. Figure adapted from Lau et. al.[2]

5.3.2 Cleavage of the second amide bond: $[b_2' - H]^{\bullet+}$ and $[b_3]^+$

Another dissociation pattern that is common in all of the $[A_4Y_{oxa}]^{\bullet+}$, $[A_4M_{oxa}]^{\bullet+}$, and $[A_4G_{oxa}]^{\bullet+}$ ions is the cleavage of the second amide bond to give the complementary pair of $[b_2' - H]^{\bullet+}$ ion and $[b_3]^+$ ion, although both ions appear in low relative abundance. All isotopic-labelling experiments done for these peptides indicated that they are the ions formed by second amide bond cleavage from the sequence $[AAAXA_{oxa}]^{\bullet+}$ (X = G, Y, or M). This implies that formation of the $[b_2' - H]^{\bullet+}$ ion and $[b_3]^+$ ion from other sequences must have rearrangement of the $[b_5 - H]^{\bullet+}$ ion before dissociation.

Formation of the $[b_3]^+$ ion by loss of a dialanine radical is also present in the CID of the $[A_4W_{\alpha\text{-Me oxa}}]^{\bullet+}$ ions, with the difference that these ions do not isomerize, and such a loss is absent in the sequence $[AW_{\alpha\text{-Me}}AAA_{oxa}]^{\bullet+}$ because it cannot occur without rearrangement. Here, we can suggest a similar mechanism for the cleavage of the second amide bond (**Scheme 5.4**). Starting with a captodative structure of the $[b_5 - H]^{\bullet+}$ ion with the radical at the N-terminal α-carbon, proton transfer to the second amide nitrogen followed by nucleophilic attack by the N-terminal oxygen, results in cleavage of the second amide bond. Initially, a solvated complex is formed; this consists of the $[b_2' - H]^{\bullet+}$ of the two alanine residues from the N-terminus, and another oxazolone structure, the $[b_3]^+$ ion, with the remaining three residues from the C-terminus. These two species will compete for proton affinity within the complex. Eventually, the complex dissociates, and both ions have sufficiently similar proton affinities to acquire the proton and be detected.

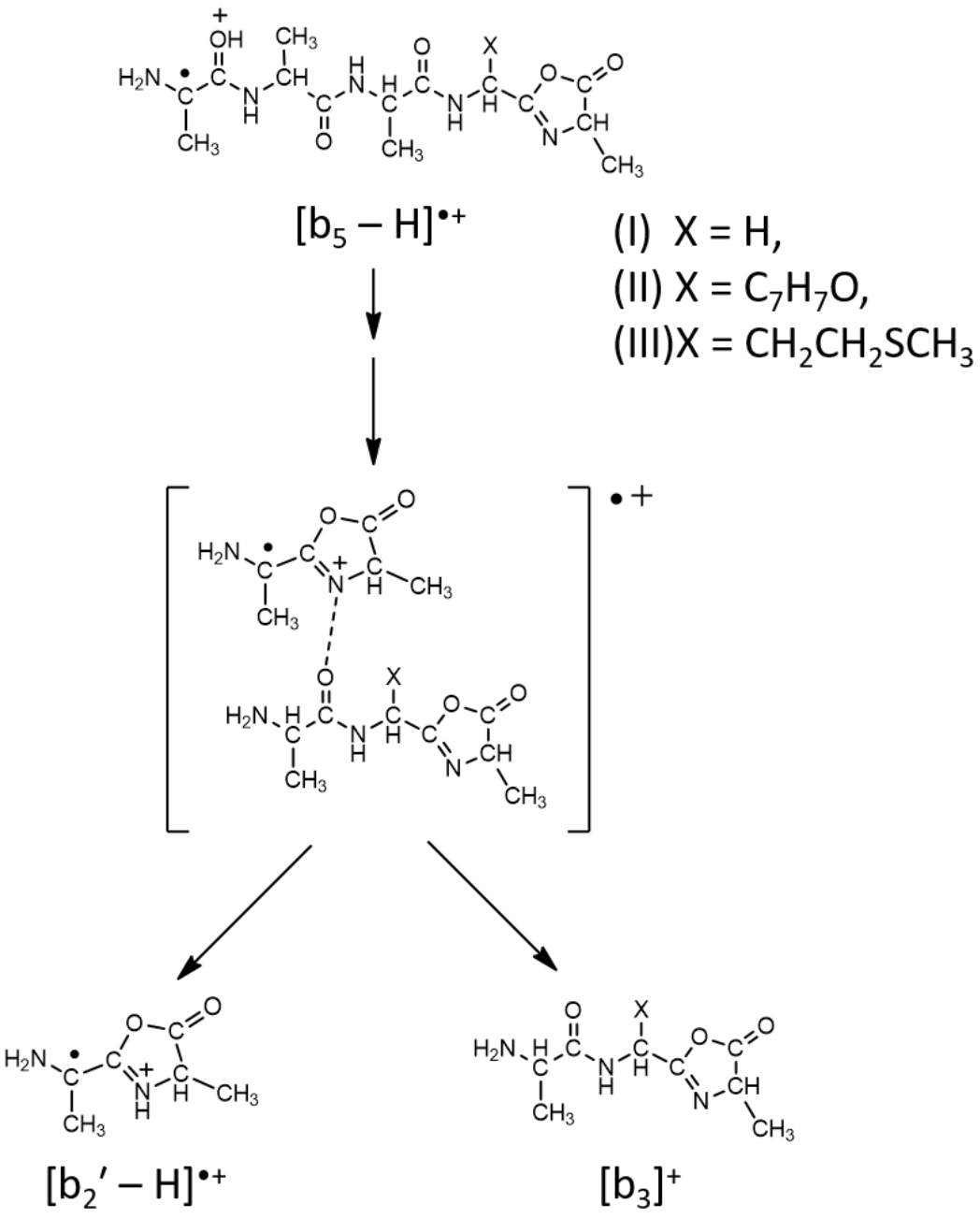

Scheme 5.4 Proposed mechanism for cleavage of the second amide bond from the N-terminus, for CID of **(I)** $[A_4G_{oxa}]^{\bullet+}$ **(II)** $[A_4Y_{oxa}]^{\bullet+}$, and **(III)** $[A_4M_{oxa}]^{\bullet+}$ ions.

5.3.3 Loss of alanine residues

In the CID spectra of all three series of $[b_5 - H]^{\bullet+}$ ions ($[A_4Y_{oxa}]^{\bullet+}$, $[A_4M_{oxa}]^{\bullet+}$, and $[A_4G_{oxa}]^{\bullet+}$ ions), $[b_4 - H]^{\bullet+}$, $[b_3 - H]^{\bullet+}$, and $[b_2 - H]^{\bullet+}$ ions are present, the product of the loss of one, two, or three alanine residue, respectively. Loss of one residue from a closed-shell b-type ion is usually achieved by an initial loss of CO, giving an a-type ion, followed by the loss of the remainder of the residue. Based on the isotopic-labeling experiment, loss of one alanine residue in all three series consists of a mixture, indicating that the $[b_4 - H]^{\bullet+}$ ion is formed from the dissociation of more than one isomer.

Loss of two alanine residues is mostly from the N-terminus of the sequence $[AAAXA_{oxa}]^{\bullet+}$ (X = G, Y, or M), with also a minor mixture. This is supported by isotopic-labeling of $[AAAXA_{oxa}]^{\bullet+}$ for all three series (**Figure 5.6** and **Figure 5.8**).[51]

Loss of three alanine residues as an oxazolone, is in very low abundance from isomer $[AAAXA_{oxa}]^{\bullet+}$ in all three series, and for X = tyrosine, the loss is definitely from the N-terminus (**Figure 5.6**). The loss of three alanine residues from $[AYAAA_{oxa}]^{\bullet+}$ and $[AMAAA_{oxa}]^{\bullet+}$, forming the $[b_2 - H]^{\bullet+}$ ion, is one of the major pathways (60% - 100% relative abundance), compared to the very minor product when the hetero-residue is at other positions. ^{18}O-labeled $[AG^{\bullet}AAA_{oxa}]^{+}$ revealed that the $[b_2 - H]^{\bullet+}$ ion (*m/z* 128) is from the loss of three alanine residues from the C-terminus of the original sequence (**Figure 5.12**).

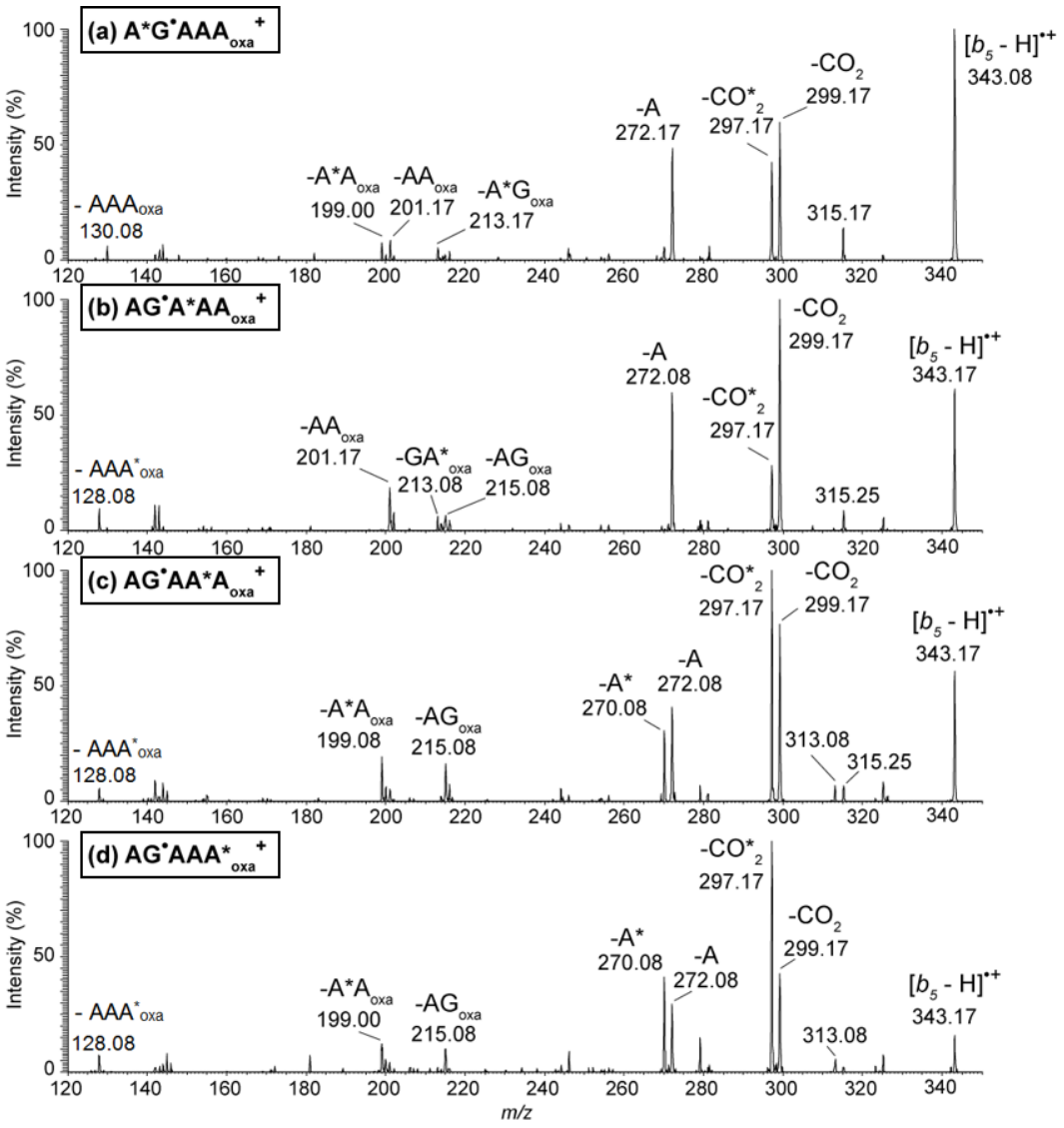

Figure 5.12 CID spectra of $[AG^{\bullet}AAA_{oxa}]^+$, with ^{18}O label at different positions. "*" indicates the ^{18}O label. Figure adapted from Lau et. al.[2]

5.3.4 Loss of the hetero-residue

In both the $[A_4Y_{oxa}]^{\bullet+}$ and $[A_4M_{oxa}]^{\bullet+}$ ions, there is a corresponding $[b_4' - H]$, ion at *m/z* 284 via loss of the hetero-residue (Y or M) in all sequence, although the relative abundance varies and is present at very low abundance in some spectra (**Figure 5.3** and **Figure 5.4**). This species is not observed in the $[A_4G_{oxa}]^{\bullet+}$, $[A_4W_{oxa}]^{\bullet+}$, or the $[A_4W_{\alpha\text{-Me oxa}}]^{\bullet+}$ ions. Loss of the hetero-residue is a sign of sequence scrambling.

5.3.5 Loss of the side chain

In the study of α-methyltryptophan-containing hexapeptides, we observed the loss of side chain fragments. CID of the hexapeptide radical cations showed losses of 129 Da, which is a closed-shell fragment; in contrast, the $[b_5 - H]^{\bullet+}$ ions showed losses of 130 Da, corresponding to an open-shell radical fragment (**Figure 5.13 a)**). CID of the $[A_4Y_{oxa}]^{\bullet+}$ ions also showed a loss of the open-shell radical side chain (107 Da) in all sequences, although the relative abundance varies (**Figure 5.13 b)**). However, we cannot conclude that all $[b_5 - H]^{\bullet+}$ ions lose the radical side chain, since the $[A_4M_{oxa}]^{\bullet+}$ ions showed losses of the closed-shell side chain fragment (74 Da) (**Figure 5.12 c)**). The fact that the $[A_4M_{oxa}]^{\bullet+}$ ions can also lose parts of the side chain ($HSCH_3$, CH_3SCH_3, and $\bullet CH_2SCH_3$) and that the ion after loss of 74 Da tends to further lose an NH_3 indicates that the $[A_4M_{oxa}]^{\bullet+}$ ions may undergo unique pathways for the loss of side chain fragments.

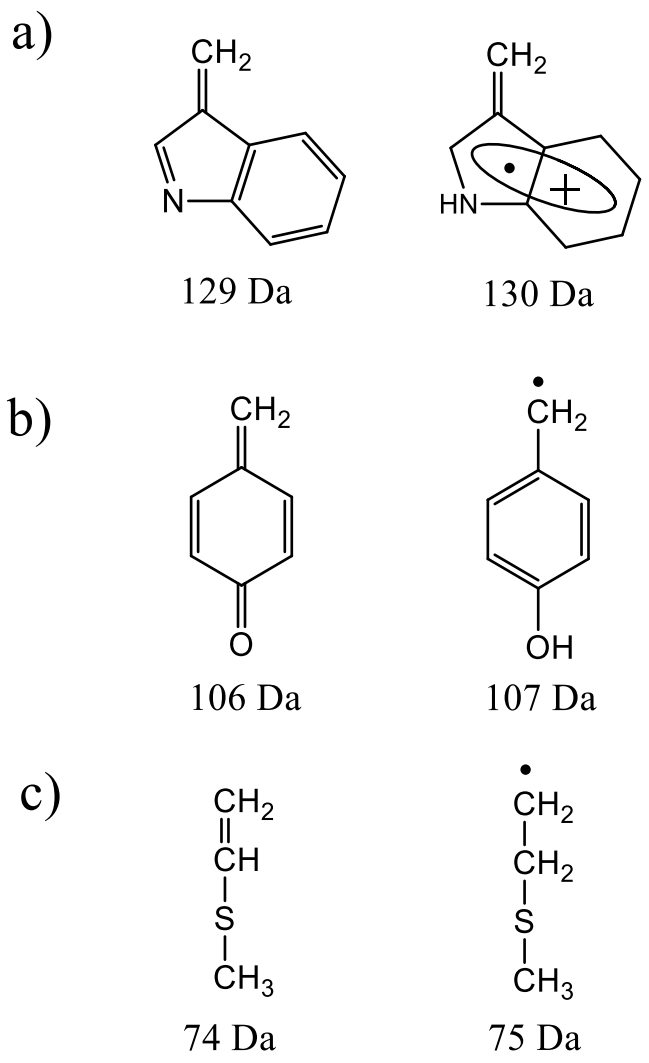

Figure 5.13 Structures and corresponding molecular weights of both the closed-shell and open-shell side chain fragments for a) tryptophan, b) tyrosine, and c) methionine.

5.4 Summary

We have studied the fragmentation behavior of $[A_4Y_{oxa}]^{\bullet+}$ and $[A_4M_{oxa}]^{\bullet+}$ ions and found similar behaviors between the dissociation of $[A_4Y_{oxa}]^{\bullet+}$, $[A_4M_{oxa}]^{\bullet+}$ and $[A_4G_{oxa}]^{\bullet+}$ ions. For all three series, CID of the $[b_5 - H]^{\bullet+}$ ions with the hetero-residue at different positions showed non-identical spectra; the fragment ions are identical but there are different relative abundances, and there is evidence for rearrangement of the $[b_5 - H]^{\bullet+}$ ions before dissociation. Key characteristics for the dissociation of the $[b_5 - H]^{\bullet+}$ ions from these three series have been summarized. The most dominant peak in all the spectra from these three series is always the loss of CO_2, which is found to have the lowest onset energy based on the energy-resolved breakdown diagram of $[A^{1N}A^{D3}AMA_{oxa}]^{\bullet+}$. Spectra of isotopically-labeled $[AAAXA_{oxa}]^{\bullet+}$ ions indicated that majority of the fragment ions are from the original sequence. However, it remains unclear whether these dissociation pathways apply on the original structure of each sequence, or if the $[b_5 - H]^{\bullet+}$ ions macrocyclize and the sequence $[AAAXA_{oxa}]^{\bullet+}$ is the most preferred structure for ring-opening and dissociation. Further isotopic-labelling experiment with the tyrosine or methionine residue on other positions is required.

CHAPTER 6: Summary and Future Works

In this thesis, we have answered the question to whether the α-methyl substituent on the tryptophan residue affects fragmentation patterns of protonated peptides, peptide radical cations, closed-shell $[b_5]^+$ ions, and open-shell $[b_5 - H]^{\bullet+}$ ions. For dissociation of protonated peptides, having the methyl group on the α-carbon of the tryptophan does not affect the dissociation. Protonated peptide ions with or without the α-methyl group both produce the $[b_5]^+$ ion as the most dominant fragment. For dissociation of the peptide radical cations, however, ions with a normal tryptophan residue predominantly produce $[b_5 - H]^{\bullet+}$ ions, while ions with the α-methyl substituent tend to dissociate by cleavages around the α-carbon due to steric crowding. This produces mainly the $[z_m - H]^{\bullet+}$ ions and the ion after the loss of 3-methyleneindolenine, with very little $[b_5 - H]^{\bullet+}$ ions produced.

Fragmentation of the $[b_5]^+$ ions with the α-methyltryptophan residue is also very different from those with a normal tryptophan residue, despite the fact that both showed sequence scrambling. Dissociations of $[A_4W_{\alpha\text{-Me oxa}} + H]^+$ ions produce high abundance of the $[a_5]^+$ ion, as well as the complementary pair of internal $[a_1]^+$ ion and $[b_4']^+$ ion by cleavage between the four alanine residues and the α-methyltryptophan residue from the $[a_5]^+$ ion of $[AAAAW_{\alpha\text{-Me oxa}} + H]^+$. The $[b_5]^+$ ions with the α-methyltryptophan residue also lose CO_2, and this becomes the dominant pathway at higher collision energies. With sufficient collision energy, these $[b_5]^+$ ions also lose a fragment of 117 Da, which corresponds to a combined loss of a neutral fragment of the oxazolone

ring and a water molecule that are from alanine residues on both sides of the α-methyltryptophan residue from the ion $[AAAW_{\alpha\text{-}Me}A_{oxa} + H]^+$.

For the $[b_5 - H]^{\bullet+}$ ions with the α-methyl substituent on the tryptophan residue clearly showed that, by preventing the formation of the α-radical on the tryptophan residue proposed for $[b_5 - H]^{\bullet+}$ ions with normal tryptophan residues, the best structure for the $[b_5 - H]^{\bullet+}$ ion would have a captodative radical at the N-terminal α-carbon. This reduces the nucleophilicity of the N-terminal nitrogen, and prevents head-to-tail cyclization and sequence scrambling. One marked observation is that a loss of 116 Da, which appears to be a combined loss of the oxazolone with a radical and a water, is only observed in the dissociation of $[AAAW_{\alpha\text{-}Me}A_{oxa}]^{\bullet+}$, consistent with the observation that no isomerization occurs in this set of ions. This provided a further support for the proposed dissociation mechanism for the analogous loss of 117 Da from the ion $[AAAW_{\alpha\text{-}Me}A_{oxa} + H]^+$.

Studies done for the $[A_4Y_{oxa}]^{\bullet+}$ and $[A_4M_{oxa}]^{\bullet+}$ systems indicated that they shared similarities in fragmentation patterns with the $[A_4G_{oxa}]^{\bullet+}$ system and may be grouped together. These three systems all showed indications of rearrangement before dissociation, but relative abundance of the fragment ions differ significantly between spectra with the hetero-residue at different positions. Isotopic-labelling experiments done for each system all implies that the fragment ions are mixtures of products from more than one structure, while the majority is from the original sequence $[AAAXA_{oxa}]^{\bullet+}$ (X = G, Y, or M) that was selected for isotopic-labelling.

Although the experiments were well-designed, and reliable data were obtained and analyzed, there are some potential limitations in this work that need to be addressed. First, since no calculation work has yet been done for any of the work related to the open-shell ions except for

the structure of the $[A_4W_{\alpha\text{-Me oxa}}]^{\bullet+}$ ions, all of the dissociation mechanisms drawn for these ions are simply proposed mechanisms. These hypotheses are based on general gas-phase chemistry, without knowing the actual energy barriers and energies of the intermediate products. Secondly, most of the labeling works in the open-shell studies were done on peptides with the linear sequence where the hetero-residue is on the fourth position ($[AAAXA_{oxa}]^{\bullet+}$). This sequence was chosen because it generally produces richer fragmentation, including some unique features such as the loss of 116 Da from the $[AAAW_{\alpha\text{-Me}}A_{oxa}]^{\bullet+}$ ion, compared to other sequences. However, since the $[b_5 - H]^{\bullet+}$ ions that we studied showed either no scrambling or incomplete scrambling, it is not enough to generalize dissociation patterns for all sequences by studying one particular sequence, especially without calculation supports. All of these potential pitfalls may lead to future directions for this work, which will include labeling on sequences where the hetero-residue is not at the fourth position; and DFT calculations on the intermediate structures and energy barriers of all proposed dissociation pathways.

CHAPTER 7: References

1. R. Aebersold, M. Mann, Mass spectrometry-based proteomics, *Nature*. 422 (2003) 198–207.

2. J.B. Fenn, M. Mann, C.K.A.I. Meng, S.F. Wong, C.M. Whitehouse, Electrospray ionization for mass spectrometry of large biomolecules, *Science*, 246 (1989) 64–71.

3. X. Han, A. Aslanian, J.R. Yates, Mass spectrometry for proteomics, *Curr. Opin. Chem. Biol.* 12 (2008) 483–490.

4. S. Kollipara, N. Agarwal, B. Varshney, J. Paliwal, Technological advancements in mass spectrometry and its impact on proteomics, *Anal. Lett.* 44 (2011) 1498–1520.

5. K.A. Resing, N.G. Ahn, Proteomics strategies for protein identification, *FEBS Lett.* 579 (2005) 885–889.

6. H. Steen, M. Mann, The ABC's (and XYZ's) of peptide sequencing., *Nat. Rev. Mol. Cell Biol.* 5 (2004) 699–711.

7. M. Tyers, M. Mann, From genomics to proteomics, *Nature*. 422 (2003) 193–197.

8. C.C. Wu, J.R. Yates 3rd, J.R. Yates, The application of mass spectrometry to membrane proteomics, *Nat Biotechnol.* 21 (2003) 262–267.

9. T. Masuda, M. Tomita, Y. Ishihama, Phase transfer surfactant-aided trypsin digestion for membrane proteome analysis, *J. Proteome Res*. 7 (2008) 731–740.

10. E.I. Chen, D. Cociorva, J.L. Norris, J.R. Yates, Optimization of mass spectrometry-compatible surfactants for shotgun proteomics, *J. Proteome Res*. 6 (2007) 2529–2538.

11. F. Meng, B.J. Cargile, S.M. Patrie, J.R. Johnson, S.M. Mcloughlin, N.L. Kelleher, Processing complex mixtures of intact proteins for direct analysis by mass spectrometry, *Anal. Chem*. 74 (2002) 2923–2929.

12. Y. Yu, M. Gilar, P.J. Lee, E.S.P. Bouvier, J.C. Gebler, Enzyme-friendly, mass spectrometry-compatible surfactant for in-solution enzymatic digestion of proteins, *Anal. Chem*. 75 (2003) 6023–6028.

13. C.C. Wu, J.R. Yates 3rd, J.R. Yates, The application of mass spectrometry to membrane proteomics, *Nat. Biotechnol*. 21 (2003) 262–267.

14. T. Yalcin, C. Khouw, I.G. Csizmadia, M.R. Peterson, A.G. Harrison, Why are b ions stable species in peptide spectra*?, J. Am. Soc. Mass Spectrom*. 6 (1995) 1165–1174.

15. A.G. Harrison, To b or not to b: the Ongoing saga of peptide b ions, *Mass Spectrom. Rev*. 28 (2009) 640–654.

16. V.H. Wysocki, G. Tsaprailis, L.L. Smith, L.A. Breci, Mobile and localized protons: a framework for understanding peptide dissociation, *J. Mass Spectrom*. 35 (2000) 1399–1406.

17. C.F. Rodriquez, A. Cunje, T. Shoeib, I.K. Chu, A.C. Hopkinson, K.W.M. Siu, Proton migration and tautomerism in protonated triglycine, *J. Am. Chem. Soc*. 123 (2001) 3006–3012.

18. I.K. Chu, C.K. Siu, J.K.C. Lau, W.K. Tang, X. Mu, C.K. Lai, X. Guo, X. Wang, N. Li, Y. Xia, X. Kong, H. Bin Oh, V. Ryzhov, F. Tureček, A.C. Hopkinson, K.W.M. Siu, Proposed nomenclature for peptide ion fragmentation, *Int. J. Mass Spectrom*. 390 (2015) 24–27.

19. B. Paizs, Z. Szlávik, G. Lendvay, K. Vékey, S. Suhai, Formation of b_2^+ ions from protonated peptides: an ab initio study, *Rapid Commun. Mass Spectrom*. 14 (2000) 746–755.

20. M.J. Nold, C. Wesdemiotis, T. Yalcin, A.G. Harrison, Amide bond dissociation in protonated peptides. structures of the N -terminal ionic and neutral fragments, *Int. J. Mass Spectrom Ion Process*. 164 (1997) 137–153.

21. N.C. Polfer, J. Oomens, S. Suhai, B. Paizs, Spectroscopic and theoretical evidence for oxazolone ring formation in collision-induced dissociation of peptides, *J. Am. Chem. Soc*. 127 (2005) 17154–17155.

22. B. Paizs, S. Suhal, Fragmentation pathways of protonated peptides, *Mass Spectrom. Rev*. 24 (2005) 508–548.

23. T. Yalcin, I.G. Csizmadia, M.R. Peterson, A.G. Harrison, The structure and fragmentation of b_n ($n \geq 3$) ions in peptide spectra, *J. Am. Soc. Mass Spectrom*. 7 (1996) 233–242.

24. M.J. Wells, S.A. McLuckey, Collision-induced dissociation (CID) of peptides and proteins, *Methods Enzym*. 402 (2005) 148–185.

25. March, R. E., Todd, J. F.: Dynamics of ion trapping. quadrupole ion trap mass spectrometry. 2, 73-132 (2005)

26. J.H. Gross, Tandem Mass spectrometry. mass spectrometry – a textbook. 2, Springer-Verlag Berlin Heidelberg (2011)

27. R.G. Cooks, Collision spectroscopy, Springer US (1978)

28. S. A. McLuckey, Principles of collisional activation in analytical mass spectrometry, *J. Am. Soc. Mass Spectrom*. 3 (1992) 599–614.

29. M.J. Charles, S. a. McLuckey, G.L. Glish, competition between resonance ejection and ion dissociation during resonant excitation in a quadrupole ion trap, *J. Am. Soc. Mass Spectrom*. 5 (1994) 1031–1041.

30. E.M. Marzluff, S. Campbell, M.T. Rodgers, J.L. Beauchamp, Collisional activation of large molecules is an efficient process, *J. Am. Chem. Soc*. 116 (1994) 6947–6948.

31. I.A. Papayannopoulos, The interpretation of collision-induced dissociation tandem mass spectra of peptides, *Mass Spectrom. Rev*. 14 (1995) 49–73.

32. R. A. Zubarev, Electron-capture dissociation tandem mass spectrometry, *Curr. Opin. Biotechnol*. 15 (2004) 12–16.

33. Y. Qi, D.A. Volmer, Electron-based fragmentation methods in mass spectrometry: an overview, *Mass Spectrom. Rev*. 9999 (2015) 1–12.

34. K.O. Zhurov, L. Fornelli, M.D. Wodrich, A. Laskay, Y.O. Tsybin, Principles of electron capture and transfer dissociation mass spectrometry applied to peptide and protein structure analysis, *Chem. Soc. Rev*. 42 (2013) 5014–5030.

35. R. Zubarev, N.L. Kelleher, F.W. McLafferty, Electron capture dissociation of multiply charged protein cations. a nonergodic process, *J. Am. Chem. Soc*. 120 (1998) 3265–3266.

36. J.E.P. Syka, J.J. Coon, M.J. Schroeder, J. Shabanowitz, D.F. Hunt, Peptide and protein sequence analysis by electron transfer dissociation mass spectrometry., *Proc. Natl. Acad. Sci. U.S.A.* 101 (2004) 9528–9533.

37. M.-S. Kim, A. Pandey, Electron transfer dissociation mass spectrometry in proteomics., *Proteomics*. 12 (2012) 530–42.

38. J.J. Coon, J.E.P. Syka, J.C. Schwartz, J. Shabanowitz, D.F. Hunt, Anion dependence in the partitioning between proton and electron transfer in ion/ion reactions, *Int. J. Mass Spectrom*. 236 (2004) 33–42.

39. D.F. Hunt, J.J. Coon, J.E.P. Syka, J.A. Marto: Electron transfer dissociation for biopolymer sequence mass spectrometric analysis. US 7,534,622 B2 (2009)

40. Thermo Fisher Scientific: Orbitrap Elite Hardware Manual. P/N 1288170. Revision A (2011)

41. M.L. Nielsen, B. A. Budnik, K.F. Haselmann, J. V. Olsen, R. A. Zubarev, Intramolecular hydrogen atom transfer in hdrogen-deficient polypeptide radical cations, *Chem. Phys. Lett.* 330 (2000) 558–562.

42. H. Lioe, R.A J. O'Hair, Comparison of collision-induced dissociation and electron-induced dissociation of singly protonated aromatic amino acids, cystine and related simple peptides using a hybrid linear ion trap-FT-ICR mass spectrometer, *Anal. Bioanal. Chem*. 389 (2007) 1429–1437.

43. M.L. Nielsen, B. A. Budnik, K.F. Haselmann, R. A. Zubarev, Tandem MALDI/EI ionization for tandem fourier transform ion cyclotron resonance mass spectrometry of polypeptides, *Int. J. Mass Spectrom*. 226 (2003) 181–187.

44. R.H. Wills, P.B. O'Connor, Structural characterization of actinomycin D using multiple ion isolation and electron induced dissociation, *J. Am. Soc. Mass Spectrom.* 25 (2014) 186–195.

45. J. A. Mosely, M.J.P. Smith, A.S. Prakash, M. Sims, A.W.T. Bristow, Electron-induced dissociation of singly charged organic cations as a tool for structural characterization of pharmaceutical type molecules, *Anal. Chem*. 83 (2011) 4068–4075.

46. B. A. Budnik, K.F. Haselmann, R. A. Zubarev, Electron detachment dissociation of peptide di-anions: an electron-hole recombination phenomenon, *Chem. Phys. Lett*. 342 (2001) 299–302.

47. M. Huzarska, I. Ugalde, D. A. Kaplan, R. Hartmer, M.L. Easterling, N.C. Polfer, Negative electron transfer dissociation of deprotonated phosphopeptide anions: choice of radical cation reagent and competition between electron and proton transfer, *Anal. Chem.* 82 (2010) 2873–2878.

48. H.J. Yoo, N. Wang, S. Zhuang, H. Song, K. Håkansson, Negative-ion electron capture dissociation: radical-driven fragmentation of charge-increased gaseous peptide anions, *J. Am. Chem. Soc*. 133 (2011) 16790–16793.

49. I.K. Chu, C.N.W. Lam, S.O. Siu, Facile generation of tripeptide radical cations in vacuo via intramolecular electron transfer in Cu^{II} tripeptide complexes containing sterically encumbered terpyridine ligands, *J. Am. Soc. Mass Spectrom*. 16 (2005) 763–771.

50. I.K. Chu, C.F. Rodriquez, T. Lau, A.C. Hopkinson, K.W.M. Siu, molecular radical cations of oligopeptides, *J. Phys. Chem. B.* 104 (2000) 3393–3397.

51. J.K.-C. Lau, J. Zhao, D. Williams, B.-H.B. Wu, Y. Wang, S. Ma, I.S. Saminathan, K.W.M. Siu, A.C. Hopkinson, Radical-induced dissociation leading to the loss of CO_2 from the oxazolone ring of $[b_5 - H]^{\bullet +}$ ions, *Phys. Chem. Chem. Phys*. 18 (2016) 18119–18127.

52. I.K. Chu, S.O. Siu, C.N.W. Lam, J.C.Y. Chan, C.F. Rodriquez, Formation of molecular radical cations of aliphatic tripeptides from their complexes with Cu^{II} (12-crown-4), *Rapid Commun. Mass Spectrom*. 18 (2004) 1798–1802.

53. J.L. Holmes, Assigning structures to ions in the gas phase, *Org. Mass Spectrom*. 20 (1985) 169–183.

54. A.G. Harrison, Peptide sequence scrambling through cyclization of b_5 ions, *J. Am. Soc. Mass Spectrom*. 19 (2008) 1776–1780.

55. C. Bleiholder, S. Osburn, T.D. Williams, S. Suhai, M. Van Stipdonk, A.G. Harrison, B. Paizs, Sequence-scrambling fragmentation pathways of protonated peptides, *J. Am. Chem. Soc.* 130 (2008) 17774–17789.

56. A.G. Harrison, A.B. Young, C. Bleiholder, Scrambling of sequence information in collision-induced dissociation of peptides, *J. Am. Chem. Soc*. 128 (2006) 10364–10365.

57. U. Erlekam, B.J. Bythell, D. Scuderi, M.V. Stipdonk, B. Paizs, and P. Maître, Infrared spectroscopy of fragments of protonated peptides: direct evidence for macrocyclic structures of b_5 ions, *J. Am. Chem. Soc*. 131 (2009) 11503-1108.

58. S. Molesworth, S. Osburn, and M.V. Stipdonk, Influence of size on apparent scrambling of sequence during CID of b-type ions, *J. Am. Soc. Mass Spectrom.* 20 (2009) 2174-2181.

59. D. Williams, J.K.-C. Lau, J. Zhao, S. Mädler, Y. Wang, I.S. Saminathan, A.C. Hopkinson, K.W.M. Siu, Radical-induced, proton-transfer-driven fragmentations in $[b_5 - H]^{\bullet+}$ ions derived from pentaalanyl tryptophan., *Phys. Chem. Chem. Phys*. 17 (2015) 10699–10707.

60. A.C. Hopkinson, Radical cations of amino acids and peptides: structures and stabilities, *Mass Spectrom. Rev.* 28 (2009) 655–671.

61. T. Song, Q. Hao, C. Law, C. Siu, I.K. Chu, Novel Cβ–Cg bond cleavages of tryptophan-containing peptide radical cations, *J. Am. Soc. Mass Spectrom*. 23 (2012) 264–273.

62. G. Hao, S.S. Gross, Electrospray tandem mass spectrometry analysis of S- and N-nitropeptides: facile loss of NO and radical-induced fragmentation, *J. Am. Soc. Mass Spectrom.* 17 (2006) 1725-1730.

63. V. Ryzhov, A.K.Y. Lam, R.A.J. O'Hair, Gas-phase fragmentation of long-lived cysteine radical cations formed via NO loss from protonated S-nitrosocysteine, *J. Am. Soc. Mass Spectrom*. 20 (2009) 985–995.

64. M. Lesslie, J.K. Lau, J.T. Lawler, K.W.M. Siu, V. Steinmetz, P. Maître, A.C. Hopkinson, V. Ryzhov, Cysteine radical / metal ion adducts : a gas-phase structural elucidation and reactivity study, *Chempluschem*. 81 (2016) 444–452.

65. A.K.Y. Lam, V. Ryzhov, R.A.J. O'Hair, Mobile protons versus mobile radicals : gas-phase unimolecular chemistry of radical, *J. Am. Soc. Mass Spectrom*. 21 (2010) 1296–1312.

66. J.K.C. Lau, S. Lo, J. Zhao, K.W.M. Siu, A.C. Hopkinson, Fragmentation chemistry of $[Met\text{-}Gly]^{\bullet+}$, $[Gly\text{-}Met]^{\bullet+}$, and $[Met\text{-}Met]^{\bullet+}$ radical cations, *J. Am. Soc. Mass Spectrom.* 24 (2013) 543–553.

67. J. Zhao, C.M.D. Ng, I.K. Chu, K.W.M. Siu, A.C. Hopkinson, Methionine, α-methylmethionine and s-methylcysteine radical cations: generations and dissociations in the gas phase, *Phys. Chem. Chem. Phys.*11 (2009) 7629-7639.

68. L. Sleno, D.A. Volmer, Ion activation methods for tandem mass spectrometry, *J. Mass Spectrom*. 39 (2004) 1091–1112.

69. G.L. Glish, R.W. Vachet, The basics of mass spectrometry in the twenty-first century, *Nat. Rev. Drug Discov*. 2 (2003) 140–150.

70. P. Kebarle, U.H. Verkerk, Electrospray: from ions in solution to ions in the gas phase, what we know now, *Mass Spectrom. Rev*. 28 (2009) 898–917.

71. HESI-II prob user guide, United States, Thermo Fisher Scientific Inc. (2009)

72. W. Paul, Electromagnetic traps for charged and neutral particles, *Rev. Mod. Phys.* 62 (1990) 531-540.

73. Y. Huang, S. Guan, H. S. Kim, A. G. Marshall, Ion transport through a strong magnetic field gradient by r.f.-only octupole ion guides, *Int. J. Mass Spectrom Ion Process*. 152 (1996) 121-133

74. LTQ series hardware manual, United States, Thermo Fisher Scientific Inc. (2009)

75. J. Marecek, B. Song, S. Brewer, J. Belyea, R. B. Dyer, D. P. Raleigh, A simple and economical method for the production of ^{13}C, ^{18}O-labeled fmoc-amino acids with high levels of enrichment: applications to isotope-edited IR studies of proteins, *Org. Lett*. 9 (2007) 4935-4937.

76. W. C. Cheng, P.D. White, Fmoc solid phase peptide synthesis: a practical approach, Oxford: New York, (2000).

77. B.J. Bythell, A.G. Harrison, Formation of a_1 ions directly from oxazolone b_2 ions: an energy-resolved and computational study, *J. Am. Soc. Mass Spectrom*. 26 (2015) 774–781.

78. Gaussian 09, Revision D.01, M. J. Frisch, G. W. Trucks, H. B. Schlegel, G. E. Scuseria, M. A. Robb, J. R. Cheeseman, G. Scalmani, V. Barone, G. A. Petersson, H. Nakatsuji, X. Li, M. Caricato, A. Marenich, J. Bloino, B. G. Janesko, R. Gomperts, B. Mennucci, H. P. Hratchian, J. V. Ortiz, A. F. Izmaylov, J. L. Sonnenberg, D. Williams-Young, F. Ding, F. Lipparini, F. Egidi, J. Goings, B. Peng, A. Petrone, T. Henderson, D. Ranasinghe, V. G. Zakrzewski, J. Gao, N. Rega, G. Zheng, W. Liang, M. Hada, M. Ehara, K. Toyota, R. Fukuda, J. Hasegawa, M. Ishida, T. Nakajima, Y. Honda, O. Kitao, H. Nakai, T. Vreven, K. Throssell, J. A. Montgomery, Jr., J. E. Peralta, F. Ogliaro, M. Bearpark, J. J. Heyd, E. Brothers, K. N. Kudin, V. N. Staroverov, T. Keith, R. Kobayashi, J. Normand, K. Raghavachari, A. Rendell, J. C. Burant, S. S. Iyengar, J. Tomasi, M. Cossi, J. M. Millam, M. Klene, C. Adamo, R. Cammi, J. W. Ochterski, R. L. Martin, K. Morokuma, O. Farkas, J. B. Foresman, and D. J. Fox, Gaussian, Inc., Wallingford CT, 2016.

79. A.D. Becke, Density-functional exchange-energy approximation with correct asymptotic behavior, *Phys. Rev.* A38 (1988) 3098–3100.

80. A.D. Becke, Density-functional thermochemistry. III. The role of exact exchange, *J. Chem. Phys*. 98 (1993) 5648–5652.

81. C. Lee, W. Yang, R.G. Parr, Development of the Colle-Salvetti correlation-energy formula into a functional of the electron density, *Phys. Rev*. B37 (1988) 785–789.

82. W.J. Hehre, R. Ditchfield, J.A. Pople, Self—consistent molecular orbital methods. XII. further extensions of Gaussian—type basis sets for use in molecular orbital studies of organic molecules, *J. Chem. Phys.* 56 (1972) 2257–2261.

83. M.J. Frisch, J. A. Pople, J.S. Binkley, Self-consistent molecular orbital methods 25. Supplementary functions for Gaussian basis sets, *J. Chem. Phys*. 80 (1984) 3265–3269.

84. C. Gonzalez, H.B. Schlegel, An improved algorithm for reaction path following, *J. Chem. Phys*. 90 (1989) 2154–2161.

85. S. Mädler, J. K.-C. Lau, D.Williams, Y.Wang, I. S. Saminathan, J. Zhao, K. W. M. Siu and A. C. Hopkinson, *J. Phys. Chem. B.* 118 (2014) 6123–6133.

THE END